Source: HANDBOOK OF OPTICS

PART 5

DETECTORS

Downloaded from Digital Engineering Library @ McGraw-Hill (www.accessengineeringlibrary.com)
Copyright © 2010 The McGraw-Hill Companies. All rights reserved.
Any use is subject to the Terms of Use as given at the website.

Downloaded from Digital Engineering Library @ McGraw-Hill (www.accessengineeringlibrary.com)
Copyright © 2010 The McGraw-Hill Companies. All rights reserved.
Any use is subject to the Terms of Use as given at the website.

Source: HANDBOOK OF OPTICS

24 PHOTODETECTORS

Paul R. Norton

U.S. Army Night Vision and Electronics Directorate
Fort Belvoir, Virginia

*Second revision and update from an article by Stephen F. Jacobs**

24.1 SCOPE

The purpose of this chapter is to describe the range of detectors commercially available for sensing optical radiation. Optical radiation over the range from vacuum ultraviolet to the far-infrared or submillimeter wavelength (25 nm to 1000 μm) is considered. We will refer to the following spectral ranges:

25–200 nm	vacuum ultraviolet	VUV
200–400 nm	ultraviolet	UV
400–700 nm	visible	VIS
700–1000 nm	near infrared	NIR
1–3 μm	short-wavelength infrared	SWIR
3–5 μm	medium-wavelength infrared	MWIR
5–14 μm	long-wavelength infrared	LWIR
14–30 μm	very long wavelength infrared	VLWIR
30–100 μm	far-infrared	FIR
100–1000 μm	submillimeter	SubMM

We begin by giving a brief description of the photosensitive mechanism for each type of detector. The usefulness and limitations of each detector type are also briefly described. Definitions of the technical terms associated with the detection process are listed. The concept of sensitivity is defined, and D-star (D^*) is presented as a measure of ideal performance. Examples are then given of the limiting cases for D^* under several conditions. In addition, other detector performance parameters are described which may be of critical interest in a specific application, including spectral response, responsivity, quantum efficiency, noise, uniformity, speed, and stability. Finally, manufacturers' specifications for a range of available detectors are compiled and a list of manufacturers is included for each type of detector.

*In *Handbook of Optics*, first edition, McGraw-Hill, 1978. Section 4, "Nonimaging Detectors," by Stephen F. Jacobs, Optical Sciences Center, University of Arizona, Tucson, Arizona.

Downloaded from Digital Engineering Library @ McGraw-Hill (www.accessengineeringlibrary.com)
Copyright © 2010 The McGraw-Hill Companies. All rights reserved.
Any use is subject to the Terms of Use as given at the website.

The sensitivity of many detectors has reached the limit set by room-temperature background photon fluctuations (radiation shot noise). For these detectors, sensitivity may be enhanced by providing additional cooling, while restricting their spatial field of view and/or spectral bandwidth. At some point, other factors such as amplifier noise may limit the improvement.

Techniques for evaluating detector performance are not covered in this treatment but can be found in Refs. 1–6.

24.2 THERMAL DETECTORS

Thermal detectors sense the change in temperature produced by absorption of incident radiation. Their spectral response can therefore be as flat as the absorption spectrum of their blackened coating and window* will allow. This makes them useful for spectroscopy and radiometry. These detectors are generally operated at room temperature, where their sensitivity is limited by thermodynamic considerations[7,8] to 3 pW for 1-s measurement time and 1-mm^2 sensitive area. This limit has been very nearly reached in practice, whereas cooled bolometers have been made to reach the background photon noise limit. Figure 1 illustrates the basic structural elements of a thermal detector.

Construction of the detector seeks to minimize both the thermal mass of the sensitive element and the heat loss from either conductive or convective mechanisms. Heat loss may ideally be dominated by radiation. This allows the incident photon flux to give a maximum temperature rise (maximum signal), but results in a correspondingly slow response time for this class of detectors. The response time τ of thermal detectors is generally slower than 1 ms, depending on thermal capacity C and heat loss per second per degree G, through the relation

$$\tau = C/G$$

A short time constant requires a small C. However, for room-temperature operation, ultimate sensitivity is limited by the mean spontaneous temperature fluctuation:

$$\Delta T = T\sqrt{\frac{k}{C}}$$

where k is Boltzmann's constant. There is thus a trade-off between time constant and ultimate sensitivity.

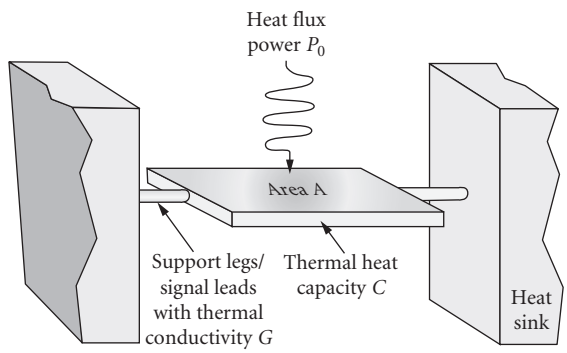

FIGURE 1 Structural elements of a thermal detector. Sensitive area A with a thermal heat capacity of C, supported by leads having thermal conductivity G, and with a heat flux of P_0 incident on the pixel.

*No windows exist without absorption bands anywhere between the visible and millimeter region. Some useful window materials for the far-infrared are diamond, silicon, polyethylene, quartz, and CsI.

Downloaded from Digital Engineering Library @ McGraw-Hill (www.accessengineeringlibrary.com)
Copyright © 2010 The McGraw-Hill Companies. All rights reserved.
Any use is subject to the Terms of Use as given at the website.

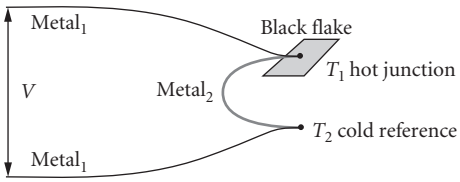

FIGURE 2 Thermocouple detector structure.

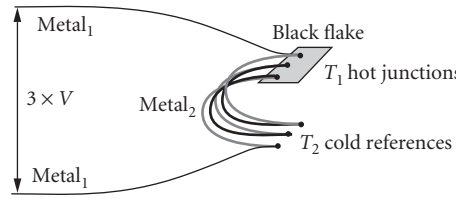

FIGURE 3 Thermopile detector structure.

Thermocouple/Thermopile

The thermocouple receiver, illustrated in Fig. 2, is a thin, blackened flake connected thermally to the junction of two dissimilar metals or semiconductors. Heat absorbed by the flake causes a temperature rise of the junction, and hence a thermoelectric emf is developed which can be measured, for example, with a voltmeter.

Thermocouples are limited in sensitivity by thermal (Johnson-Nyquist) noise but are nevertheless respectably sensitive. Their usefulness lies in the convenience of room temperature operation, wide spectral response, and their rugged construction. Thermocouples are widely used in spectroscopy.

Thermopiles consist of thin-film arrays of thermocouples in series, as illustrated in Fig. 3. This device multiplies the thermocouple signal corresponding to the number of junctions in series. The device may be constructed with half the thermocouples acting as reference detectors attached to a heat sink.

Bolometer/Thermistor

The receiver is a thin, blackened flake or slab, whose impedance is highly temperature dependent—see Fig. 4. The impedance change may be sensed using a bridge circuit with a reference element in the series or parallel arm. Alternatively, a single bolometer element in series with a load and voltage source may be used.

Most bolometers in use today are of the thermistor type made from oxides of manganese, cobalt, or nickel. Their sensitivity closely approaches that of the thermocouple for frequencies higher than 25 Hz. At lower frequencies there may be excess or $1/f$ noise. Construction can be very rugged for systems applications. Some extremely sensitive low-temperature semiconductor and superconductor bolometers are available commercially.

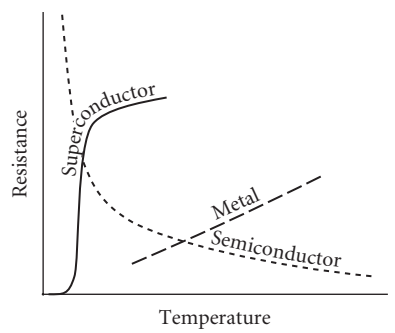

FIGURE 4 Temperature dependence characteristics of three bolometer material types.

Downloaded from Digital Engineering Library @ McGraw-Hill (www.accessengineeringlibrary.com)
Copyright © 2010 The McGraw-Hill Companies. All rights reserved.
Any use is subject to the Terms of Use as given at the website.

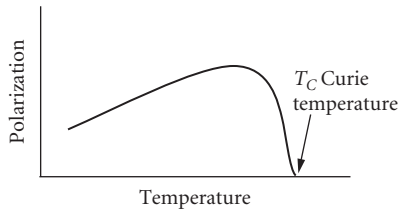

FIGURE 5 Ferroelectric materials exhibit residual polarization with no applied bias.

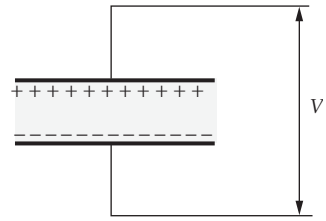

FIGURE 6 The pyroelectric effect produces a surface charge when the temperature changes.

Pyroelectric

Ferroelectric material exhibits a residual polarization in the absence of any electric field, as illustrated in Fig. 5. Dipole moments, initially aligned by applying an external field, result in a surface charge which is normally slowly neutralized by leakage. This polarization is temperature-dependent (pyroelectric effect), and when incident radiation heats an electroded sample, there is a change in surface charge (open-circuit voltage) which is proportional to the incident radiation power—see Fig. 6. Electrically, the device behaves like a capacitor, requiring no bias and therefore exhibiting no current noise. The signal, however, must be chopped or modulated. Sensitivity is limited either by amplifier noise or by loss-tangent noise. Response speed can be engineered, with a proportional decrease in sensitivity, making pyroelectric detectors useful for moderately fast laser pulse detection. Other common applications include power meters. Microphonic noise in applications associated with vibrations can be a problem with some of these devices.

24.3 QUANTUM DETECTORS

Photon detectors respond in proportion to incident photon rates (quanta) rather than to photon energies (heat). Thus, the spectral response of an ideal photon detector is flat on an incident-photon-rate basis but linearly rising with wavelength on an incident-power (per watt) basis. The sensitivity of efficient quantum detectors can approach the limits of photon noise fluctuations provided that the detector temperature is sufficiently low for photon-induced mechanisms to dominate thermally induced mechanisms in the detector. Quantum detectors generally have submicrosecond time constants. Their main disadvantage is the associated cooling required for optimum sensitivity. (These remarks do not apply to photographic detection, which measures cumulative photon numbers.)

Photoemissive

The radiation is absorbed by a photosensitive surface which usually contains alkali metals (cesium, sodium, or potassium). Incident quanta release photoelectrons (Fig. 7), via the photoelectric effect, which are collected by a positively biased anode. This is called a diode phototube; it can be made the basis for the multiplier phototube (photomultiplier phototube, or photomultiplier) by the addition of a series of biased dynodes which serve as secondary emission multipliers.

In spectral regions where quantum efficiency is high (λ <550 nm), the photoemissive detector is very nearly ideal. Sensitivity is high enough to count individual photons. Amplification does not degrade the signal-to-noise ratio. The sensitive area is conveniently large. Photomultiplier signal response time (transit spread time) can be made as short as 0.1 ns. Since the sensitivity in red-sensitive tubes is limited by thermally generated electrons, sensitivity can be improved by cooling.

Downloaded from Digital Engineering Library @ McGraw-Hill (www.accessengineeringlibrary.com)
Copyright © 2010 The McGraw-Hill Companies. All rights reserved.
Any use is subject to the Terms of Use as given at the website.

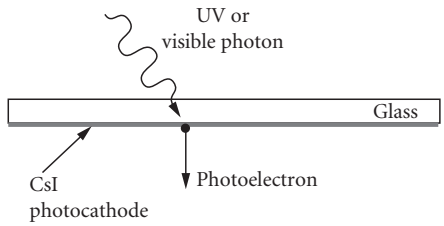

FIGURE 7 Electrons are ejected from a photoemissive surface when excited by photons.

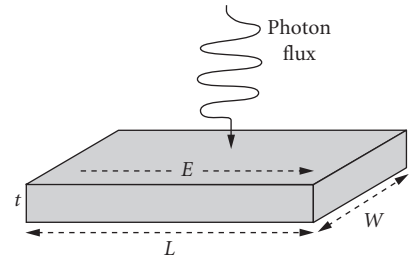

FIGURE 8 Photoconductor device structure.

Photoconductive

The radiation is absorbed by a photoconductive (PC) material, generally a semiconductor, either in thin-film or bulk form, as illustrated in Fig. 8. Each incident quantum may release an electron-hole pair or an impurity-bound charge carrier, thereby increasing the electrical conductivity. The devices are operated in series with a bias voltage and load resistor. Very low impedance photoconductors may be operated with a transformer as the load. Since the impedance of photoconductors varies with device type and operating conditions from less than 50 Ω to more than 10^{14} Ω, the load resistor and preamplifier must be chosen appropriately. Figure 9 shows the current-voltage characteristics of a photoconductor.

Photoconductors that utilize excitation of an electron from the valence to conduction band are called *intrinsic* detectors. Those which operate by exciting electrons into the conduction band or holes into the valence band from states within the band—impurity-bound states, quantum wells, or quantum dots—are called *extrinsic* detectors. Figure 10 illustrates these two mechanism types. Intrinsic detectors are most common at the short wavelengths, out to about 20 μm. Extrinsic detectors are most common at longer wavelengths. A key difference between intrinsic and extrinsic detectors is that intrinsic detectors do not require as much cooling to achieve high sensitivity at a given spectral response cutoff as extrinsic detectors. Thus, intrinsic photoconductors such as HgCdTe will operate out to 15 to 20 μm at 77 K, while comparable extrinsic detectors with similar cutoff must be cooled below 30 to 40 K.

A further distinction may be made by whether the semiconductor material has a direct or indirect bandgap. This difference shows up near the long-wavelength limit of the spectral response

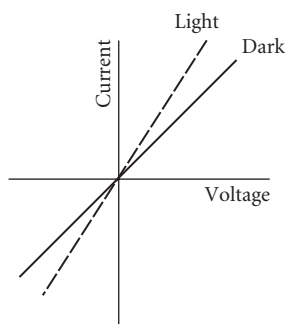

FIGURE 9 Photoconductor current-voltage characterisitics in the dark and in the light.

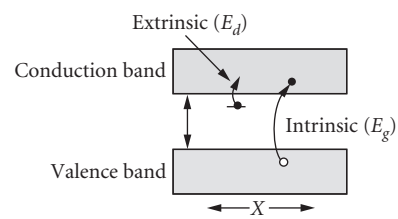

FIGURE 10 Intrinsic detectors excite electrons between the valence and conduction band. Extrinsic detectors excite electrons (or holes) from states within the band to the conduction (valence) band.

Downloaded from Digital Engineering Library @ McGraw-Hill (www.accessengineeringlibrary.com)
Copyright © 2010 The McGraw-Hill Companies. All rights reserved.
Any use is subject to the Terms of Use as given at the website.

where detectors made from direct bandgap materials such as InGaAs, InSb, or HgCdTe have a sharper spectral cutoff than indirect bandgap materials such as silicon and germanium.

Photoconductors can have high quantum efficiency from the visible region out to the far infrared but lack the nearly ideal high amplification of photomultipliers. They are therefore most commonly used in the spectral region beyond 1 μm, where efficient photoemitters are unavailable. Photoconductors do, however, provide current gain which is equal to the recombination time divided by the majority-carrier transit time. This current gain leads to higher responsivity than is possible with (nonavalanching) photovoltaic (PV) detectors. For applications where photovoltaic detection would be amplifier noise limited, the larger photoconductive responsivity makes it possible to realize greater sensitivity with the photoconductor. In general, lower-temperature operation is associated with longer-wavelength sensitivity in order to suppress noise due to thermally induced transitions between close-lying energy levels. Ideally, photoconductors are limited by generation-recombination noise in the photon-generated carriers. Response time can be shorter than 1 μs and in some cases response times can be shorter than 1 ns for small elements. Response across a photoconductive element can be nonuniform due to recombination mechanisms at the electrical contacts, and this effect may vary with electrical bias.

Photovoltaic*

The most widely used photovoltaic detector is the *pn* junction type (Fig. 11), where a strong internal electric field exists across the junction even in the absence of radiation. Photons incident on the junction of this film or bulk material produce free hole-electron pairs which are separated by the internal electric field across the junction, causing a change in voltage across the open-circuit cell or a current to flow in the short-circuited case.

As with the photoconductor, quantum efficiency can be high from the visible to the very long-wavelength infrared, generally about 20 to 25 μm. The limiting noise level can ideally be $\sqrt{2}$ times lower than that of the photoconductor, thanks to the absence of recombination noise. Lower temperatures are associated with longer-wavelength operation. Response times can be less than a nanosecond,

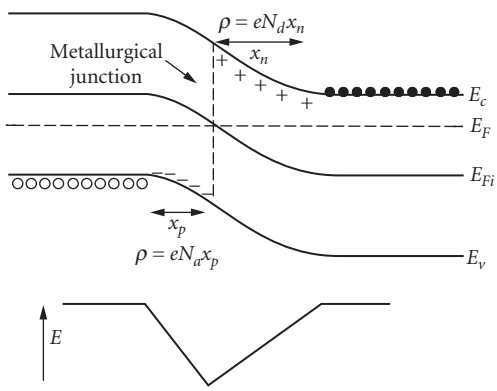

FIGURE 11 *pn* junction showing how the band bends across the junction. The junction width is given by $W = x_p + x_n$.

*The use of a photovoltaic detector at other than zero bias is often referred to as its photoconductive mode of operation because the circuit then is similar to the standard photoconductor circuit. This terminology is confusing with regard to detection mechanism and will not be used here.

Downloaded from Digital Engineering Library @ McGraw-Hill (www.accessengineeringlibrary.com)
Copyright © 2010 The McGraw-Hill Companies. All rights reserved.
Any use is subject to the Terms of Use as given at the website.

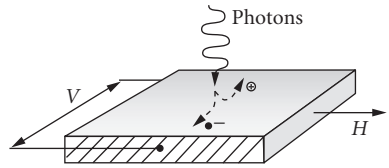

FIGURE 12 Photoelectromagnetic detector configuration—incident photons create electron-hole pairs that diffuse away from the surface. A magnetic field perpendicular to the diffusion separates the charges toward opposite sides, creating a voltage.

and are generally limited by device capacitance and detection-circuit resistance. The *pin* diode has been developed to minimize capacitance for high-bandwidth applications. The advantages of nearly ideal internal amplification have now become available in avalanche photodiodes sensitive out to 1.55 μm. This internal gain is most important for high-frequency operation, where external load resistance must be kept small and would otherwise introduce limiting thermal noise, and for situations involving low signal flux where amplifier noise is otherwise dominant.

Photoelectromagnetic

A thin slab of photoconductive material is oriented with radiation incident on a large face and a magnetic field perpendicular to it, as illustrated in Fig. 12. Electron-hole pairs generated by the incident photons diffuse through the material and are separated by the magnetic field, causing a potential difference at opposite ends of the detector.

These detectors require no cooling or biasing electric field but do require a (permanent) magnetic field. Photoelectromagnetic InSb at room temperature has response up to 7.5 μm, where it is as sensitive as a thermocouple of equal size, and has a response time less than 1 μs. Another competing uncooled detector is InAs, which is far more sensitive out to 3.5 μm. HgCdTe is also available in the photoelectromagnetic (PEM) configuration out to the LWIR spectral region. Cooled infrared detectors are one to two orders of magnitude more sensitive.

Photographic

The receiver is an emulsion containing silver halide crystals. Incident photons are absorbed by the halide ion, which subsequently loses its electron. This electron eventually recombines with a silver ion and reduces it to a neutral silver atom. As more photons are absorbed, this process is repeated until a small but stable cluster of reduced silver atoms is formed within the crystal (latent image). Internal amplification is provided by introduction of an electron donor (photographic) developer, which, using the latent image as a catalytic center, reduces all the remaining silver ions within the exposed crystal to neutral silver atoms. The density of reduced crystals is a measure of the total radiation exposure.

The spectral region of sensitivity for photographic detection coincides rather closely with that of the photoemissive detector. For $\lambda > 1.2$ μm (~1 eV) there is too little energy in each photon to form a stable latent image. The basic detection process for both detectors operates well for higher energy, shorter wavelength radiation. The problem in ultraviolet and x-ray operation is one of eliminating nonessential materials, for example, the emulsion which absorbs these wavelengths.

The photographic process is an integrating one in that the output (emulsion density) measures the cumulative effect of all the radiation incident during the exposure time. The efficiency of the photographic process can be very high, but it depends upon photon energy; for example, in the

Downloaded from Digital Engineering Library @ McGraw-Hill (www.accessengineeringlibrary.com)
Copyright © 2010 The McGraw-Hill Companies. All rights reserved.
Any use is subject to the Terms of Use as given at the website.

PHOTODETECTORS

visible region it takes only 10 to 100 photons to form a stable latent image (developable grain). The photographic process enjoys a large and efficient internal amplification ability (development) wherein the very small energy of the photons' interaction is converted into readily observed macroscopic changes. An extensive discussion of photographic detection is found in Chap. 29, "Photographic Films."

Photoionization

The radiation is absorbed by a gas. If the photon energy exceeds the gas-ionization threshold, ion pairs can be produced with very high efficiency. They are collected by means of an applied voltage. Operating in a dc mode, these detectors are known as ionization and gas-gain chambers. When a pulse mode is used, the detectors are known as proportional and photon (Geiger) counters.

Photoionization detectors have a high sensitivity and a low noise level. They may also be quite selective spectrally since the choice of window and gas independently set upper and lower limits on detectable photon energies. Manufacturers' specifications are not discussed for these detectors as applications are still few enough to be treated as individual cases.[9]

24.4 DEFINITIONS

The following definitions will be used:

Avalanche photodiode (*APD*) A photodiode designed to operate in strong reverse bias where electron and/or hole impact ionization produces multiplication of photogenerated carriers.

Background temperature The effective temperature of all radiation sources viewed by the detector exclusive of the signal source.

Blackbody D star D^*_{BB} (cm $Hz^{1/2}$/W also called "Jones") Similar to $D^*(\lambda)$ or $D^*(T_B f)$ except that the source is a blackbody whose temperature must be specified.

Blackbody detectivity D_{BB} (W^{-1}) A measure of detector sensitivity, defined as DBB $(NEP_{BB})^{-1}$.

Blackbody noise-equivalent power NEP_{BB} Same as spectral NEP, except that the source has blackbody spectral character whose temperature must be specified, for example, NEP (500 K, 1, 800) means 500-K blackbody radiation incident, 1-Hz electrical bandwidth, and 800-Hz chopping frequency.

Blackbody responsivity R_{BB} Same as spectral sensitivity except that the incident signal radiation has a blackbody spectrum (whose temperature must be specified).

Blip detector or blip condition Originally meaning background-limited impurity photoconductor, this term has come to mean performance of any detector where the limiting noise is due to fluctuations in the arrival rate of background photons.

Cutoff wavelength λ_c The wavelength at which the detectivity has degraded to one-half its peak value.

Dark current The output current which flows even when input radiation is absent or negligible. (Note that although this current can be subtracted out for the dc measurements, the shot noise on the dark current can become the limiting noise.)

Detective quantum efficiency The square of the ratio of measured detectivity to the theoretical limit of detectivity.

Detective time constant $\tau_d = 1/2\pi f_d$ where f_d is the frequency at which D^* drops to 0.707 $(1/\sqrt{2})$ times its maximum value. A physics convention defines it as $1/e$, or 0.368 of the maximum value.

Dewar A container (cryostat) for holding detector coolant.

Downloaded from Digital Engineering Library @ McGraw-Hill (www.accessengineeringlibrary.com)
Copyright © 2010 The McGraw-Hill Companies. All rights reserved.
Any use is subject to the Terms of Use as given at the website.

Equivalent noise input (*ENI*) A term meaning nearly the same thing as NEP_{BB} (287 K, 1, f). The difference is that the peak-to-peak value of square-wave chopped input flux is used, rather than the rms value of the sinusoidally chopped input flux. (See recommendation IRE.[2])

Excess noise A term usually referring to noises other than generation-recombination, shot, or thermal.

Extrinsic semiconductor transition Incident photons produce a free electron in the conduction band and bound hole at a donor impurity site or a bound electron at an acceptor impurity site and a free hole in the valence band by excitation of an impurity level.

Field of view (*FOV*) The solid angle from which the detector receives radiation.

Flicker noise See Modulation noise.

Generation noise Noise produced by the statistical fluctuation in the rate of production of photoelectrons.

Generation-recombination (*GR*) *noise* Charge carriers are generated both by (optical) photons and (thermal) phonons. Fluctuations in these generation rates cause noise; fluctuations in carrier-recombination times cause recombination noise. The phonon contribution can be removed by cooling. The remaining photon contribution is indistinguishable from radiation shot noise (photon noise). With photovoltaic *pn* junctions, carriers are swept away before recombination, so that recombination noise is absent.

Guard ring An electrically biased field plate or surrounding diode used in some photodiodes, usually used to control surface recombination effects and thus reduce the leakage current in the detection circuit.

Intrinsic semiconductor transition Incident photons produce a free electron-free hole pair by direct excitation across the forbidden energy gap (valence to conduction band).

Johnson noise Same as Thermal noise.

Jones Unit of measure for D^* cm $Hz^{1/2}/W$.

Maximized D star, $D^*(\lambda_{pk} f_o)$, cm $Hz^{1/2}/W$ *or Jones* The value of $D^*(\lambda_{pk} f)$ corresponding to wavelength λ_{pk} and chopping frequency of maximum D^*.

Modulation (*or 1/f*) *noise* A consensus regarding the origin(s) of the mechanism has not been established, and although a quantum theory has been proposed, other mechanisms may dominate. As its name implies, it is characterized by a $1/f^n$ noise power spectrum, where $0.8 < n < 2$. This type of noise is prominent in thermal detectors and may dominate the low-frequency noise characteristics of photoconductive and photovoltaic quantum detectors as well as other electronic devices such as transistors and resistors.

Multiplier phototube or multiplier photodiode Phototube with built-in amplification via secondary emission from electrically biased dynodes.

NEI photons/(cm^2 sec) noise equivalent irradiance is the signal flux level at which the signal produces the same output as the noise present in the detector. This unit is useful because it directly gives the photon flux above which the detector will be photon noise limited. See also Spectral noise equivalent power (NEP).

Noise spectrum The electrical power spectral density of the noise.

Nyquist noise Same as Thermal noise.

Photo cell See Photodiode.

Photoconductive gain The ratio of carrier lifetime divided by carrier transit time in a biased photoconductor.

Photodiode The term photodiode has been applied both to vacuum- or gas-filled photoemissive detectors (diode phototubes, or photo cells) and to photovoltaic detectors (semiconductor *pn* junction devices).

Photomultiplier Same as Multiplier phototube.

Downloaded from Digital Engineering Library @ McGraw-Hill (www.accessengineeringlibrary.com)
Copyright © 2010 The McGraw-Hill Companies. All rights reserved.
Any use is subject to the Terms of Use as given at the website.

Photon counting Digital counting of individual photons from the photoelectrons produced in the detector in contrast to averaging of the photocurrent. This technique leads to very great sensitivity but can be used only for quite low light levels.

Quantum efficiency The ratio of the number of countable output events to the number of incident photons, for example, photoelectrons per photon, usually referred to as a percentage value.

RMS noise $V_{n,\text{rms}}$ That component of the electrical output which is not coherent with the radiation signal (generally measured with the signal radiation removed).

RMS signal $V_{s,\text{rms}}$ That component of the electrical output which is coherent with the input signal radiation.

Response time τ Same as Time constant.

Responsive quantum efficiency See Quantum efficiency.

Sensitivity Degree to which detector can sense small amounts of radiation.

Shot noise This current fluctuation results from the random arrival of charge carriers, as in a photodiode. Its magnitude is set by the size of the unit charge.

$$i_{n,\text{rms}} = (2ei_{\text{dc}}\Delta f)^{1/2}$$

Spectral D-double-star $D^{**}(\lambda, f)$ A normalization of D^* to account for detector field of view. It is used only when the detector is background-noise-limited. If the FOV is 2π sr, $D^{**} = D^*$.

Spectral D-star $D^*(\lambda, f)$ (*cm* $Hz^{1/2}/W$ or *Jones*) A normalization of spectral detectivity to take into account the area and electrical bandwidth dependence, for example, D^*(1 μm, 800 Hz) means D^* at $\lambda = 1$ μm and chopping frequency 800 Hz; unit area and electrical bandwidth are implied. For background-noise-limited detectors the FOV and the background characteristics must be specified. For many types of detectors this normalization is not valid, so that care should be exercised in using D^*.

Spectral detectivity $D(\lambda)$ (W^{-1}) A measure of detector sensitivity, defined as $D(\lambda) = (\text{NEP}_\lambda)^{-1}$. As with NEP, the chopping frequency electrical bandwidth, sensitive area, and, sometimes, background characteristics should be specified.

Spectral noise equivalent power NEP_λ The rms value of sinusoidally modulated monochromatic radiant power incident upon a detector which gives rise to an rms signal voltage equal to the rms noise voltage from the detector in a 1-Hz bandwidth. The chopping frequency, electrical bandwidth, detector area, and, sometimes, the background for characteristics should be specified. NEP (1 μm, 800 Hz) means noise equivalent power at 1-μm wavelength, 1-Hz electrical bandwidth, and 800-Hz chopping rate. Specification of electrical bandwidth is often simplified by expressing NEP in units of $W/Hz^{1/2}$.

Spectral responsivity $R(\lambda)$ The ratio between rms signal output (voltage or current) and the rms value of the monochromatic incident signal power or photon flux. This is usually determined by taking the ratio between a sample detector and a thermocouple detector. The results are given as relative response/watt or relative response/photon, respectively.

Temperature noise Fluctuations in the temperature of the sensitive element, due either to radiative exchange with the background or conductive exchange with a heat sink, produce a fluctuation in signal voltage. For thermal detectors, if the temperature noise is due to the former, the detector is said to be at its theoretical limit. For thermal detectors:

$$\overline{(\Delta T)^2} = \frac{4kT^2G\Delta f}{K^2 + 4\pi^2 f^2 C^2}$$

where $\overline{(\Delta T)^2}$ = mean square temperature fluctuations
K = thermal conductance
C = heat capacity

Downloaded from Digital Engineering Library @ McGraw-Hill (www.accessengineeringlibrary.com)
Copyright © 2010 The McGraw-Hill Companies. All rights reserved.
Any use is subject to the Terms of Use as given at the website.

Thermal noise (*also known as Johnson or Nyquist noise*) Noise due to the random motion of charge carriers in a resistive element:

$$V_{n,\text{rms}} = (4kTR\Delta f)^{1/2} \qquad k = \text{Boltzmann's constant}$$

Thermopile A number of thermocouples mounted in series in such a way that their thermojunctions lie adjacent to one another in the plane of irradiation.

Time constant τ (see also *detective time constant*) A measure of the detector's speed of response. $\tau = 1/(2\pi f_c)$, where f_c is that chopping frequency at which the responsivity has fallen to 0.707 $(1/\sqrt{2})$ times its maximum value. Sometimes a physics convention defines it as 1/e, or 0.368 of the maximum value:

$$R(f) = \frac{R_0}{(1+4\pi^2 f^2 \tau^2)^{1/2}}$$

24.5 DETECTOR PERFORMANCE AND SENSITIVITY

*D**

A figure of merit defined by Jones in 1958 is used to compare the sensitivity of detectors.[10] It is called D^*. Although the units of measure are cm $\text{Hz}^{1/2}/\text{W}$, this unit is now referred to as a *Jones*. D^* is the signal-to-noise (S/N) ratio of a detector measured under specified test conditions, referenced to a 1-Hz bandwidth and normalized by the square root of the detector area (A) in square centimeters. Specified test conditions usually consist of the blackbody signal source temperature, often 500 K for infrared detectors, and the signal chopping frequency. If the background temperature is other than room temperature (295 or 300 K in round numbers), then that should be noted.

By normalizing the measured S/N ratio by the square root of the detector area, the D^* figure of merit recognizes that the statistical fluctuations of the background photon flux incident on the detector (photon noise) are dependent upon the square root of the number of photons and thus increase as the square root of the detector area, while the signal will increase in proportion to the detector area itself. This figure of merit therefore provides a valid comparison of detector types that may have been made and tested in different sizes.

The ultimate limit in S/N ratio for any radiation power detector is set by the statistical fluctuation in photon arrival times. For ideal detectors which are photon-noise-limited, and where only generation noise is present, we shall discuss limiting detectivity for three cases:

1. Photon detector where arrival rate of signal photons far exceeds that of background photons (all other noise being negligible)
2. Photon detector where background photon arrival rate exceeds signal photon rate (all other noise being negligible)
3. Thermal detector, background limited

The rate of signal-carrier generation is

$$n = \eta \text{AN}_s \tag{1}$$

where η = detector quantum efficiency and AN_s = average rate of arrival of signal photons.

It can be shown[11] that in a bandwidth Δf, the rms fluctuation in carrier-generation rate is

$$\delta n_{\text{rms}} = (2P_N \Delta f)^{1/2} \tag{2}$$

Downloaded from Digital Engineering Library @ McGraw-Hill (www.accessengineeringlibrary.com)
Copyright © 2010 The McGraw-Hill Companies. All rights reserved.
Any use is subject to the Terms of Use as given at the website.

where P_N is the frequency dependence of the mean square fluctuations in the rate of carrier generation, that is,

$$P_N = A\int_0^\infty \eta(\nu)(\Delta N)^2 d\nu \tag{3}$$

where $(\Delta N)^2$ is the mean square deviation in the total rate of photon arrivals per unit area and frequency interval including signal and background photons. For thermally produced photons of frequency ν (see Ref. 12).

$$(\Delta N)^2 = \overline{N}\frac{e^{h\nu/kT}}{e^{h\nu/kT}-1} = \frac{2\pi\nu^2}{c^2}\frac{e^{h\nu/kT}}{(e^{h\nu/kT}-1)^2} \tag{4}$$

where $\overline{N}$ is the average rate of photon arrivals per unit area and frequency interval. Then, for the special case of $h\nu >> kT$

$$\delta n_{\text{rms}} = (2A\eta\overline{N}\Delta f)^{1/2} \tag{5}$$

This is also the case for a laser well above threshold. Here the photon statistics become Poisson, and $(\Delta N)^2 = \overline{N}$ even when $h\nu$ is not greater than kT.

Photon Detector, Strong-Signal Case This is generally a good approximation for visible and higher photon energy detectors since the background radiation is often weak or negligible. When signal photons arrive at a much faster rate than background photons

$$\delta n_{\text{rms}} = (2A\eta\overline{N}_s\Delta f)^{1/2} \tag{6}$$

then

$$\text{NEP} = \frac{N_s A h\nu}{n/\delta n_{\text{rms}}(\Delta f)^{1/2}} = \left(\frac{2N_s A}{\eta}\right)^{1/2} h\nu \tag{7}$$

or the noise-equivalent quantum rate is

$$\text{NEQ} = \left(\frac{2\times \text{incident photon rate}}{\text{quantum efficiency}}\right)^{1/2} \tag{8}$$

Photon Detector, Background-Limited Case This is usually a good approximation for detecting low signal levels in the infrared where background flux levels exceed signal flux levels in many applications. When the background photon noise rate N_B exceeds the signal photon rate ($N_B >> N_S$)

$$\delta n_{\text{rms}} \approx (2A\eta\overline{N}_B\Delta f)^{1/2} \tag{9}$$

the noise-equivalent power is

$$\text{NEP} = \frac{N_s A h\nu}{(n/\delta n_{\text{rms}})(\Delta f)^{1/2}} = \left(\frac{2N_B A}{\eta}\right)^{1/2} h\nu \tag{10}$$

The noise-equivalent quantum rate is

$$\text{NEQ} = \left(\frac{2\times \text{incident background photon rate}}{\text{quantum efficiency}}\right)^{1/2} \tag{11}$$

Downloaded from Digital Engineering Library @ McGraw-Hill (www.accessengineeringlibrary.com)
Copyright © 2010 The McGraw-Hill Companies. All rights reserved.
Any use is subject to the Terms of Use as given at the website.

or

$$D^* = \frac{A^{1/2}}{\text{NEP}} = \left(\frac{\eta}{2N_B}\right)^{1/2} \frac{1}{h\nu} \tag{12}$$

or

$$\text{Area-normalized quantum detectivity} = \frac{A^{1/2}}{\text{NEQ}} = \left(\frac{\eta}{2\bar{N}_B}\right)^{1/2} \tag{13}$$

For the general case of a detector with area A seeing 2π sr of blackbody background at temperature T, $(\Delta N)^2$ is that in Eq. (4)

$$\overline{(\delta n)^2} = 2A\Delta f \int_0^\infty \eta(\nu)(\Delta N)^2 d\nu = 4\pi A\Delta f \int_0^\infty \eta(\nu)\nu^2 \frac{e^{h\nu/KT}}{(e^{h\nu/kT}-1)^2} d\nu \tag{14}$$

Then for $\Delta f = 1$ Hz,

$$\text{NEP} = \frac{h\nu}{c\eta}\left[4\pi A\int_0^\infty \eta(\nu)\frac{\nu^2 e^{h\nu/kT}}{(e^{h\nu/kT}-1)} d\nu\right]^{1/2} \tag{15}$$

or

$$D^*(T,\lambda) = \frac{c\eta}{2\pi^{1/2}h\nu}\left[\int_0^\infty \eta(\nu)\nu^2 \frac{e^{h\nu/kT}}{(e^{h\nu/kT}-1)^2} - d\nu\right]^{-1/2} \tag{16}$$

Assuming $\eta(\nu)$ is independent of frequency but falls back to zero for $\nu < \nu_c$

$$D^*(T,\lambda) = \frac{c\eta^{1/2}}{2\pi^{1/2}h\nu}\left[\int_0^\infty \nu^2 \frac{e^{h\nu/kT}}{(e^{h\nu/kT}-1)^2} - d\nu\right]^{-1/2} \tag{17}$$

Figure 13 shows photon-noise-limited D^* versus cutoff wavelength λ_c for various thermal-background temperatures.[13] Note that these curves are not independent. $D^*(T, \lambda_c)$ is related to $D^*(T, \lambda'_c)$ by the formula

$$D^*(T,\lambda_c) = \left(\frac{T'}{T}\right)^{5/2} D^*(T,\lambda'_c) \qquad \text{where } \lambda'_c = \frac{T}{T'}\lambda_c \tag{18}$$

This relation is useful for determining values of $D^*(T, \lambda_c)$, which do not appear in Fig. 13, in terms of a value of $D^*(T', \lambda'_c)$, which does appear. For example, to find D^*(1000 K, 4 μm) from the 500-K curve

$$D^*(1000,4) = \left(\frac{500}{1000}\right)^{5/2} D^*\left(500, 4\times\frac{1000}{500}\right) = 2.3\times10^9 \text{ Jones} \tag{19}$$

If higher accuracy is desired than can be determined from Fig. 13, one can use the preceding formula in combination with Table 1, which gives explicit values of $D^*(\lambda_c)$ versus λ_c for $T = 295$ K.

The effect on D^* of using a narrow bandwidth detection system is illustrated in Fig. 14. Such a system may be configured with a cold narrow bandwidth filter, or with a narrow bandwidth amplifier—in order to limit the background flux noise or the electrical bandwidth noise, respectively. Q refers to the factor of the reduction provided.

Downloaded from Digital Engineering Library @ McGraw-Hill (www.accessengineeringlibrary.com)
Copyright © 2010 The McGraw-Hill Companies. All rights reserved.
Any use is subject to the Terms of Use as given at the website.

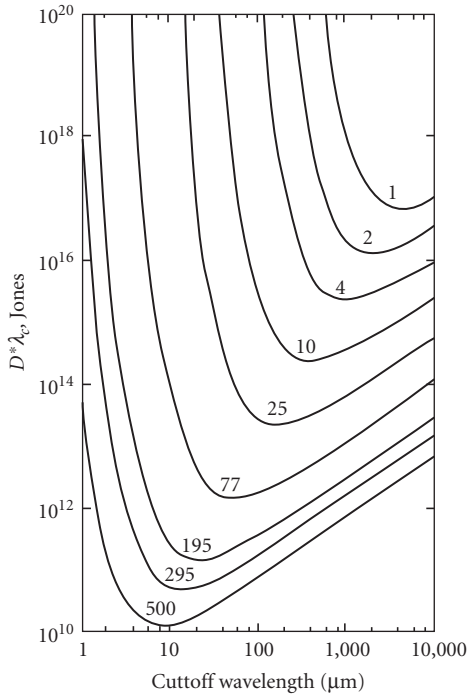

FIGURE 13 Photon-noise-limited D^* at peak wavelength—assumed to be cut-off wavelength—for background temperatures 1, 2, 4, 10, 25, 77, 195, 295, and 500 K (assumes 2π FOV and $\eta = 1$). (*Reprinted from Ref. 13.*)

TABLE 1 D^* versus λ_c for $T = 295$ K

λ_c, μm	$D^*(\lambda_c)$	λ_c, μm	$D^*(\lambda_c)$	λ_c, μm	$D^*(\lambda_c)$	λ_c, μm	$D^*(\lambda_c)$
1	2.19×10^{13}	10	5.35×10^{10}	100	1.67×10^{11}	1000	1.55×10^{12}
2	4.34×10^{13}	20	5.12×10^{10}	200	3.20×10^{11}	2000	3.10×10^{12}
3	1.64×10^{12}	30	6.29×10^{10}	300	4.74×10^{11}	3000	4.64×10^{12}
4	3.75×10^{11}	40	7.68×10^{10}	400	6.28×10^{11}	4000	6.19×10^{12}
5	1.70×10^{11}	50	9.13×10^{10}	500	7.82×10^{11}	5000	7.73×10^{12}
6	1.06×10^{11}	60	1.06×10^{11}	600	9.36×10^{11}	6000	9.28×10^{12}
7	7.93×10^{10}	70	1.21×10^{11}	700	1.09×10^{12}	7000	1.08×10^{13}
8	6.57×10^{10}	80	1.36×10^{11}	800	1.24×10^{12}	8000	1.24×10^{13}
9	5.80×10^{10}	90	1.52×10^{11}	900	1.40×10^{12}	9000	1.39×10^{13}

Downloaded from Digital Engineering Library @ McGraw-Hill (www.accessengineeringlibrary.com)
Copyright © 2010 The McGraw-Hill Companies. All rights reserved.
Any use is subject to the Terms of Use as given at the website.

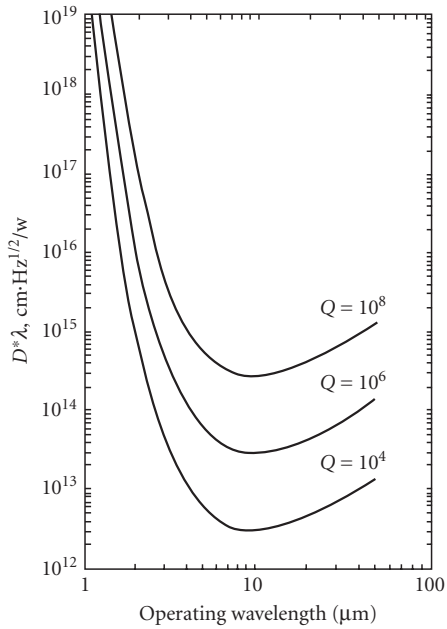

FIGURE 14 Photon noise limit of a narrow-band quantum counter as a function of operating wavelength for a 290-K background, 2π FOV, and $\eta = 1$. (*From Ref. 14.*)

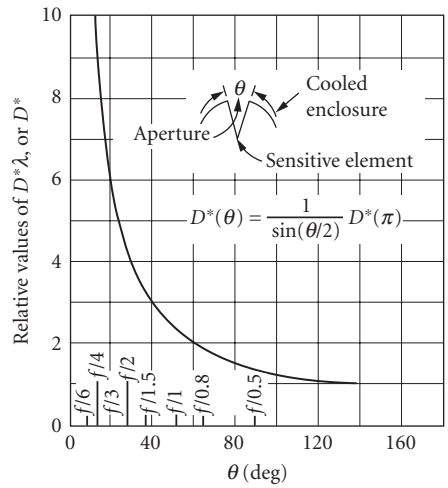

FIGURE 15 Relative increase in photon-noise-limited $D^*(\lambda_{pk})$ or D^* achieved by using a cooled aperture in front of lambertian detector. (*From Ref. 14.*)

Figure 15 shows the relative increase in photon-noise-limited D^* achievable by limiting the FOV through use of a cooled aperture.

The photon-noise-limited sensitivity shown in Fig. 13 and Table 1 apply to photovoltaic and photoemissive detectors. Figure 14 is for photoconductors. For photoconductors, recombination noise results in a $\sqrt{2}$ reduction in D^* at all wavelengths.

Thermal Detectors Limiting sensitivity of an ideal thermal detector has been discussed previously.[12,14,15] Assuming no shortwave- or long-wavelength cutoffs exist,

$$D^* = \frac{\varepsilon}{[8\varepsilon\sigma k(T_1^5 + T_2^5)]^{1/2}} = \frac{4\times10^{16}\,\varepsilon^{1/2}}{(T_1^5 \times T_2^5)^{1/2}} \text{ Jones} \tag{20}$$

where T_1 = detector temperature
T_2 = background temperature
ε = detector emissivity
σ = Stefan-Boltzmann constant
k = Boltzmann constant

D^* versus T_2 is plotted for various T_1 in Fig. 16. Figure 17 shows the effect of both short- and long-wavelength cutoffs on bolometer sensitivity,[16] with the ideal photoconductor curve for reference. D^* can be seen to increase rapidly when the cutoff is set to avoid the high flux density from the 300-K background that peaks around 10 μm.

Downloaded from Digital Engineering Library @ McGraw-Hill (www.accessengineeringlibrary.com)
Copyright © 2010 The McGraw-Hill Companies. All rights reserved.
Any use is subject to the Terms of Use as given at the website.

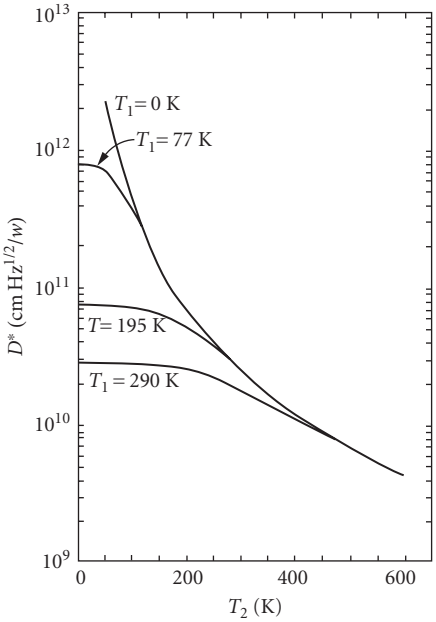

FIGURE 16 Photon-noise-limited D^* for thermal detectors as a function of detector temperature T_1 and background temperature T_2 (2π FOV: $\eta = 1$). (*From Ref. 14.*)

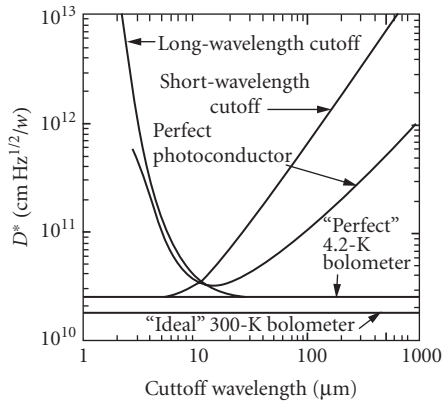

FIGURE 17 The detectivity of a "perfect" bolometer plotted as a function of both short- and long-wavelength cutoffs. Plots for a perfect photoconductor and two other cases are included for comparison. The background temperature is 300 K. (*From Ref. 16.*)

24.6 OTHER PERFORMANCE PARAMETERS

Spectral Response

Spectral response provides key information regarding how the detector will respond as a function of wavelength or photon energy. Spectral response may be limited by the intrinsic detector material properties, a coating on the detector, or by a window through which the radiation must pass. Relative response is the spectral response ratioed against a detector with a nominally wavelength independent response, such as a thermocouple having a spectrally-broad black coating. Relative response is plotted as a function of wavelength with either a vertical scale of W^{-1} or photon^{-1}. Thermal detectors tend to be spectrally flat in the first case while quantum detectors are generally flat in the second case. The curves are typically shown with the peak value of the spectral response normalized to a value of 1. The spectral response curve can be used together with the blackbody D^* to calculate D^* as a function of wavelength, which is shown in Fig. 18 for selected detectors.

Responsivity and Quantum Efficiency

Responsivity and quantum efficiency are important figures of merit relating to the detector signal output. Responsivity is a measure of the transfer function between the input signal photon power or flux and the detector electrical signal output. Thermal detectors will typically give this responsivity in volts/watt. Photoconductors will usually quote the same units, but will also frequently reference the value to the peak value of relative response per watt from the spectral response curve. This value

Downloaded from Digital Engineering Library @ McGraw-Hill (www.accessengineeringlibrary.com)
Copyright © 2010 The McGraw-Hill Companies. All rights reserved.
Any use is subject to the Terms of Use as given at the website.

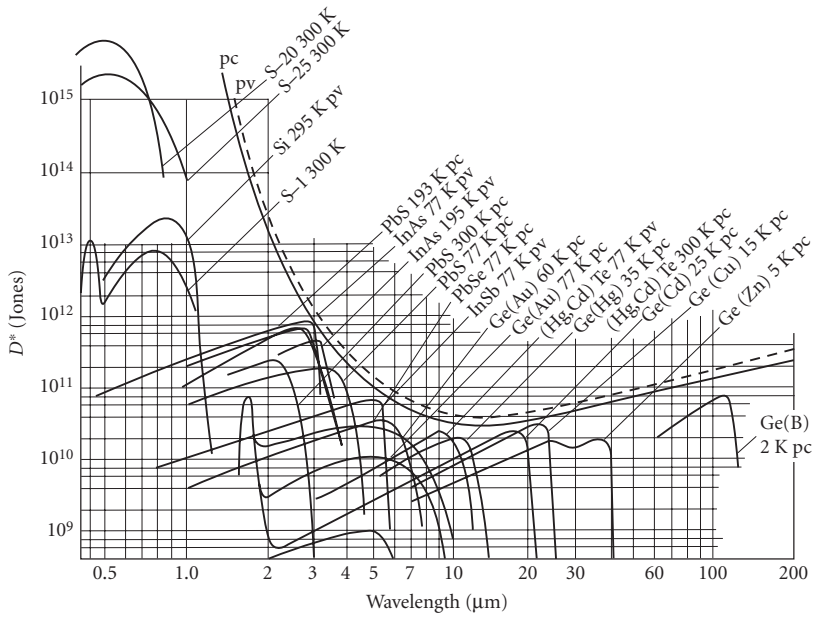

FIGURE 18 D^* versus λ for selected detectors.

is actually realized if the detector bias circuit load resistor is significantly larger than the detector resistance. Photoconductor responsivity is given by:

$$\text{Responsivity}_{\text{peak}} = \frac{\eta \mathbf{q} \mathbf{R}_d \mathbf{E} \tau (\mu_n + \mu_p)}{h\nu \ell} \tag{21}$$

where η is the quantum efficiency, $\mathbf{q}$ is the electronic charge, $\mathbf{R}_d$ is the detector resistance, $\mathbf{E}$ is the electric field, τ is time constant, μ are the mobilities for electrons (n) and holes (p), $h\nu$ is the photon energy, and ℓ is the device length. Photomultiplier tubes and photovoltaic detectors will usually reference the responsivity in amperes per watt, again referenced to peak spectral response.

Detector response performance is also conveyed from the detector quantum efficiency. In the case of photovoltaic detectors which, in the absence of avalanche operation have a gain of unity, quantum efficiency is essentially the current per photon. For a blip photovoltaic detector, the quantum efficiency also determines the D^*. Quantum efficiency is not readily measured for photoconductors and photomultiplier tubes unless the internal gain is carefully calibrated. It is sometimes inferred from the measured D^* for photoconductive devices which are blip—see definition of detective quantum efficiency.

Noise, Impedance, Dark and Leakage Current

Noise has a number of potential origins. Background photon flux–limited detectors have noise dominated by the square root of the number of background photons striking the detector per second [see Eq. (9)]. Other noise sources may contribute or dominate. Among these are

- Johnson, Nyquist, or thermal noise which is defined by the detector temperature and impedance
- Modulation or $1/f$ noise which may dominate at lower frequencies
- Amplifier noise
- Shot noise from dark or leakage current

Downloaded from Digital Engineering Library @ McGraw-Hill (www.accessengineeringlibrary.com)
Copyright © 2010 The McGraw-Hill Companies. All rights reserved.
Any use is subject to the Terms of Use as given at the website.

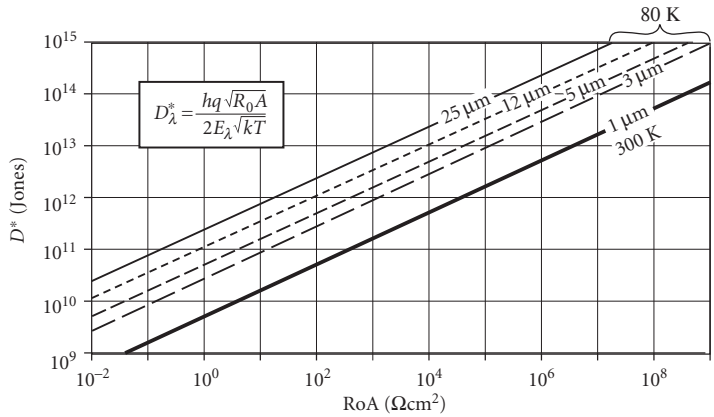

FIGURE 19 Zero-bias impedance-area product (R_0A or shunt resistance per unit area) of a photodiode can limit the D^* as shown. The limiting D^* depends on R_0A, temperature, and photon energy or wavelength. Examples are illustrated for a 1-μm cutoff diode at 300 K, and for 3-, 5-, 12-, and 25-μm cutoff devices at 80 K. Other noise mechanisms, such as photon noise, typically limit D^* to lower values than the highest values shown here.

The impedance of a photodiode may limit performance, depending upon the detector operating conditions. Figure 19 illustrates the diode impedance per unit area (R_0A) limiting value of D^* for silicon detectors at room temperature and longer-wavelength infrared photodiodes at 80 K.

Measurement of the noise as a function of frequency can be valuable for characterizing the relevant noise sources. Selection of an appropriate preamplifier is also critical, particularly for detectors having very low or very high impedance. Integration of preamplifiers together with detectors has significantly improved the overall performance of many detectors. The use of phase-sensitive lock-in amplifiers in combination with a modulated signal can also improve the signal-to-noise ratio.

Uniformity

One cannot assume that the response of a detector will be uniform across its sensitive area. Material inhomogeneity and defects and/or fabrication variables can give rise to nonuniformity. Lateral collection from near the perimeter of a photodiode may give a gradual response decrease away from the edge—this effect will typically be accompanied by a change in response speed as well. Recombination at the electrical contacts to a photoconductor can limit the lifetime, and hence the photoconductive gain, for carriers generated near the contact, a phenomenon called sweep-out. Recombination may be enhanced at surfaces and edges also. Laser spot scanning is useful to check the detector spatial uniformity, although laser sources may not be readily available at all the wavelengths of interest. An alternative method is to move the detector around under a fixed small aperture in conjunction with a light source.

Speed

Detector response speed is often related inversely to detector sensitivity. Thermal detectors often show this characteristic because the signal is proportional to the inverse of response speed, while the noise is amplifier or Johnson limited. Excluding detectors with internal carrier multiplication mechanisms, the best detectors from broad experience seem limited to a D^*f^* product of a few times 10^{17} Jones Hz. D^*f^* may be proportionally higher for devices with gain, since speed can be increased to a greater extent by using a lower value of load resistance without becoming Johnson-noise-limited. The user should be aware that with many detectors it is possible to operate them in a circuit to maximize

Downloaded from Digital Engineering Library @ McGraw-Hill (www.accessengineeringlibrary.com)
Copyright © 2010 The McGraw-Hill Companies. All rights reserved.
Any use is subject to the Terms of Use as given at the website.

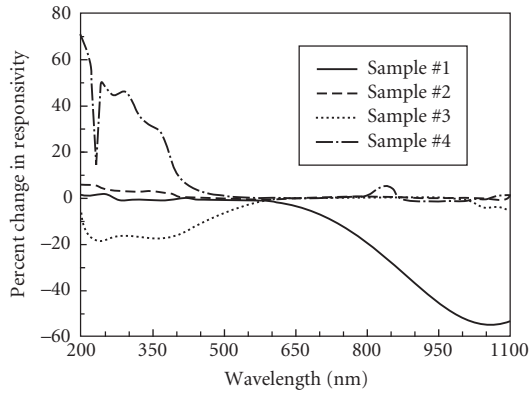

FIGURE 20 After only 3 hours of UV irradiation, these silicon detectors showed great variations in responsivity. (*Reprinted from the September 1993 issue of Photonics Spectra, © Laurin Publishing Co., Inc.*)

sensitivity or speed, but not both at the same time. Speed may vary across the sensitive area of the detector and with temperature, wavelength, and electrical bias.

Stability

Detector performance may change or drift with time. Changes in operating temperature, humidity, and exposure to elevated temperatures as well as to visible, ultraviolet, and high-energy radiation can affect device operation. These effects arise from the temperature dependence of electronic properties in solids, as well as from the critical role played by electrical charge conditions near the surface of many device types. Sensitivity changes in a sample of silicon detectors from four vendors illustrate this point. Wide variations in responsivity change after UV exposure, as shown in Fig. 20. In applications where stability is of significant concern, these effects must be carefully reviewed along with the detector supplier's experience in these matters.

24.7 DETECTOR PERFORMANCE

Manufacturers' Specifications

Table 2 lists the detector materials covered in Sec. 24.7.

TABLE 2 Detector Materials Covered in Sec. 24.7

Thermocouple	GaAsP	Ge:Au
Thermopile	CdS, CdSe	HgCdTe
Thermistor bolometer	CdTe	PbSnTe
Pyroelectric	GaAs	Ge:Hg
InSb hot electron bolometer	Si	Si:Ga
Ge:Ga bolometer	InGaAs	Si:B
Photoemissive	Ge	Ge:Cu
GaN, InGaN	PbS	Ge:Zn
SiC	InAs	Ge:Ga
TiO_2	PbSe	Photographic
GaP	InSb	

Downloaded from Digital Engineering Library @ McGraw-Hill (www.accessengineeringlibrary.com)
Copyright © 2010 The McGraw-Hill Companies. All rights reserved.
Any use is subject to the Terms of Use as given at the website.

Detector sensitivity can be the determining factor in the design and performance of a sensor system. Detector performance is subject to the development of improved materials, fabrication techniques, and the ingenuity of device engineers and inventors. The descriptions given here may improve with time, and consultation with manufacturers and users is recommended. Today, the internet can be the quickest and most up-to-date source of currently available manufacturers and specifications for the devices they offer. Many suppliers noted in this section may have gone out of business—a search on the internet is the best choice for finding active vendors. Other than a general Web search, some collections of device suppliers can be found at

http://www.photonics.com/bgHome.aspx

http://laserfocusworld.365media.com/laserfocusworld/search.asp

http://www.physicstoday.org/ptbg/search.jsp

Thermocouple The thermocouple offers broad uniform spectral response, a high degree of stability, and moderate sensitivity. Its slow response and relative fragility have limited its use to laboratory instruments, such as spectrometers.

Compared with thermistors, thermocouples are slower, require no bias, and have higher stability but much lower impedance and responsivity. This increases the amplification required for the thermocouple; however, the only voltage appearing is the signal voltage, so that the serious thermistor problem of bridge-circuit bias fluctuations is avoided. With proper design, performance should not be amplifier-limited but limited instead by the Johnson noise of the thermocouple. Thermocouples perform stably in dc operation, although the instability of dc amplifiers usually favors ac operation.

The inherent dc stability of thermocouples is attractive for applications requiring no moving parts, and recently a relatively rugged solid-backed evaporated thermocouple has been developed whose sensitivity approaches that of the thermistor bolometer.

Sensitivity: D^* 1×10^9 Jones for 20-ms response time; spectral response depends on black coating (usually gold black) (see Fig. 21)

Noise: White Johnson noise, falling off with responsivity (see Fig. 22)

Resistance: 5 to 15 Ω typical

Responsivity: 5 V/W (typical), 20 to 25 V/W (selected)

Time constant: 10 to 20 ms (typical)

Operating temperature: Normally ambient

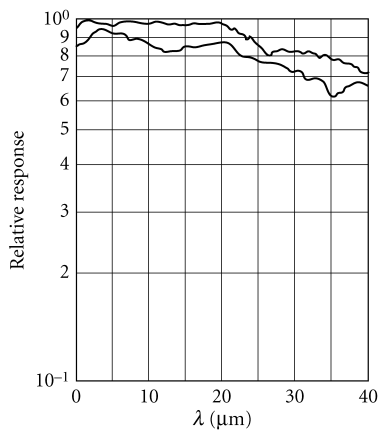

FIGURE 21 Typical thermocouple spectral response curves (CsI window) for two different manufactures.

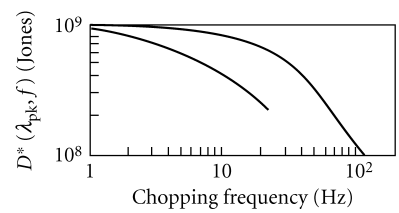

FIGURE 22 Typical thermocouple D^* (noise) frequency response for two manufacturers. (*From Ref. 1.*)

Downloaded from Digital Engineering Library @ McGraw-Hill (www.accessengineeringlibrary.com)
Copyright © 2010 The McGraw-Hill Companies. All rights reserved.
Any use is subject to the Terms of Use as given at the website.

Sensitive area: 0.1 × 1 to 0.3 × 3 or 0.6 × 2 mm (typical)

Linearity: 0.1 percent in region investigated (6×10^{10} to 6×10^{8} W incident)

Recommended circuit: Transformer coupled into low-noise (bipolar or JFET) amplifier with good low-frequency noise characteristics

Manufacturers: Perkin-Elmer, Charles Reeder, Beckman Instruments, Farrand, Eppley Laboratory

Thermopile Thermopiles are made by evaporating an array of metal junctions, such as chromel-constantan or manganin-constantan, onto a substrate. The thin-film construction is rugged, but the Coblentz-type may be quite delicate. Wire-wound thermopile arrays are also available which are very robust. Devices with arrays of semiconductor silicon junctions are also available. The array may typically be round, square, or rectangular (for matching a spectrometer slit) and consist of 10 to 100 junctions. Configuration options include matched pairs of junction arrays or compensated arrays to provide an unilluminated reference element. A black coating, such as 3M black or lampblack, is used to provide high absorption over a broad spectral range, as illustrated in Figs. 23 and 24. The housing window may limit the spectral range of sensitivity. Typical applications include power meters and radiometers.

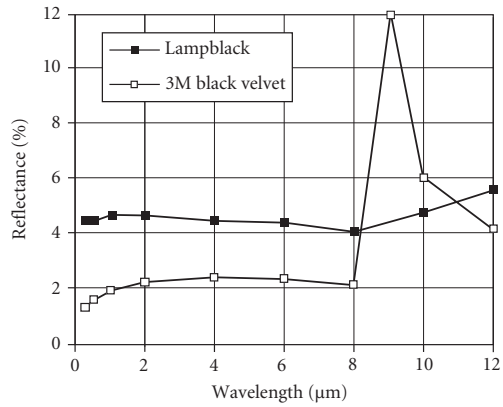

FIGURE 23 Spectral reflectance of two black coatings used in the construction of thermopile detectors. (*From Eppley Laboratory studies.*)

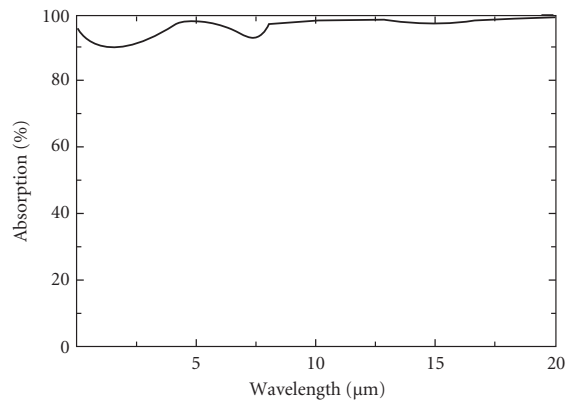

FIGURE 24 Spectral absorption of a thermopile detector coating made from a black metal oxide. (*Oriel Corporation.*)

Downloaded from Digital Engineering Library @ McGraw-Hill (www.accessengineeringlibrary.com)
Copyright © 2010 The McGraw-Hill Companies. All rights reserved.
Any use is subject to the Terms of Use as given at the website.

Sensitivity: D^* 0.5 to 4×10^8 Jones for 30-ms typical response time. D^* may be dependent upon sensitive area; spectral response depends on black coating and window (see Fig. 23 and Fig. 24)

Noise: White Johnson noise, falling off with responsivity, typical range is 5 to 30 $nV/Hz^{1/2}$

Resistance: 2Ω to 60 kΩ typical

Responsivity: 4 to 250 V/W (typical) depends on the number of junctions and time constant

Time constant: 10 ms to 2 s (typical)

Operating temperature: Normally ambient

Sensitive area: 0.5 to 6-mm diameter, 0.025×0.025 to 3×3 mm, various rectangular, 0.4×3, 0.6×2, 0.6×4 mm (typical)

Recommended circuit: Low noise (0.5 $V_{p\text{-}p}$, dc to 1 Hz), low drift with voltage gain of 1000 and input impedance of 1 MΩ

Manufacturers: Armtech, Beckman Instruments, Concept Engineering, Dexter Re search Center, Edinburgh Instruments, Eppley Laboratory, Farrand, Gentech, Molectron Detector, Ophir Optronics, Oriel, Scientech, Scitec, Swan Associates

Thermistor Bolometer Thermistors offer reliability, moderate sensitivity, and broad spectral coverage without cooling. Construction is rugged and highly resistant to vibration, shock, and other extreme environments. Response is slower than 1 ms, and trade-off exists between speed and sensitivity.

Thermistor elements are made of polycrystalline Mn, Ni, and Co oxides. In their final form they are semiconductor flakes 10 μm thick, which undergo a temperature resistance change of ~4 percent per Kelvin. Since thermistor resistance changes with ambient temperature enough to alter the biasing significantly, it is usually operated in a bridge circuit, with a nearly identical thermistor shielded from signal radiation and used for a balance resistor.

Sensitivity:

$$\text{NEP} = 8.9 \times 10^{-10} \sqrt{\frac{A(\text{mm}^2)}{\tau_{\text{rms}}}} \text{ W}$$

$$D^* = 1.1 \times 10^9 \sqrt{\tau_{\text{rms}}} \text{ Jones}$$

Spectral response: Depends on coating (usually Zapon lacquer); see Fig. 25.

Quantum efficiency: Depends on blackening coating, typically 80 percent.

Noise: Thermal-noise-limited above 20 Hz ($V_{\text{noise}} = \sqrt{4kTR\Delta f}$); below that, $1/f$ type noise—see Fig. 26. Used in balanced-bridge circuit (two flakes in parallel); limiting noise due to thermal noise in both flakes.

Resistance: For standard 10-μm-thick flakes, two different resistivities are available: 2.5 MΩ/sq or 250 kΩ/sq. Note that in a bolometer bridge, the resistance between the output connection and ground is half that of single flake.

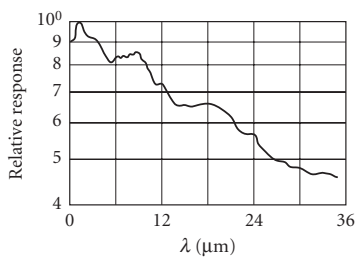

FIGURE 25 Typical thermistor spectral response (no window).

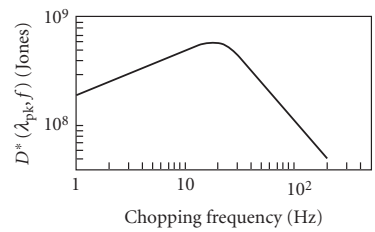

FIGURE 26 Typical thermistor D^* (noise) frequency spectrum. (*From Ref. 1.*)

Downloaded from Digital Engineering Library @ McGraw-Hill (www.accessengineeringlibrary.com)
Copyright © 2010 The McGraw-Hill Companies. All rights reserved.
Any use is subject to the Terms of Use as given at the website.

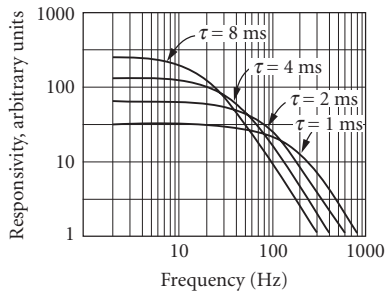

FIGURE 27 Relative response vs. frequency for various time-constant thermistor detectors ($A = 1 \times 1$ mm). (*From Barnes Engineering, Bull. 2–100.*)

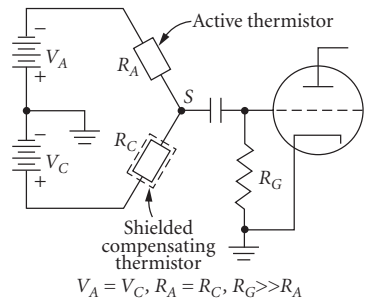

FIGURE 28 Bolometer electrical circuit. (*From Barnes Engineering, Bull. 2–100.*)

Time constant: τ is 1- to 20-ms standard for nonimmersed detectors and 2- to 10-ms standard for immersed detectors.

Sensitive area: 0.1×0.1 mm, 5×5 mm standard.

Operating temperature: Normally ambient, 285–370 K.

Responsivity: Depends on bias, resistance, area, and time constant $\mathcal{R} \propto \sqrt{R\tau/A} \approx 10^3$ V/W for 0.1×0.1 mm area, 250 kΩ resistance, and $\tau = 4$ ms (see Fig. 27 for frequency-time-constant dependence with given area). Output voltage (responsivity) can be increased to a limited degree by raising bias voltage. Figure 29 shows the deviation from Ohm's law due to heating. Bias should be held below 60 percent of peak voltage. Listed responsivity is that of active flake. In the bridge circuit, responsivity is half this value.

Sensitivity profile: Approximately 10 percent for 10-μm scan diameter over a 1×1 mm cell.

Linearity: ±5 percent 10^{-6} to 10^{-1} W/cm^2.

Recommended circuit: See Figs. 28 and 29.

Manufacturers: Servo Corporation of America, Thermometrics.

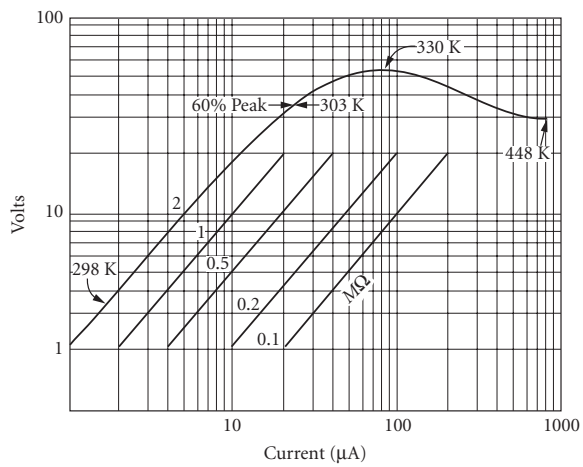

FIGURE 29 Thermistor voltage-current characteristics, showing typical flake temperatures under different conditions. (*From Barnes Engineering, Bull. 2–100.*)

Downloaded from Digital Engineering Library @ McGraw-Hill (www.accessengineeringlibrary.com)
Copyright © 2010 The McGraw-Hill Companies. All rights reserved.
Any use is subject to the Terms of Use as given at the website.

Pyroelectric Lithium tantalate ($LiTaO_3$), triglycine sulfate (TGS), and other pyroelectric materials provide an uncooled thermal detector with good sensitivity. The devices are capable of fast response, limited inversely by the preamplifier feedback resistance, but with responsivity and D^* traded for speed. This detector's, principle of operation is the pyroelectric effect, which is the change of electric polarization with temperature. Pyroelectric detectors offer rugged construction and the absence of $1/f$ noise because no bias is involved.

Lack of $1/f$ noise, combined with the ability to easily trade off speed and sensitivity, makes pyroelectric detectors useful for scanning applications and energy measurement of pulsed optical sources. In addition, the NEP is independent of area at low frequencies (10 Hz), so that these detectors are useful for large-area applications (preamplifier $1/f$ noise may limit, however). Pyroelectric detectors are useful for calorimetry since the pyroelectric effect is an integrated volume effect and the output signal is unaffected by spatial or temporal distribution of the radiation, up to damage threshold or depolarizing temperature. For higher damage thresholds, lead zirconate titanate ceramic (Clevite PZT-5) exhibits a much smaller pyroelectric effect than TGS, but its high Curie temperature of 638 K makes it more useful than TGS for high-energy applications.

Sensitivity: Sensitive from ultraviolet to millimeter wavelengths. For $\lambda < 2$ μm, TGS must be blackened, which slows response. Normally ($\lambda > 2$ μm) a transparent electrode is used, since TGS absorption is high from 2 to 300 μm. Beyond 300 μm, poor absorption and increased reflectivity reduce sensitivity. Spectral response depends largely on coating. See Fig. 30 for spectral response with modified 3M black. Figure 31 illustrates the relative spectral response for a $LiTaO_3$ device.

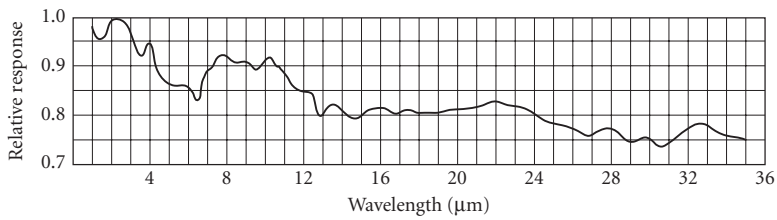

FIGURE 30 Relative spectral response of TGS detectors with modified 3M black. (*From Barnes Engineering, Bull. 2–100.*)

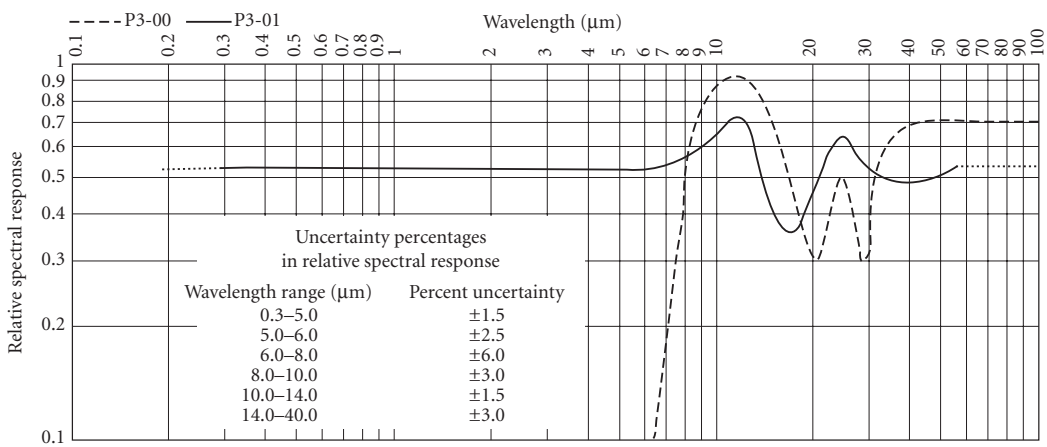

FIGURE 31 Relative spectral response of $LiTaO_3$, pyroelectric detectors showing both a black spectral coating and an optional coating tuned to the 8 to 14-μm LWIR band. (*From Molectron Detector, Inc.*)

Downloaded from Digital Engineering Library @ McGraw-Hill (www.accessengineeringlibrary.com)
Copyright © 2010 The McGraw-Hill Companies. All rights reserved.
Any use is subject to the Terms of Use as given at the website.

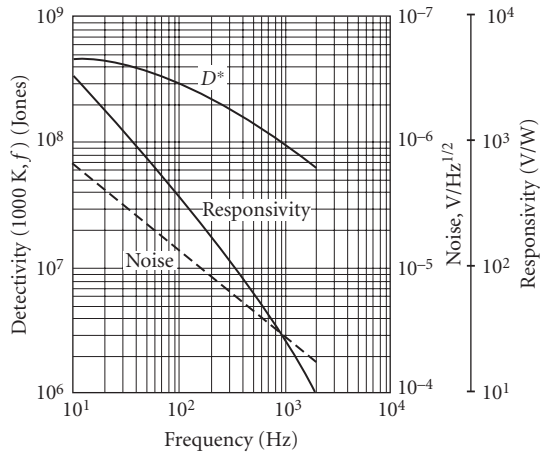

FIGURE 32 Typical D^*, responsivity, and noise versus frequency for TGS ($A = 1 \times 1$ mm; $T = 296$ K). (*From Barnes Engineering, Bull. 2–220A.*)

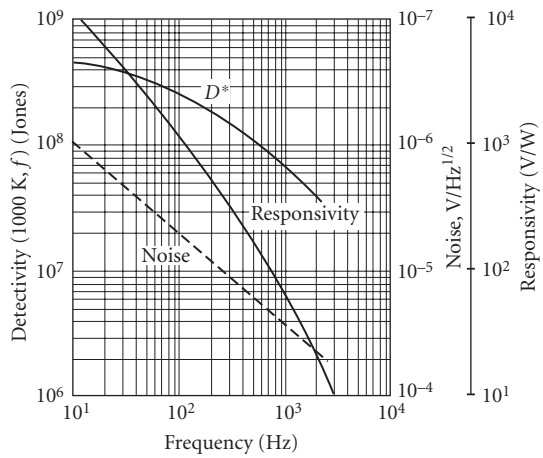

FIGURE 33 Typical D^*, responsivity, and noise versus frequency for TGS ($A = 1 \times 1$ mm; $T = 296$ K). (*From Barnes Engineering, Bull. 2–220A.*)

D^* is independent of A at low frequencies (10 Hz) (see Figs. 32 and 33). Figure 34 shows NEP versus A for various frequencies.

Quantum efficiency: Depends on coating absorptivity (for 3M black typically η >75 percent).

Noise: (See Figs. 32 and 33). Limited by loss-tangent noise up to frequencies that become limited by amplifier short-circuit noise (see Fig. 35).

Operating temperature: Ambient, up to 315 K. Can be repolarized if $T > T_{curie} = 322$ K for TGS. Irreversible damage at $T = 394$ K (see Fig. 36). Other pyroelectric materials have significantly higher Curie temperatures (398 to 883 K).

Downloaded from Digital Engineering Library @ McGraw-Hill (www.accessengineeringlibrary.com)
Copyright © 2010 The McGraw-Hill Companies. All rights reserved.
Any use is subject to the Terms of Use as given at the website.

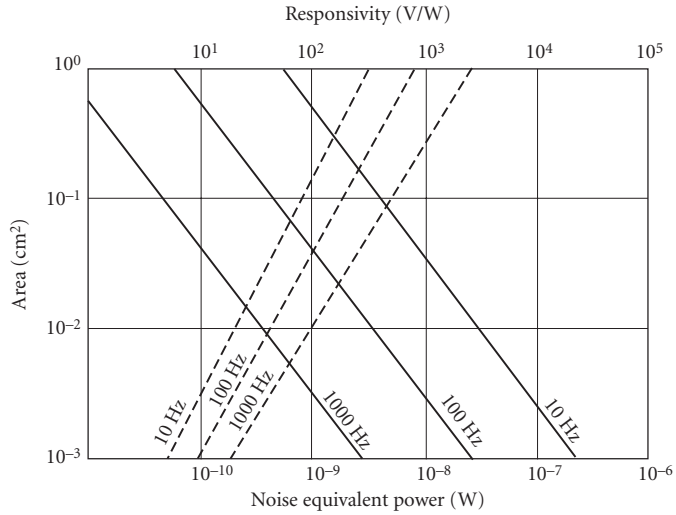

FIGURE 34 Noise equivalent power in watts (broken lines) and responsivity (solid lines) versus TGS detector area for various frequencies. (*From Barnes Engineering, Bull. 2–220B.*)

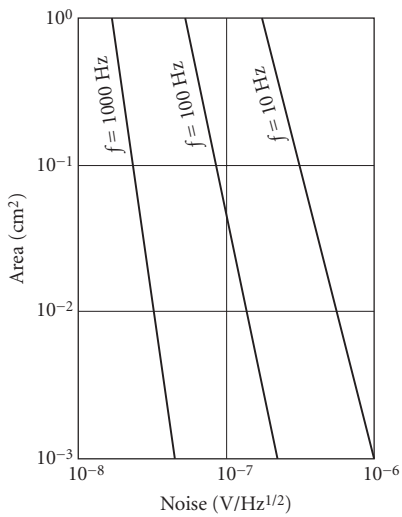

FIGURE 35 TGS noise versus detector area for various operating frequencies. (*From Barnes Engineering, Bull. 2–100.*)

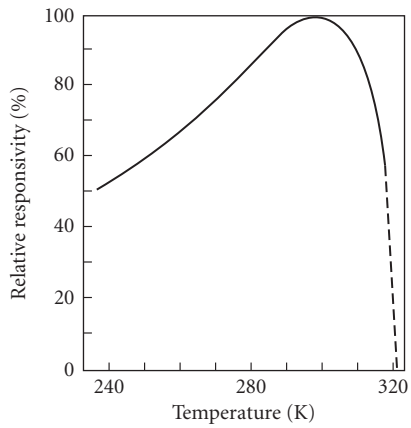

FIGURE 36 Relative responsivity versus temperature for TGS. (*From Barnes Engineering, Bull. 2–220B.*)

Output impedance: 50 Ω to 10 KΩ, set by built-in amplifier (see Fig. 37).

Responsivity: See Figs. 32 to 34, 36, and 38.

Capacitance: 5 pF for 0.5 × 0. 5 mm; 20 pF for 1 × 1 mm; 100 pF for 5 × 5 mm.

Sensitive area: 2 to 50-mm diameter round, 0.5 × 0. 5-mm to 10 × 10-mm square, typical.

Time constant: Not pertinent, response speed set by the preamplifier feedback resistor (see Fig. 38).

Downloaded from Digital Engineering Library @ McGraw-Hill (www.accessengineeringlibrary.com)
Copyright © 2010 The McGraw-Hill Companies. All rights reserved.
Any use is subject to the Terms of Use as given at the website.

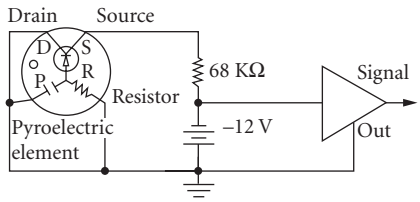

FIGURE 37 Pyroelectric detector amplifier circuit. (*From Barnes Engineering, Bull. 2–220A.*)

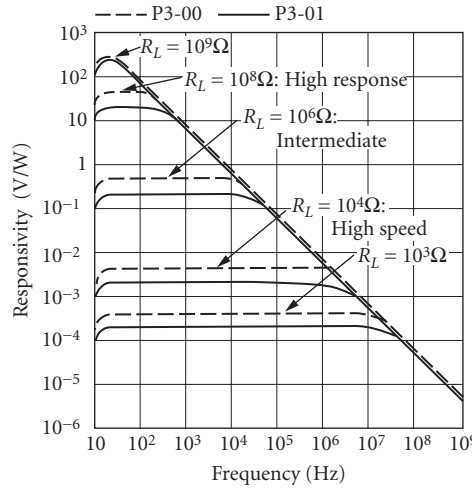

FIGURE 38 Responsivity vs. frequency for two pyroelectric models using various feedback resistors. (*From Molectron Detector, Inc.*)

Linearity: 5 percent between 10^{-6} and 10^{-1} W/cm^2.

Sensitivity profile: Depends on coating or transparent electrode; 5 to 7 percent across 12 × 12-mm; spot size < 250 μm.

Recommended circuit: See Figs. 37 and 39. Field effect transistor (FET) amplification stage usually built in. Since $\mathcal{R} \propto 1/f$, use of an amplifier with $1/f$ noise and gain $\propto f$ is recommended. Then output signal and signal-to-noise ratio are independent of frequency.

Manufacturers: Alrad Instruments, Belov Technology, CSK Optronics, Delta Developments, EG&G Heimann, Electro-Optical Systems, Eltec, Gentec, Graseby, International Light, Laser Precision, Molectron Detector, Oriel, Phillips Infrared Defence Components, Sensor-Physics, Servo Corporation of America, Spiricon, Thermometrics.

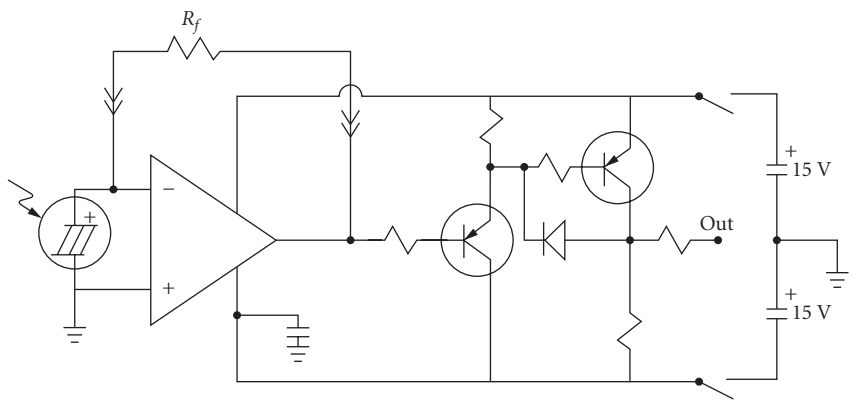

FIGURE 39 Resistive feedback circuit used with $LiTaO_3$ detectors. (*From Molectron Detector, Inc.*)

Downloaded from Digital Engineering Library @ McGraw-Hill (www.accessengineeringlibrary.com)
Copyright © 2010 The McGraw-Hill Companies. All rights reserved.
Any use is subject to the Terms of Use as given at the website.

InSb Hot-Electron Bolometer At temperatures of liquid helium and lower, free carriers in indium antimonide (InSb) can absorb radiation in the far-infrared and submillimeter spectral region. Because the mobility of the electrons varies as $T_e^{3/2}$ under these conditions, the conductivity of the material is modulated. This mechanism offers submicrosecond response and broad far-infrared coverage out to millimeter wavelengths but requires liquid-helium cooling and very sophisticated receiver design.

Technically, these devices may be classed as bolometers, since incident radiation power produces a heating effect which causes a change in free-charge mobility. In the normal bolometer, the crystal lattice absorbs energy and transfers it to the free carriers via collisions. However, in InSb bolometers incident radiation power is absorbed directly by free carriers, the crystal lattice temperature remaining essentially constant. Hence the name electron bolometer. Note that this mechanism differs from photoconductivity in that free-electron mobility rather than electron number is altered by incident light (hence there is no photoconductive gain).

Sensitivity: $D^*(2\text{ mm}, 900) = 4 \times 10^{11}$ Jones (see Fig. 40).

Noise: See Figs. 41 and 42.

Responsivity: 1000 V/W.

Time constant: 250 ns.

Sensitive area: 5 × 5 mm typical.

Operating temperature: 1.5 to 4.2 K.

Impedance: Without bias, 200 Ω; optimum bias, 150 Ω, depends on bias (see Fig. 29).

Recommended circuit: Optimum bias 0.5 mA (see Fig. 43).

Manufacturer: Infrared Laboratories.

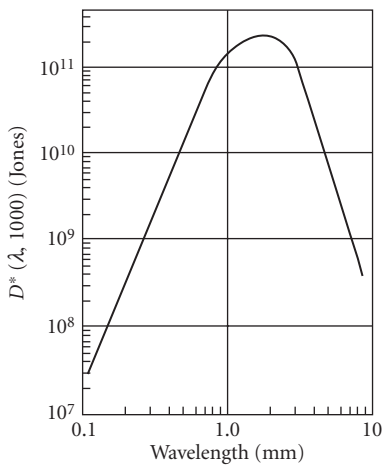

FIGURE 40 D^* versus λ for InSb electron bolometer ($H = 0$). (*From Raytheon, IR Millimeter Wave Detector, 1967.*)

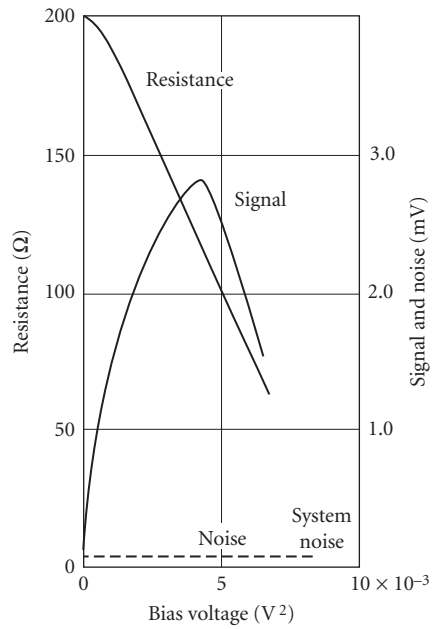

FIGURE 41 InSb electron bolometer, typical resistance, signal, and noise versus bias voltage squared ($T = 5$ K; $R_L = 200$ Ω; gain = 2.4×10^4; $F = 1100$ Hz). (*From Santa Barbara Research Center, Prelim. Res. Rep., 1967.*)

Downloaded from Digital Engineering Library @ McGraw-Hill (www.accessengineeringlibrary.com)
Copyright © 2010 The McGraw-Hill Companies. All rights reserved.
Any use is subject to the Terms of Use as given at the website.

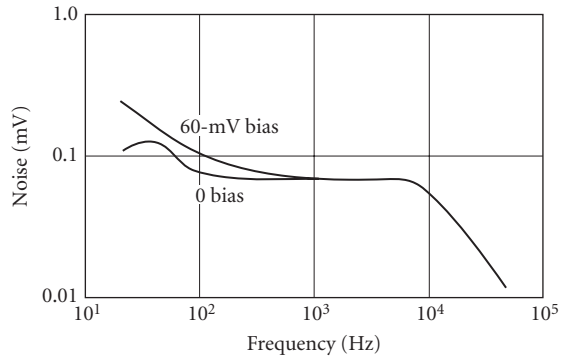

FIGURE 42 InSb electron bolometer, typical noise spectrum ($T = 5$ K; $R_L = 200\ \Omega$; gain $= 2.4 \times 10^4$; $\Delta f = 5.6$ Hz). (*From Santa Barbara Research Center, Prelim. Res. Rep., 1967.*)

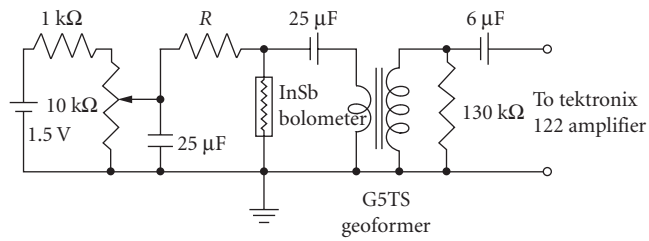

FIGURE 43 Electron bolometer biasing circuit. (*From Santa Barbara Research Center, Prelim. Res. Rep., 1967.*)

Ge(Ga) Low-temperature Bolometer The Ge(Ga) bolometer offers very high sensitivity and broad spectral coverage in the region 1.7 to 2000 μm. Liquid-helium cooling is required. A trade-off exists between response time (seconds) and sensitivity (10^{-14}-W NEP). Operation at 1000 Hz can be achieved still maintaining 2×10^{-13} W NEP.

Sensitivity: Depends on thermal conductance G (see Figs. 44 and 45). NEP(λ, 10 Hz) $= V_n/S = 3 \times 10^{-14}$ W for $G = 1$ μW/K; $A = 1$ mm^2, $D^*(\lambda, 10\text{ Hz}) = 3 \times 10^{13}$ Jones ($Q < 0.2$ μW). For this detector, NEP $\approx 4T\ (kG)^{1/2}$ and does not vary with $A^{1/2}$ (T is heat-sink temperature, and k is Boltzmann's constant). Thus D^* cannot be used as a valid means of comparison with other detectors; 300-K background-limited performance is achievable for 2π FOV when the bolometer is operated at 4.25 K with $G = 10^{-3}$ W/K. (For $A = 0.1$ cm^2, the time constant is 50 s.)

Responsivity: Typically, responsivity $= 2.5 \times 10^5$ V/W $= 0.7(R/TG)^{1/2}$, where R = resistance. Responsivity, and hence NEP, depends on thermal conductance G, which in turn is set by background power. G ranges from 0.4 to 1000 μW/K.

Thermal conductance: Typically $G = 1$ μW/K for background $Q < 0.2$ μW; note that $Q < 1/2$ (optimum bias power P).

Sensitive area: 0.25×0.25 to 10×10 mm.

Resistance: 0.5 MΩ.

Operating temperature: 2 K (see Fig. 44). In applications where radiation noise can be eliminated there is much to be gained by operating at the lowest possible temperature. Figure 45 shows the theoretical NEP and time constant at 0.5 K, assuming that current noise remains unimportant.

Downloaded from Digital Engineering Library @ McGraw-Hill (www.accessengineeringlibrary.com)
Copyright © 2010 The McGraw-Hill Companies. All rights reserved.
Any use is subject to the Terms of Use as given at the website.

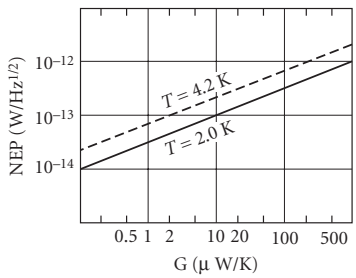

FIGURE 44 Germanium bolometer NEP versus conductance. (*Infrared Laboratories, Inc.*)

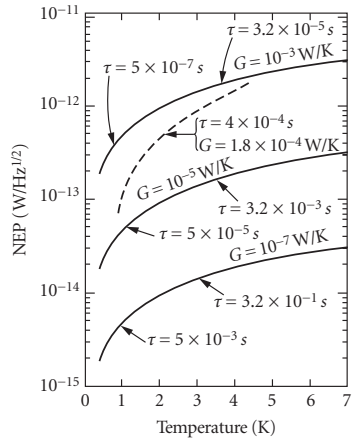

FIGURE 45 Germanium bolometer NEP versus temperature. Solid curves are theoretical: NEP $\approx 4T(kG)^{1/2}$.(*From Ref. 17.*)

Quantum efficiency: Depends on blackened coating and window. For λ <100 μm, absorptivity exceeds 95 percent. For λ >100 μm, efficiency varies with geometry.

Time constant: Response time constant is proportional to G^{-1}. Therefore, if G must be increased to accommodate larger background, the time constant is decreased proportionally. Responsivity and NEP, however, are degraded as $G^{-1/2}$.

Noise: $V_n = 1 \times 10^{-8}$ V/Hz$^{1/2}$; thermal noise is due to R and R_L.

Recommended circuit: Standard photoconductive circuit, with load resistor, grid resistor, and blocking capacitor at low temperature (see Fig. 46). See Fig. 47 for typical electrical characteristics. Bias power $P = 0.1$ *TG*.

Manufacturer: Infrared Laboratories, Inc.

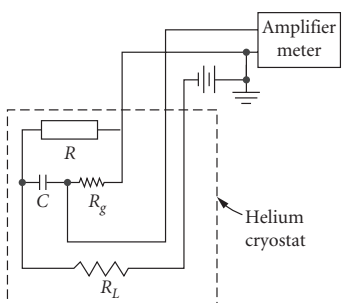

FIGURE 46 Germanium bolometer circuit and cryostat.

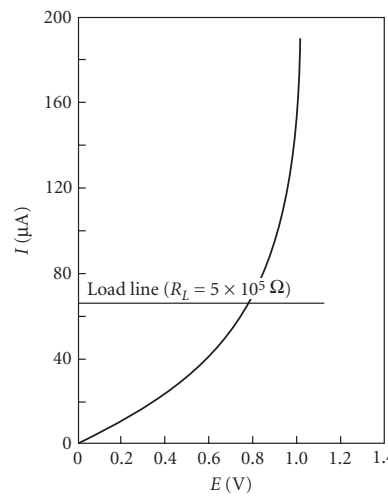

FIGURE 47 Load curve for a typical germanium bolometer ($T = 2.15$ K) with load line, showing optimum operating point. (*From Ref. 17.*)

Downloaded from Digital Engineering Library @ McGraw-Hill (www.accessengineeringlibrary.com)
Copyright © 2010 The McGraw-Hill Companies. All rights reserved.
Any use is subject to the Terms of Use as given at the website.

Photoemissive Detectors Photoemissive detector is generally the detector of choice in the UV, visible, and near-IR where high quantum efficiency is available. In the spectral region $\lambda < 600$ nm, the photomultiplier, or multiplier phototube, has close to ideal sensitivity; that is, selected photomultiplier tubes (PMT) are capable of detecting single photon arrivals (but at best only with about 30 percent quantum efficiency) and amplifying the photocurrent (pulse) enormously without seriously degrading the signal-to-noise ratio. Time resolution can be as short as 0.1 ns. Only very specialized limitations have precluded their use for $\lambda < 800$ nm, for example, cost, ruggedness, uniformity of manufacture, or need for still faster response. Recently these limitations have all been met individually but generally not collectively. Where adequate light is available, the simple phototube has advantages over the multiplier phototube in that high voltages are not required, the output level is not sensitive to applied voltage, and dynode fatigue is eliminated.

Microchannel plate tubes (MCPT) are a variant of the photomultiplier tube where the current amplifying dynode structure is replaced by an array of miniature tubes in which the photocathode current is amplified. MCP tubes are more compact than PMTs and are reliable in operating conditions of high environmental stress. The same range of photocathode materials is available in MCPTs as PMTs. MCPTs can provide a wide range of electron gain as available depending upon whether a single MCP or a stack of MCPs is used. The structure of a PMT and MCPT are compared in Fig. 48.

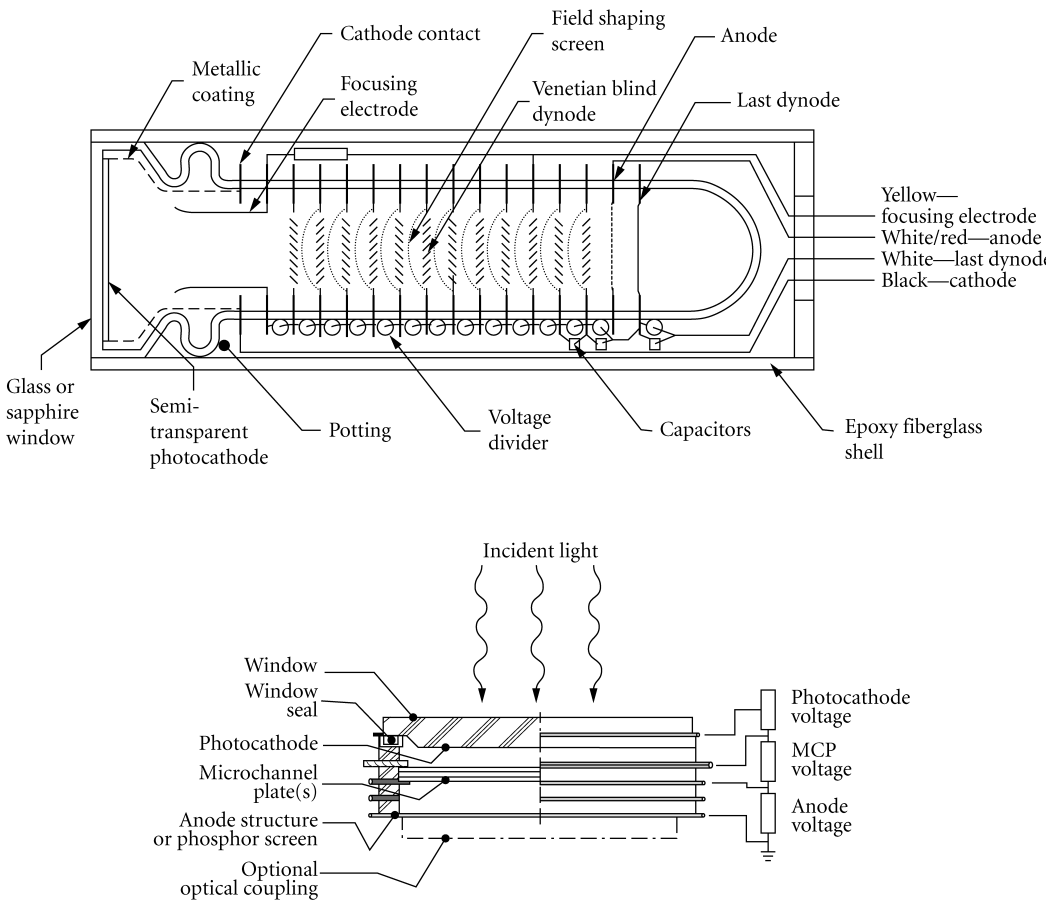

FIGURE 48 Comparison of photomultiplier tube (PMT) and microchannel plate tube (MCPT) construction. (*EMR Photoelectric.*)

Downloaded from Digital Engineering Library @ McGraw-Hill (www.accessengineeringlibrary.com)
Copyright © 2010 The McGraw-Hill Companies. All rights reserved.
Any use is subject to the Terms of Use as given at the website.

Sensitivity In modern phototubes, shot noise due to the cathode dark current is by far the most important noise source. The most common descriptions of phototube sensitivity list both current responsivity (amperes per watt), dark current, and dark noise. Several useful measures of sensitivity are noise equivalent input (NEI) (see Sec. 24.4 "Definitions"), noise equivalent power (NEP), or its reciprocal $D \equiv 1/\text{NEP}$. NEP and NEI in the range 10^{-14} to 10^{-17} W/Hz$^{1/2}$ are not uncommon.

Detectivity is generally limited by dark-current shot noise. Dark current depends on photocathode material, area, and temperature. Thus the best detectivity is obtained with small effective sensitive area. Cooling is especially useful for red-sensitive and near-IR tubes and is generally not worthwhile for others (see "Operating temperature"). Special tube housings which can provide thermoelectric cooling are available.

The spectral response curves shown in Fig. 49 are for the combination of photocathode and window. Historically, this method of description gave rise to the S-response designations, most of which are now obsolete. It is often desirable to separate photocathode response from window transmission. Thus, Fig. 50 shows the quantum efficiency (electrons per incident photon) of a number of photocathodes without window losses. For $\lambda < 400$ nm, each photocathode should maintain its peak quantum efficiency, up to photon energies where multiple photoemissions take place. In Fig. 51, the spectral dependence of quantum efficiency for a variety of modern photocathode/window combinations is illustrated.

D^* is a meaningful figure of merit for phototubes whose sensitivity is limited by dark noise (shot noise on the dark current) and whose emitting photocathode area is clearly defined, but D^* must be used with caution because, although modern phototubes are generally dark-noise-limited devices, they are often limited by noise in signal, that is, the noise content of the signal itself.[18] Serious errors in predicting the detection capability of phototubes will arise if noise in signal is ignored and D^* is presumed to be the important limiting parameter [see Eqs. (6) to (8)]. Very little reliable data are presently available on D^* for photoemitters. However D^* curves for S-1, S-20, and S-25 are shown in Figs. 52 (300 K) and 53 (PMT cooled to 200 K).

Short-wavelength considerations Window considerations are as follows:

For $\lambda > 200$ nm: Windows are essential, as all useful photocathode materials are oxidized and performance would otherwise be destroyed.

200 nm $> \lambda >$ 105 nm: Photocathode materials are not oxidized by dry air (moisture degrades performance). Windows are optional. LiF windows have shortest known cutoff, 105 nm. For $\lambda <$180 nm, it is generally advisable to flush with dry nitrogen.

$\lambda <$105 nm: No windows are available.

Since air absorbs radiation in the region 0.2 to 200 nm (ozone absorbs 200 to 300 nm), it is necessary to include the (windowless) detector in a vacuum enclosure with the source.

A useful technique for avoiding the far-ultraviolet window-absorption problem (provided $\lambda >$ vacuum ultraviolet) is to coat the outside of the window of a conventional PMT with an efficient fluorescent material, for example, sodium salicylate, which absorbs in the ultraviolet and reemits in the blue, and is efficiently detected by most photocathodes.[9]

Solar-blind considerations are as follows—although most photocathodes have high quantum efficiency at short wavelengths, background-noise considerations often preclude their use at very short wavelengths, and very wide bandgap semiconductor photocathodes such as CsI, KBr, Cs_2Te, and Rb_2Te (having peak quantum efficiency a little greater than 10 percent) often give better signal-to-noise ratio. This sacrifice in quantum efficiency to obtain insensitivity to wavelengths greater than those of interest would not be necessary if suitable short-wavelength pass filters were readily available.

For applications where it is desirable that the detector not see much solar radiation, one can use photocathodes whose high work function precludes photoemission for photons of too low an energy. Figure 54 shows quantum efficiency versus λ for three such photocathodes, tungsten, CsI, and Cs_2Te, compared with Cs_3Sb and GaAs(Cs), which are not solar blind.

Downloaded from Digital Engineering Library @ McGraw-Hill (www.accessengineeringlibrary.com)
Copyright © 2010 The McGraw-Hill Companies. All rights reserved.
Any use is subject to the Terms of Use as given at the website.

PHOTODETECTORS

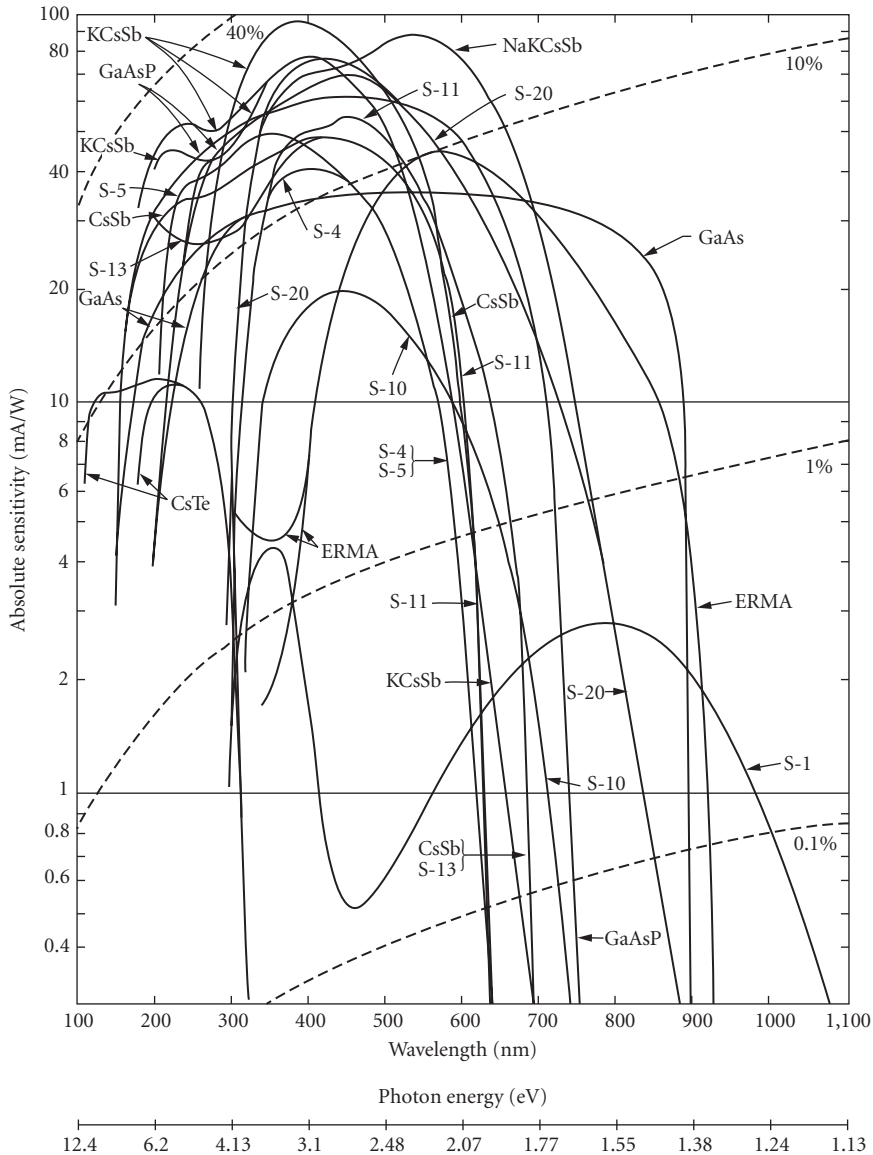

FIGURE 49 Spectral sensitivity of various photoemitters. Dotted lines indicate photocathode quantum efficiency. Chemical formulas are abbreviated to conserve space. S-1 = AgOCs with lime or borosilicate crown-glass window; S-4 = Cs_3Sb with lime or borosilicate crown-glass window (opaque photocathode); S-5 = Ss_3Sb with ultraviolet-transmitting glass window; S-8 = Cs_3Bi with lime or borosilicate crown-glass window; S-10 = AgBiOCs with lime or borosilicate crown-glass window; S-11 = Cs_3Sb with lime or borosilicate crown-glass window (semitransparent photocathode); S-13 = Cs_3Sb with fused-silica window (semitransparent photocathode); S-19 = Cs_3Sb with fused-silica window (opaque semicathode); S-20 = Na_2 KCsSb with lime or borosilicate glass window. ERMA = extended red multialkali (RCA; ITT uses MA for multialkali). This curve is representative of several manufacturers' products. Many variations of this response are available, for example, trade-offs between short- and long-wavelength response. (*From RCA Electronic Components, chart. PIT–701 B.*)

Downloaded from Digital Engineering Library @ McGraw-Hill (www.accessengineeringlibrary.com)
Copyright © 2010 The McGraw-Hill Companies. All rights reserved.
Any use is subject to the Terms of Use as given at the website.

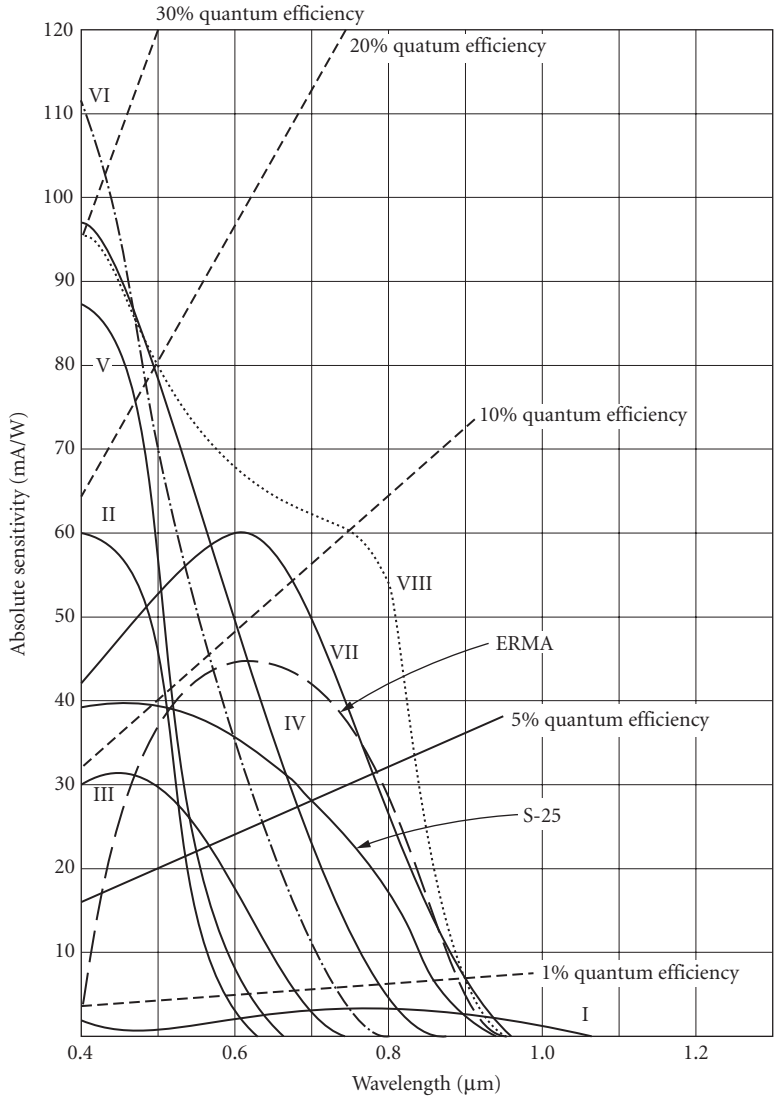

FIGURE 50 Photocathode responsivity and quantum efficiency versus wavelength (no windows). For abbreviations, see Fig. 49. I = S-1, II = S-11, III = S-10, IV = S-20, V = K_2CsSb, VI = $K_2CsSb(O)$, VII = $NaKCsSb_3$, VIII = GaAs(Cs). (*Based on material from RCA.*)

Quantum efficiency Figures 49, 50, 51, and 54 show photocathode spectral quantum efficiency (probability that one photoelectron is emitted when a single photon is incident). Note that there are fairly few basic photocathode materials and that the window often determines effective quantum efficiency at short wavelengths.

For $\lambda < 40$ nm, a wide variety of photocathode materials are available with high quantum efficiency. Many of these materials, such as tungsten, are not destroyed by being subjected to air, so that open structures can be used, consisting of a photocathode multiplier chain without window. The complete windowless structure is then placed in a vacuum enclosure with the source of radiation.

Downloaded from Digital Engineering Library @ McGraw-Hill (www.accessengineeringlibrary.com)
Copyright © 2010 The McGraw-Hill Companies. All rights reserved.
Any use is subject to the Terms of Use as given at the website.

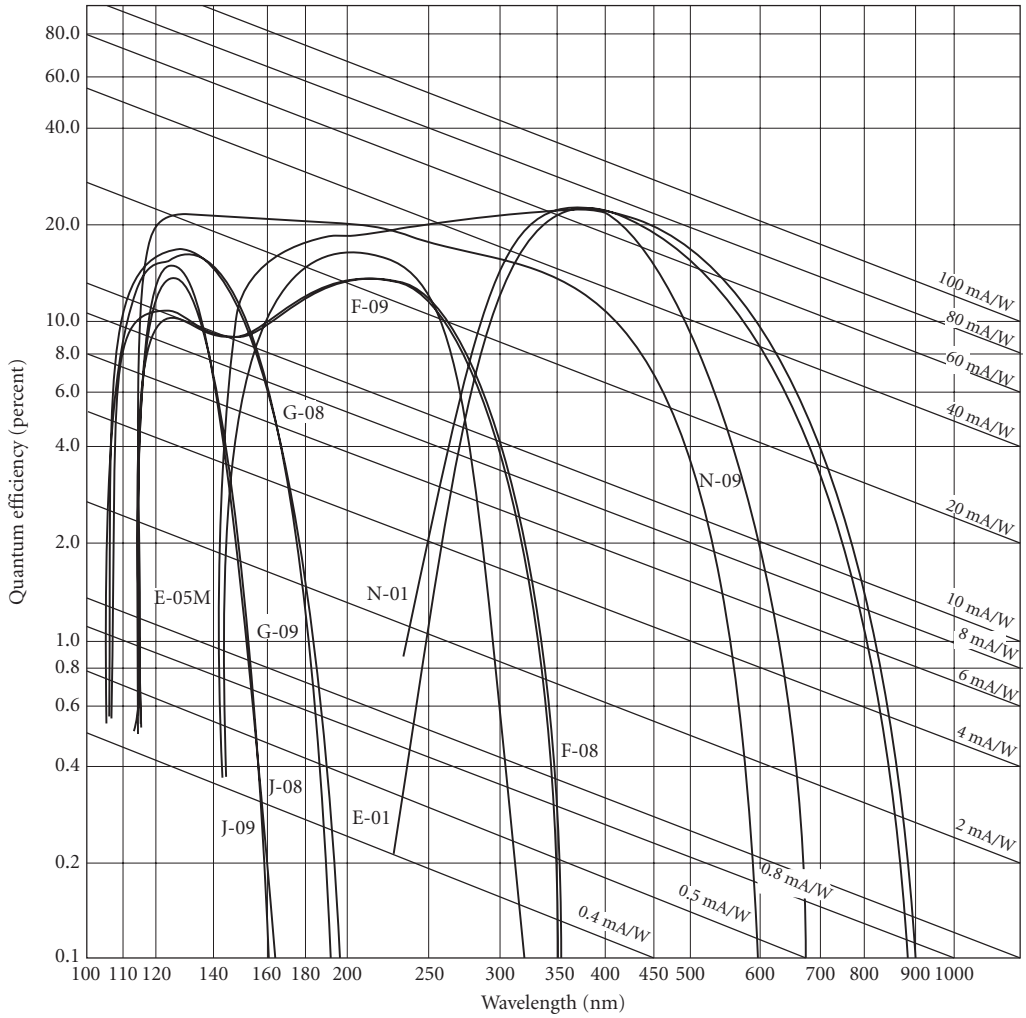

Photocathode key

Key letter	Description	Long-wavelength cutoff (Note 1)	Long-wavelength sensitivity (Note 2)
E	Tri-alkali (S-20)	850 nm	780 nm
F	Cesium telluride	355 nm	340 nm
G	Cesium iodide	195 nm	185 nm
J	Potassium bromide	165 nm	150 nm
N	High-temperature Bi-alkali	690 nm	640 nm
Q	Rubidium telluride	320 nm	300 nm

Note 1—Point at which QE becomes 1% (typical) of peak QE.
Note 2—Point at which QE is 1% (typical).

Window material key

Key no.	Description	Short-wavelength cutoff*
01	Borosilicate Glass	270 nm
05	UV Grade Sapphire	145 nm
08	UV Grade Lithium Fluoride	105 nm
09	Magnesium Fluoride	115 nm

*10% Energy transmission

FIGURE 51 Quantum efficiency of photocathode/window combinations as a funtion of wavelength. (*EMR Photoelectric*)

Downloaded from Digital Engineering Library @ McGraw-Hill (www.accessengineeringlibrary.com)
Copyright © 2010 The McGraw-Hill Companies. All rights reserved.
Any use is subject to the Terms of Use as given at the website.

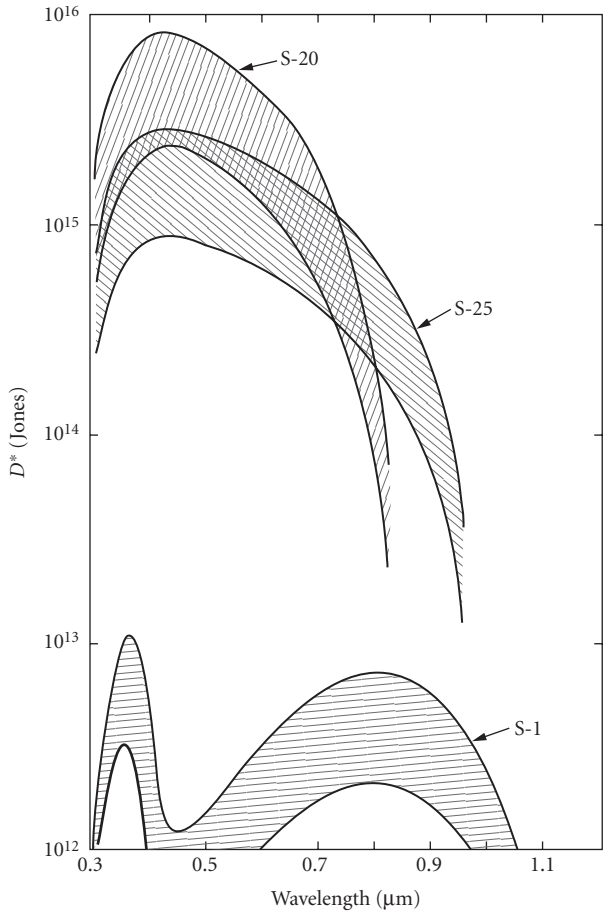

FIGURE 52 Range of D^* for uncooled photomultiplier tubes (T = 300 K). For abbreviations, see Fig. 49. S-25 = same as S-20 but different physical processing. (*Based on material from RCA*)

The quantum efficiency at any wavelength can be calculated from the formula

$$\eta = \frac{\mathcal{R} \times 1239.5}{\lambda} \tag{22}$$

where $\mathcal{R}$ = photocathode response, A/W, and λ = wavelength, nm.

A useful technique for improving quantum efficiency, reported by Livingston[19] and Gunter,[20] involves multipassing the photocathode by trapping the light inside the photocathode using a prism.

Responsivity PMT responsivity depends upon photocathode quantum efficiency and subsequent dynode gain. For most purposes, the dynode gain in a well-designed PMT introduces no significant degradation in the photocathode signal-to-noise ratio. Figure 49 shows photocathode response expressed in photocurrent (amperes) per incident radiation power (watts).

Downloaded from Digital Engineering Library @ McGraw-Hill (www.accessengineeringlibrary.com)
Copyright © 2010 The McGraw-Hill Companies. All rights reserved.
Any use is subject to the Terms of Use as given at the website.

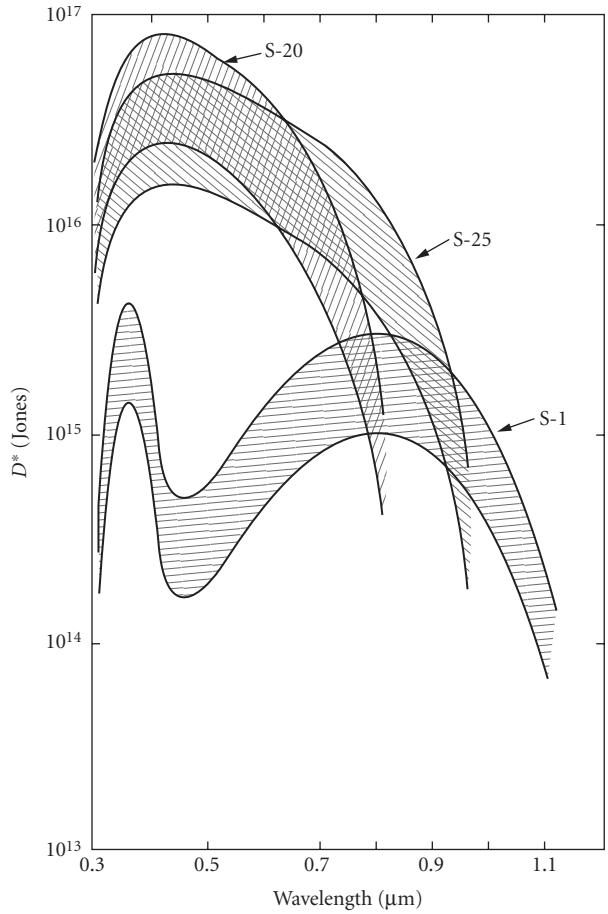

FIGURE 53 Range of D^* for uncooled photomultiplier tubes ($T = 300$ K). For abbreviations, see Fig. 49. S-25 = same as S-20 but different physical processing. (*Based on material from RCA*)2 Range of D^* for uncooled photomultiplier tubes ($T = 300$ K). For abbreviations, see Fig. 49. S-25 = same as S-20 but different physical processing. (*Based on E.H. Eberhardt, "D^* of Photomultiplier Tubes and Image Detectors", ITT Industrial Labs, 1969.*)

Noise The limiting noise in a PMT depends on the level of illumination. For low-level detection, limiting noise is the shot noise on the dark current,

$$i_n = (2ei_{\text{dark}}\Delta f)^{1/2} \tag{23}$$

For high illumination levels the shot noise on the signal photocurrent

$$i_n = (2ei_{\text{signal}}\Delta f)^{1/2} \tag{24}$$

far exceeds that on the dark current. Manufacturers usually express noise as photocathode dark current or anode dark current for given gain, which is therefore traceable to photocathode dark current.

Downloaded from Digital Engineering Library @ McGraw-Hill (www.accessengineeringlibrary.com)
Copyright © 2010 The McGraw-Hill Companies. All rights reserved.
Any use is subject to the Terms of Use as given at the website.

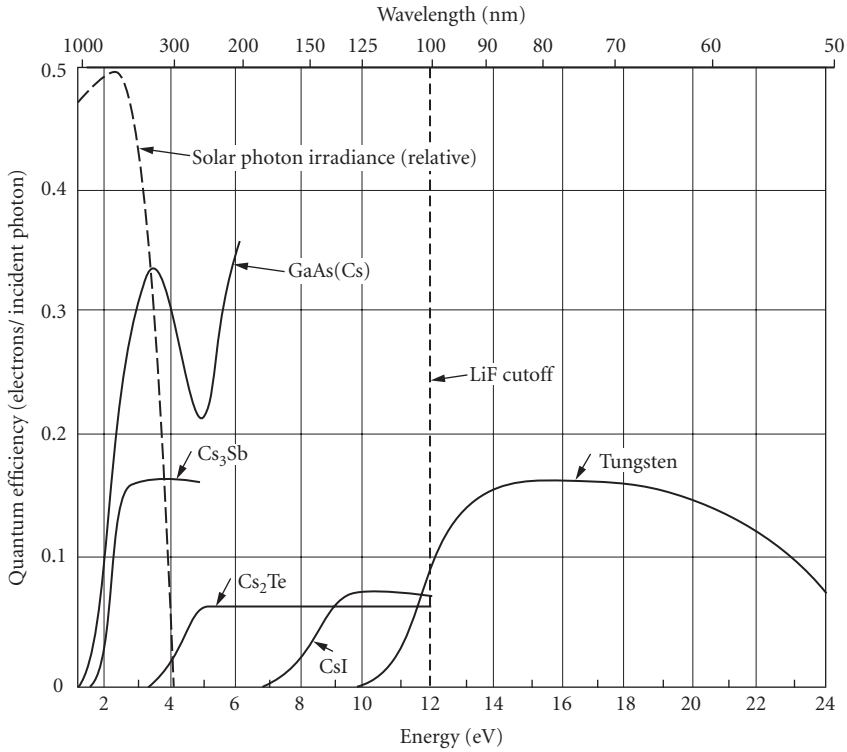

FIGURE 54 Quantum efficiency versus wavelength (photon energy) for several photoemitters.

Photocathode dark current is approximately proportional to photocathode area so that small photocathode effective areas can be expected to have reduced noise. Figure 55 shows how anode dark current and gain increase with applied voltage for a typical PMT.

Minimum detectable power is related to limiting noise through responsivity via

$$\text{NEP} = i_n / \mathcal{R} \tag{25}$$

where $\mathcal{R}$ is in amperes per watt.

Operating temperature Dark current due to thermionic emission, usually greater in red-sensitive tubes, can be reduced by cooling (see Ref. 21). The trialkali (S-20) performance does not benefit from cooling below 255 K. Maximum beneficial cooling (three to four dark counts per second) for AgOCs (S-1), (Cs)Na_2 KSb (S-20), and Cs_3Sb (S-11) is 195, 255, and 239 K, respectively. Most photocathodes become noisier as temperature rises above ambient because of increased thermionic emission. Because its thermionic emission starts at a very low value, (Cs)Na_2KSb is a useful photocathode up to temperatures of approximately 373 K.

Response time The rise time of photomultiplier tubes depends chiefly on the spread in transit time during the multiplication process. For photomultiplier tubes, this spread is about 10 ns. Some tubes with specially designed electron optics can give spread as low as 1 ns. The crossed-field PMT makes possible a spread as small as 0.1 ns. Microchannel plate tubes have response times of a nanosecond or less.

Downloaded from Digital Engineering Library @ McGraw-Hill (www.accessengineeringlibrary.com)
Copyright © 2010 The McGraw-Hill Companies. All rights reserved.
Any use is subject to the Terms of Use as given at the website.

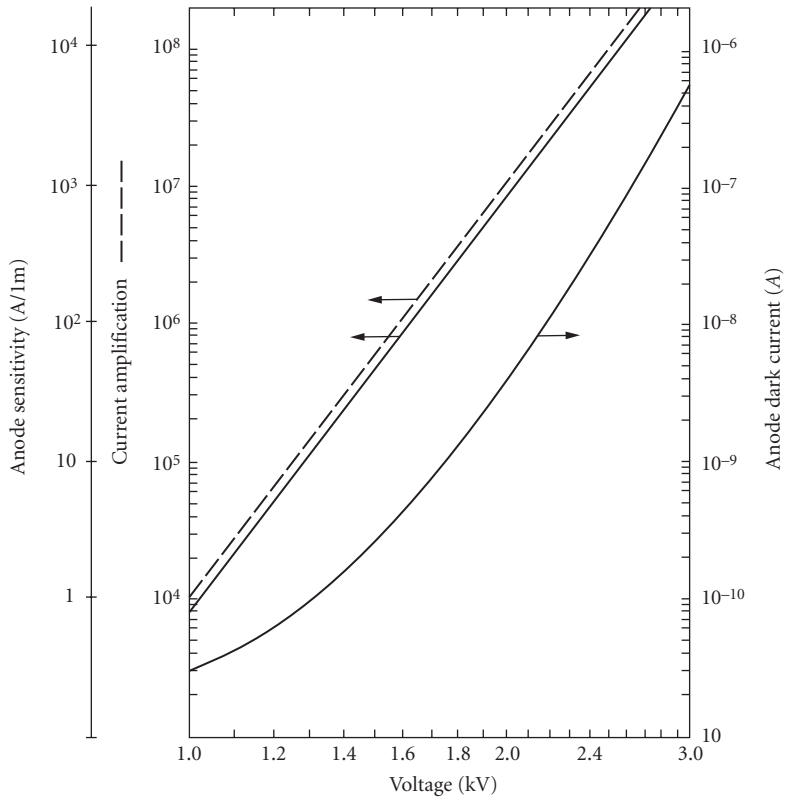

FIGURE 55 Typical current amplification and anode dark current as a function of applied voltage. (*Based on E.H. Eberhardt, "D* of Photomultiplier Tubes and Image Detectors," ITT Industrial Labs, 1969.*)

For high-speed work (<1 ns rise time), good transmission-line technique must be used to obtain impedance match and to avoid reflection. The bandwidth of the output circuit will depend upon the total capacitance (PMT circuit plus stray capacitances) and the value of the load resistance.

Linearity Photomultiplier tubes are nearly all linear to about 1 percent for cathode currents of 0.1 μA or less. Some tubes may be linear to better than 0.1 percent but must be individually selected.[22] Probably most of the nonlinearity results from the dynode structure.

Sensitive area No fundamental limitation. Only recently available with very small effective areas for extremely low dark current. Magnetic focusing has been used so that only a small fraction of the photocathode is used electron-optically.

Sensitivity profile Usually uniform within 20 to 50 percent. Microchannel plate detectors may have uniformity of ±5 percent.

Stability PMTs are subject to short- and long-term drift which can depend upon anode current, changes in anode current, storage times, and aging or anode life. They are also subject to change if exposed to magnetic fields or changes in temperature. Vibration of the tube may modulate the signal (microphonic effect).

Downloaded from Digital Engineering Library @ McGraw-Hill (www.accessengineeringlibrary.com)
Copyright © 2010 The McGraw-Hill Companies. All rights reserved.
Any use is subject to the Terms of Use as given at the website.

Recommended circuit See Fig. 56.

1. Since a PMT is a current generator, increasing output resistance R_1 increases output voltage. An upper limit to R_1 may be imposed either by the time-constant limitation or by nonlinearity, which results from a space charge produced near the anode when the anode is left nearly floating electrically.
2. The rated photocathode current (referred to anode current through gain) should not be exceeded.
3. Care should be taken not to destroy the photocathode with light (heating).
4. When large currents are drawn, it may affect later dynode interstage voltage and hence gain, causing nonlinearity; for example, in Fig. 44, if the photocurrent from DY 10 to anode becomes comparable to the biasing current, through R_{11}, the gain of the final stage is reduced. This can be avoided by biasing the dynodes with constant-voltage sources.
5. To avoid dynode damage, final dynode current must not exceed the value suggested by the manufacturer.

Photon counting At the photocathode, the shot-noise-limited signal-to-noise ratio (with negligible dark current) is

$$\frac{i_s}{i_n}\frac{i_s}{(2ei_s\Delta f)^{1/2}}\left(\frac{i_s}{2e\Delta f}\right)^{1/2}=\left(\frac{N_s}{2\Delta f}\right)^{1/2} \tag{26}$$

where N_s is the photoelectron rate at the photocathode. Thus, for extremely low levels of illumination, the ideal signal-to-noise ratio becomes very poor. At this point there is much to be gained by abandoning attempts to measure the height of the fluctuating signal (Fig. 57*a*) in favor of digitally recording the presence or absence of individual pulses (Fig. 57*e*).

Single photoelectron counting can be achieved by using a pulse amplifier (see Fig. 58), which suppresses spurious dark-noise pulses not identical in amplitude and shape to those produced by photoelectrons.

An upper practical limit for (random) photon counting is set by convenient amplifier bandwidths at about $10^5\ s^{-1}$. For reasonable (1 percent) statistical accuracy, this implies a 10-MHz bandwidth.

Gallium phosphide dynodes The development of GaP dynodes for increased secondary-electron production[23,24] makes possible unambiguous discrimination of small numbers of individual photoelectron counts which was not previously possible with lower dynode gains. This is shown in Fig. 59, where the spread in number of secondary electrons ($N\times$ gain) is just $(N\times \text{gain})^{1/2}$.

In addition to the aforementioned fundamental advantage of high dynode gain, the large gain per stage in the first dynodes also helps discriminate against noise introduced by later stages of amplification. Also, fewer stages of amplification are required.

Manufacturers ADIT, EMR Photoelectric, Bicron, Burle, Edinburgh Instruments, Galileo Electro-Optics, Hamamatsu, K and M Electronics, id Quantique, International Light, Optometrics USA, Oriel, Phillips Components, Photek, Photon Technology, Photonis, Penta Laboratories, Thorn EMI, Varo.

Downloaded from Digital Engineering Library @ McGraw-Hill (www.accessengineeringlibrary.com)
Copyright © 2010 The McGraw-Hill Companies. All rights reserved.
Any use is subject to the Terms of Use as given at the website.

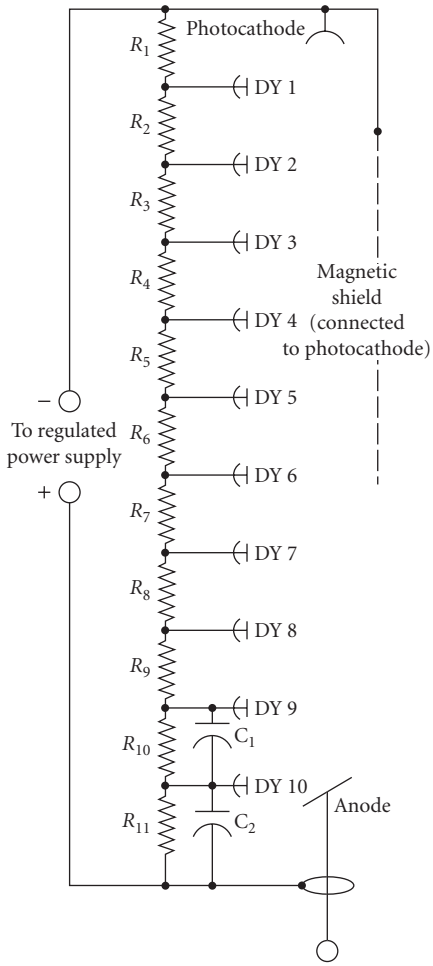

FIGURE 56 C_1 = 68 pF ±10 percent, 500 V (dc working); C_2 = 270 pF ±10 percent, 500 V (dc working); R_1 = 220 kΩ ±5 percent, 1/4 W; R_2 = 240 kΩ ±5 percent, 1/4 W; R_3 = 330 kΩ ±5 percent, 1/4 W; R_4 to R_{11} = 220 kΩ ±5 percent, 1/4 W. (*Based on E.H. Eberhardt, "D* of Photomultiplier Tubes and Image Detectors," ITT Industrial Labs, 1969.*)

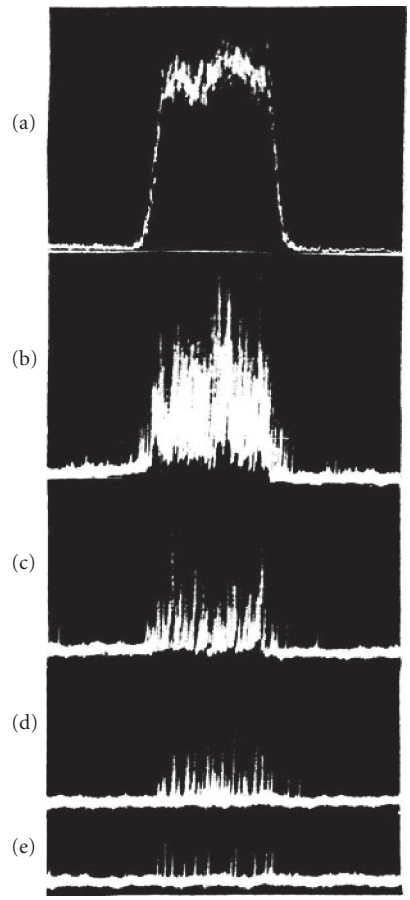

FIGURE 57 Oscilloscope presentation of PMT output when reviewing square-wave chopped light pulse. In (*a*) to (*e*) the intensity is reduced and gain is increased commensurately. (*Courtesy of E.H. Eberhardt.*)

Downloaded from Digital Engineering Library @ McGraw-Hill (www.accessengineeringlibrary.com)
Copyright © 2010 The McGraw-Hill Companies. All rights reserved.
Any use is subject to the Terms of Use as given at the website.

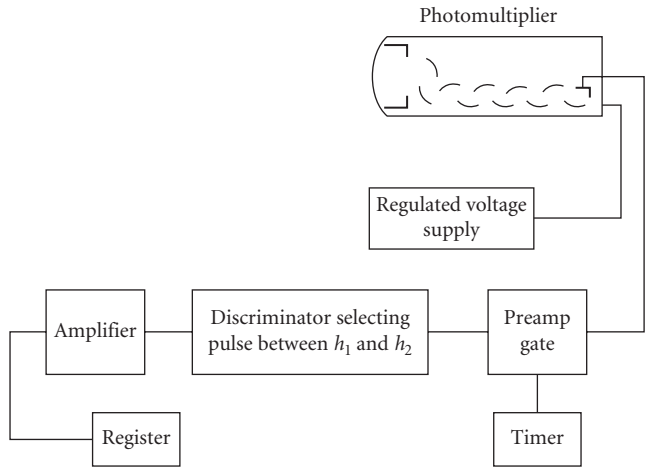

FIGURE 58 Photomultiplier and associated circuits for photon counting. (*ITT Report E5.*)

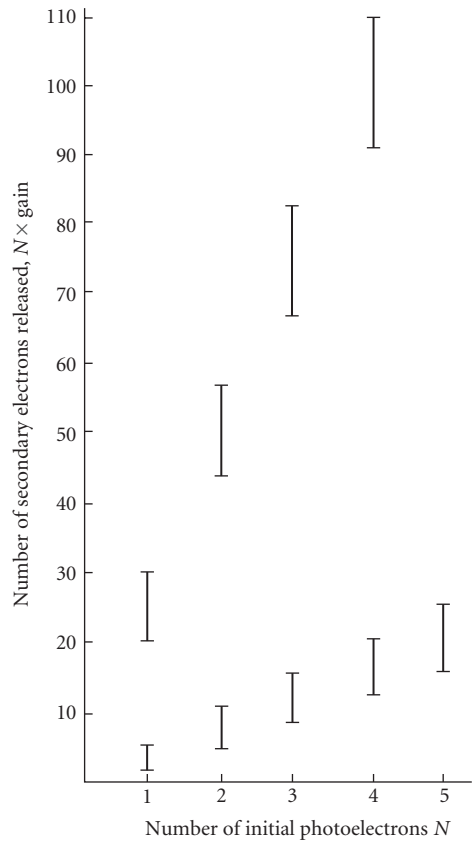

FIGURE 59 Spread in number of secondary electrons for various phototube gains.

Downloaded from Digital Engineering Library @ McGraw-Hill (www.accessengineeringlibrary.com)
Copyright © 2010 The McGraw-Hill Companies. All rights reserved.
Any use is subject to the Terms of Use as given at the website.

GaN and AlGaN Gallium nitride photovoltaic detectors, with a bandgap of 3.39 eV have spectral response in the ultraviolet (UV) from 200 to 365 nm, as illustrated in Fig. 60. By using aluminum-gallium nitride—an alloy mixture of AlN and GaN—the spectral response can be tuned to shorter wavelength cutoffs. Spectral response examples are shown in Figs. 61 to 64 to compare GaN with one particular AlGaN alloy. Some devices may be tailored to custom UV bands, such as UVA (320 to 400 nm), UVB (280 to 320 nm), or UVC (100 to 280).

Response at visible wavelengths is low or absent, so that no special filtering may be required to detect UV in the presence of visible lighting or solar radiation—but see the logrithmic spectral Figs. 62 and 64 to see the degree of longer wavelength response. These solid-state devices are potentially useful for operation at elevated temperatures, in high-vibration environments, and in other environments unsuitable for photomultiplier tubes.

The photoconductive GaN devices use interdigitated contact electrodes because of the very high impedance of the GaN films, but currently there may not be any available commercially.

Response: Photovoltaic 0.1 A/W

Dark current: 0.05-nA photovoltaic

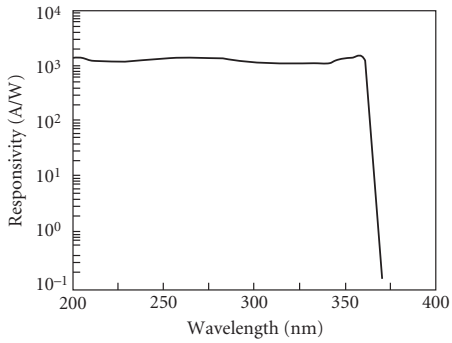

FIGURE 60 Response in amperes per watt for a GaN detector. (*Reprinted from Appl. Phys. Lett., vol. 60, no. 23, 1992, p. 2918.*)

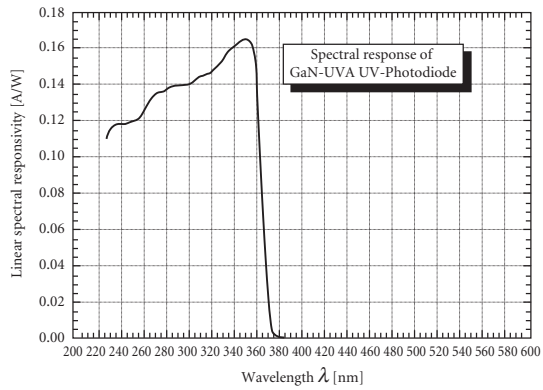

FIGURE 61 Spectral response of a UVA GaN detector shown on a linear vertical scale of amps/watt versus wavelength. (*http://www.boselec.com/products/documents/GaNAlGaNall.pdf.*)

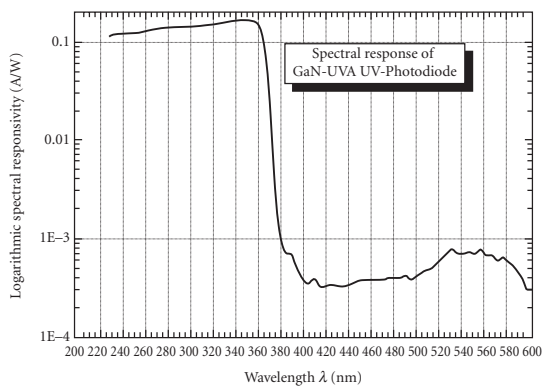

FIGURE 62 Spectral response of a UVA GaN detector shown on a logrithmic vertical scale of amperes/watt versus wavelength. (*http://www.boselec.com/products/documents/GaNAlGaNall.pdf.*)

Downloaded from Digital Engineering Library @ McGraw-Hill (www.accessengineeringlibrary.com)
Copyright © 2010 The McGraw-Hill Companies. All rights reserved.
Any use is subject to the Terms of Use as given at the website.

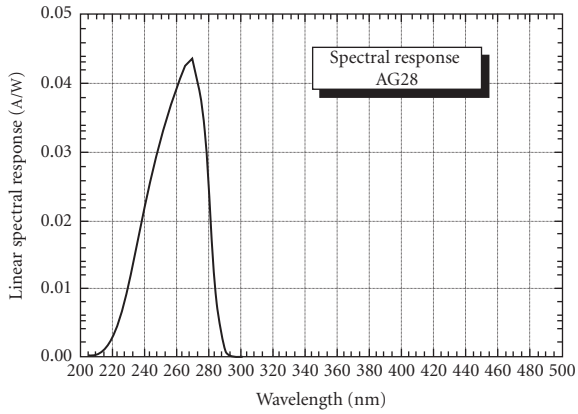

FIGURE 63 Spectral response of a UVC AlGaN detector shown on a linear vertical scale of amperes/watt versus wavelength. (*http://www.boselec.com/products/documents/GaNAlGaNall.pdf.*)

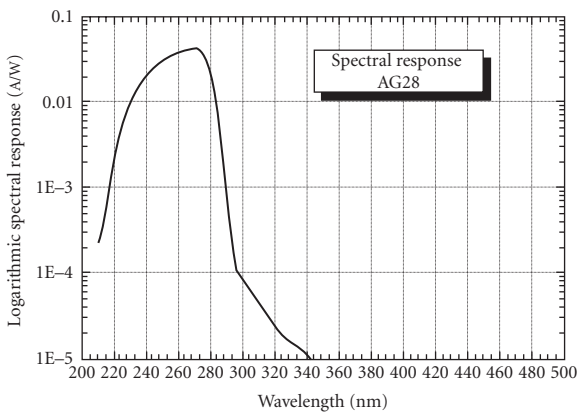

FIGURE 64 Spectral response of a UVC GaN detector shown on a logrithmic vertical scale of amperes/watt versus wavelength. (*http://www.boselec.com/products/documents/GaNAlGaNall.pdf.*)

Capacitance: 24 pF photovoltaic at 0-V bias

Time constant: Photovoltaic 0.10 ns

Size: 0.076 mm^2

Devices with AlGaN alloys have wider bandgaps and generally lower leakage currents.

Response: Photovoltaic 0.045 A/W.

Dark current: 0.1-pA photovoltaic at 0.1-V reverse bias

Capacitance: 24-pF photovoltaic at 0-V bias

Size: 0.076 mm^2

Downloaded from Digital Engineering Library @ McGraw-Hill (www.accessengineeringlibrary.com)
Copyright © 2010 The McGraw-Hill Companies. All rights reserved.
Any use is subject to the Terms of Use as given at the website.

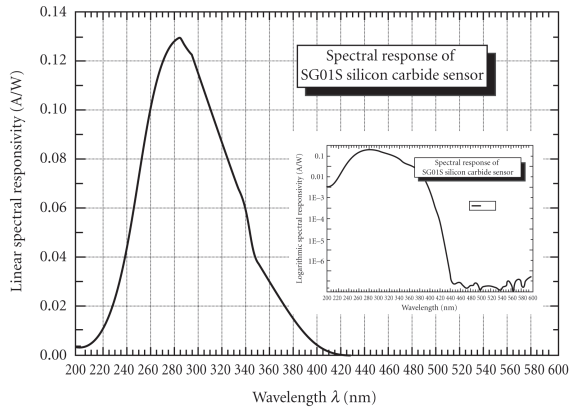

FIGURE 65 Spectral response of an unfiltered, broadband SiC detector shown on a linear vertical scale of amps/watt versus wavelength. The inset shows the same data on a logrithmic scale. (*http://www.boselec.com/products/documents/UVPhotodetectors2-08WWW.pdf.*)

Manufacturers: Advanced Photonix: http://www.advancedphotonix.com/ap_products/standard_GaN.asp?from=leftnav, Boston Electronics: http://www.boselec.com/products/detuv.html, Orion Semiconductor:http://www.orion-semi.com, SVT Associates: http://www.svta.com/products/uv/uv.htm.

SiC Silicon carbide UV detectors are available in photovoltaic structures. The 3-eV bandgap of SiC is slightly narrower than GaN, thereby giving a response may extend to slightly longer wavelength. However, because the bandgap of SiC is indirect, unlike GaN which is direct, the response cut-on is more gradual in SiC, peaking at a wavelength much shorter than the wavelength corresponding to 3 eV (413 nm)—see Fig. 65. SiC detectors with integrated filters are available.

Response: 0.13 A/W peak

Dark current: 1 fA for a 1×1 mm device

Capacitance: 195 pF for a 1×1 mm device

Sizes: 0.25×0.25 mm, 0.5×0.5 mm, 1×1 mm

Manufacturers: Boston Electronics: http://www.boselec.com/products/detuv.html, Electro Optical Components: http://www.eoc-inc.com/UV_detectors_silicon_carbide_photodiodes.htm

TiO_2 Detectors With a bandgap of 3.2 eV, TiO_2 is another UV photodetector. Photovoltaic devices are made with Schottky diodes. An unfiltered spectral response is shown in Fig. 66. TiO_2 detectors with integrated filters are available.

Response: 0.021 A/W peak

Dark current: 100 pA for a 5.4×2.9 mm device

Sizes: 2.2×1.9 mm, 5.4×2.9 mm

Manufacturer: Boston Electronics: http://www.boselec.com/products/detuv.html

GaP Gallium phosphide can provide Schottky photodiodes that cover the UV to mid-visible spectral region as shown in Fig. 67. The bandgap of GaP is 2.26 eV and is indirect, leading to a soft spectral

Downloaded from Digital Engineering Library @ McGraw-Hill (www.accessengineeringlibrary.com)
Copyright © 2010 The McGraw-Hill Companies. All rights reserved.
Any use is subject to the Terms of Use as given at the website.

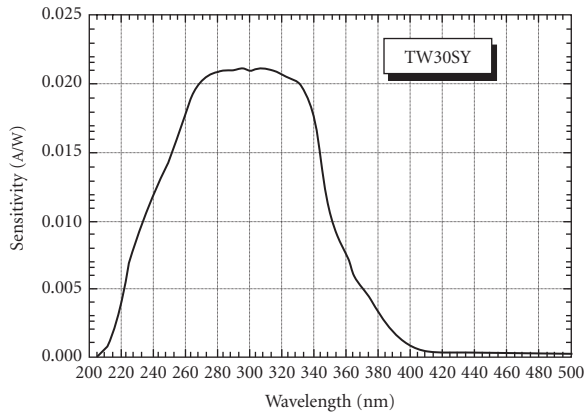

FIGURE 66 Spectral response of a TiO_2 Schottky photodiode detector shown on a linear vertical scale of amperes/watt versus wavelength. (*http://www.boselec.com/products/documents/UVPhotodetectors2-08WWW.pdf.*)

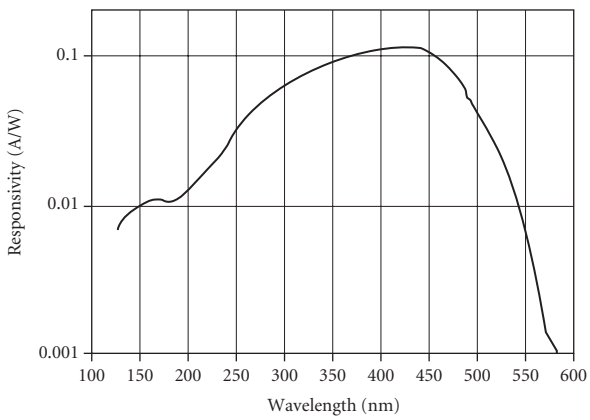

FIGURE 67 Spectral response of a GaP Schottky photodiode detector shown on a logrithmic vertical scale of amps/watt versus wavelength. (*http://www.thorlabs.com/Thorcat/12100/12174-S01.PDF.*)

turn-on and a peak quite far from the wavelength corresponding to the bandgap (549 nm). GaP devices with integrated filters to restrict the response to the UV region are also available.

Response: 0.12 A/W peak

Dark current: 1 nA max for a 2.5 × 2.5 mm device

NEP @ 440 nm: 1×10^{-14} W/√Hz @ 5 V bias

Rise time: 1 nsec @ 5 V bias for a 2.5 × 2.5 mm device

Fall time: 140 nsec @ 5 V bias for a 2.5 × 2.5 mm device

Sizes: 1.1 × 1.1 mm, 2.3 × 2.3 mm, 2.5 × 2.5 mm, 4.6 × 4.6 mm

Downloaded from Digital Engineering Library @ McGraw-Hill (www.accessengineeringlibrary.com)
Copyright © 2010 The McGraw-Hill Companies. All rights reserved.
Any use is subject to the Terms of Use as given at the website.

PHOTODETECTORS

Manufacturers: Hamamatsu: http://jp.hamamatsu.com/products/sensor-ssd/pd140/pd144/index_en.html, Electro Optical Components: http://www.eoc-inc.com/ifw/EPD-365-0-2-5.pdf, Thor Labs: http://thorlabs.com/thorProduct.cfm?partNumber=FGAP71

GaAsP Gallium arsenide phosphide alloys can provide photodiodes that cover from the UV to the near-infrared spectral region. The bandgap of GaP is 2.26 eV and is indirect, while that of GaAs is 1.43 eV and is direct. GaAsP alloys from 0 to ~50% GaP are direct bandgap materials while those with higher percentages of GaP are indirect*. A variety of alloys are available, covering the following spectral bands:

Spectral Band (nm)	λ Peak (nm)	Response at Peak (A/W)	Sizes (mm)
400–760	710	0.4	1.3 × 1.3, 2.7 × 2.7, 5.6 × 5.6
300–680	640	0.3	1.3 × 1.3, 2.7 × 2.7, 5.6 × 5.6
300–580	470	0.25	0.8 × 0.8
280–580	470	0.2	0.8 × 0.8
260–400	370	0.06	0.8 × 0.8
190–760	710	0.22	2.3 × 2.3, 4.6 × 4.6
190–680	610	0.18	10.1 × 10.1

Spectral responses of these alloys are shown in Figs. 68 to 73 (*ref: http://jp.hamamatsu.com/products/sensor-ssd/pd140/pd143/index_en.html?sort=WAVE_LENGTH4&desc=1&style=F1 for all six figures*).

Manufacturer: Hamamatsu: http://jp.hamamatsu.com/products/sensor-ssd/pd140/pd143/index_en.html

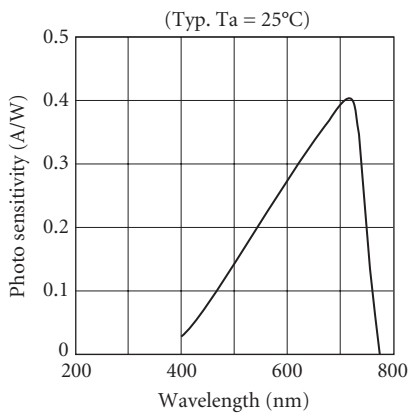

FIGURE 68 Spectral response of a 400 to 760-nm GaAsP photodiode detector with a vertical scale of amps/watt versus wavelength.

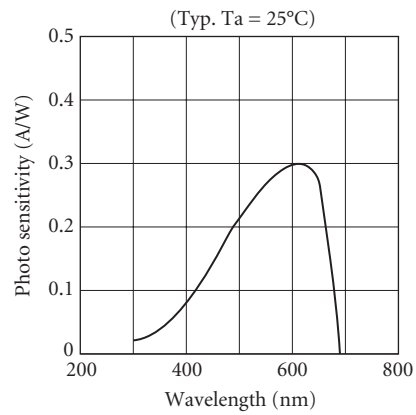

FIGURE 69 Spectral response of a 300 to 680-nm GaAsP photodiode detector with a vertical scale of amps/watt versus wavelength.

*http://www.iue.tuwien.ac.at/phd/palankovski/node37.html.

Downloaded from Digital Engineering Library @ McGraw-Hill (www.accessengineeringlibrary.com)
Copyright © 2010 The McGraw-Hill Companies. All rights reserved.
Any use is subject to the Terms of Use as given at the website.

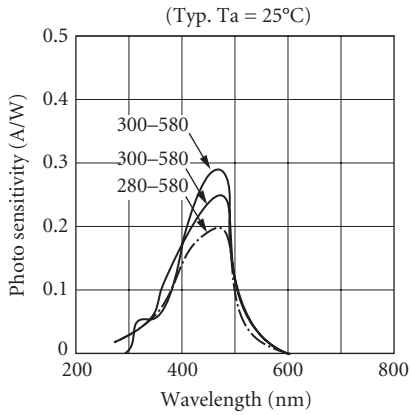

FIGURE 70 Spectral response of 300 to 580 and 280- to 580-nm GaAsP photodiode detectors with a vertical scale of amperes/watt versus wavelength.

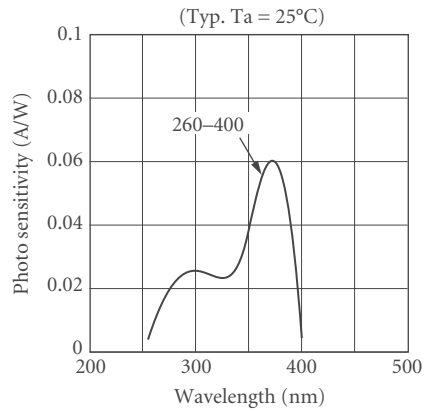

FIGURE 71 Spectral response of a 260- to 400-nm GaAsP photodiode detector with a vertical scale of amperes/watt versus wavelength.

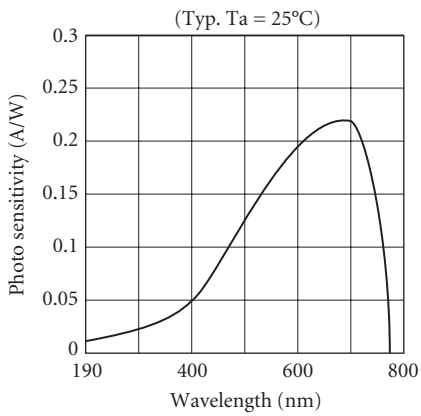

FIGURE 72 Spectral response of a 190- to 760-nm GaAsP photodiode detector vertical scale of amps/watt versus wavelength.

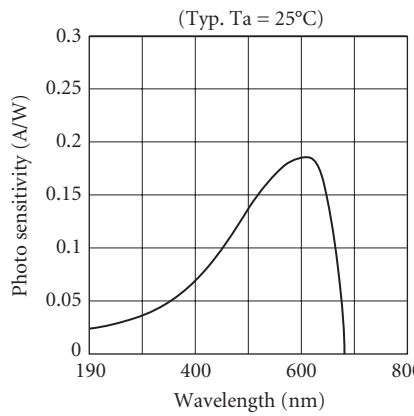

FIGURE 73 Spectral response of a 190- to 680-nm GaAsP photodiode detector vertical scale of amps/watt versus wavelength.

CdS and CdSe Cadmium sulfide and cadmium selenide photoconductors are available for detection of visible light out to 700 to 800 nm. CdS and CdSe films have sheet resistivity in the range of 20 mΩ per square at an illumination level of 2 footcandles. The devices are typically made in a linear or serpentine configuration consisting of 2 to 500 squares to maximize the length-to-width ratio. A variety of material "types" are available, offering unique spectral curves for various applications, depending upon the source color. CdS and CdSe are typically slow detectors, with response times of 5 to 100 ms, with speed improving at higher light levels. These devices exhibit "memory" or "history" effects, where the response is dependent upon the storage condition preceding use—the length of storage and time in use, and differences between the storage light level and the light level during use. These history effects may amount to changes in resistance from less than 10 percent to over 500 percent. CdSe has comparably greater memory effect than CdS.

Downloaded from Digital Engineering Library @ McGraw-Hill (www.accessengineeringlibrary.com)
Copyright © 2010 The McGraw-Hill Companies. All rights reserved.
Any use is subject to the Terms of Use as given at the website.

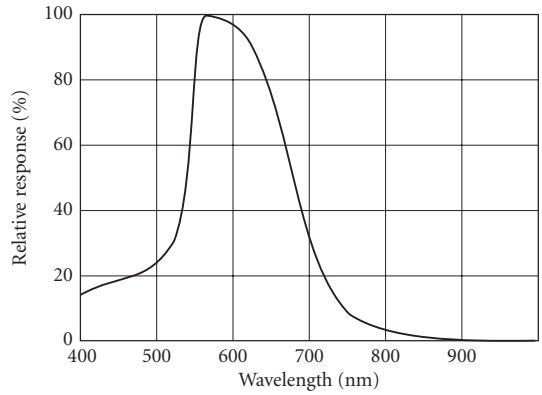

FIGURE 74 Relative spectral response of a "Type 0" CdS photocell. (*http://optoelectronics.perkinelmer.com/content/RelatedLinks/Brochures/BRO_PhotoconductiveCellsAndAnalogOptoiso.pdf.*)

CdS and CdSe are useful for a variety of commercial applications, both analog and digital, such as camera exposure control, automatic focus and brightness controls, densitometers, night light controls, etc. They are comparatively inexpensive and are available in a wide range of packages and resistance values, including dual cell configurations.

Spectral response: See Figs. 74 to 76.

Resistance and sensitivity: See Figs. 77 to 78.

Temperature coefficient of resistance: See Figs. 79, 80.

Light history effects: See Table 3.

Detector size: 4 × 4 mm to 12 × 12 mm approximate, dual elements available.

Manufacturers: In the previous edition, the listed supplier was EG&G VACTEK. Their product line has been acquired by Perkin Elmer. In this transition, all but two of the detector "types" have

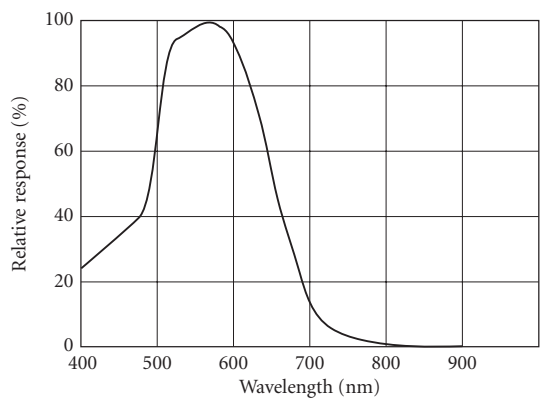

FIGURE 75 Relative spectral response of a "Type 3" CdS photocell. (*http://optoelectronics.perkinelmer.com/content/RelatedLinks/Brochures/BRO_PhotoconductiveCellsAndAnalogOptoiso.pdf.*)

Downloaded from Digital Engineering Library @ McGraw-Hill (www.accessengineeringlibrary.com)
Copyright © 2010 The McGraw-Hill Companies. All rights reserved.
Any use is subject to the Terms of Use as given at the website.

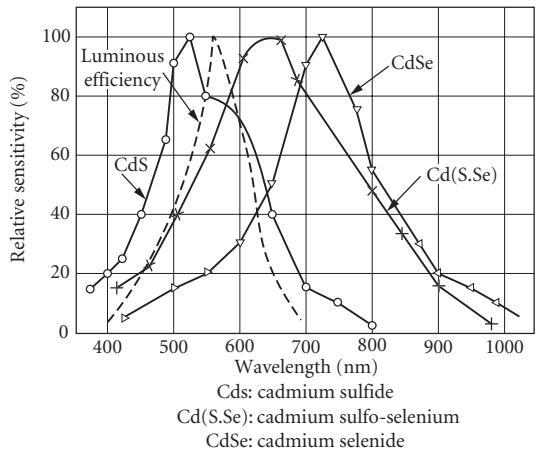

FIGURE 76 Spectral response of CdS, CdSSe, and CdSe photocell detectors together with the human eye response or luminous efficiency. (*http://www.selcoproducts.com/CFM/photocells/photocell_PDF/Selco_PhotoCells_Construct.pdf.*)

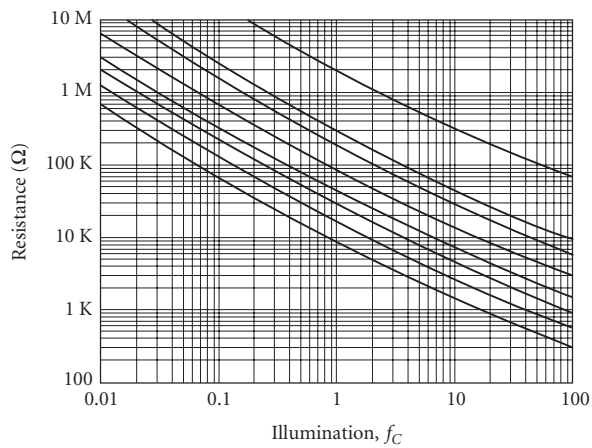

FIGURE 77 Resistance as a function of illumination for a "Type 0" CdS photocell. (*http://optoelectronics.perkinelmer.com/content/RelatedLinks/Brochures/BRO_PhotoconductiveCellsAndAnalogOptoiso.pdf.*)

been dropped—Perkin Elmer now only sells types 0 and 3. Other manufacturers offer comparable varieties and charts from at least one other producer are included.

Jameco Electronics:http://www.jameco.com/webapp/wcs/stores/servlet/CategoryDisplay?storeId=10001&catalogId=10001&langId=-1&categoryId=151080, Perkin Elmer: http://optoelectronics.perkinelmer.com/catalog/Category.aspx?CategoryName=Photocells, Selco Products: http://www.selcoproducts.com/CFM/photocell_toc.cfm, Silonex: http://www1.silonex.com/optoelectronics/optophotoc.html

Downloaded from Digital Engineering Library @ McGraw-Hill (www.accessengineeringlibrary.com)
Copyright © 2010 The McGraw-Hill Companies. All rights reserved.
Any use is subject to the Terms of Use as given at the website.

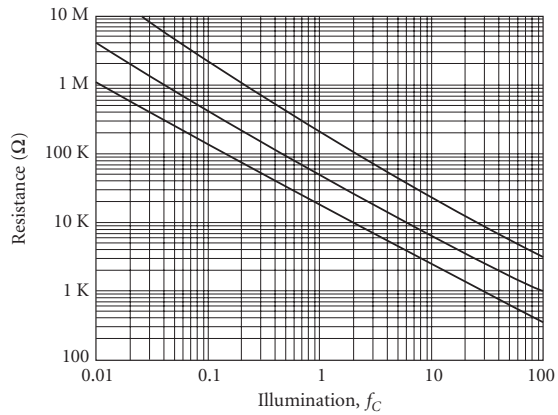

FIGURE 78 Resistance as a function of illumination for a "Type 3" CdS photocell. (*http://optoelectronics.perkinelmer.com/content/RelatedLinks/Brochures/BRO_PhotoconductiveCellsAndAnalogOptoiso.pdf.*)

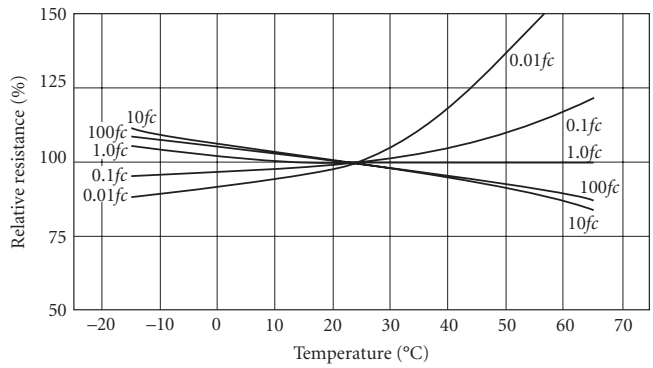

FIGURE 79 Relative resistance as a function of temperature for a "Type 0" CdS photocell. (*http://optoelectronics.perkinelmer.com/content/RelatedLinks/Brochures/BRO_PhotoconductiveCellsAndAnalogOptoiso.pdf.*)

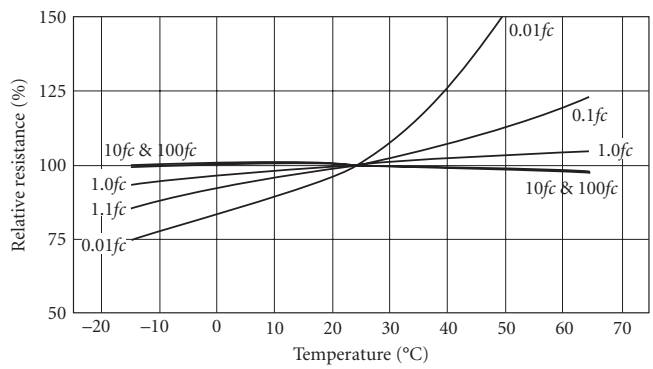

FIGURE 80 Relative resistance as a function of temperature for a "Type 3" CdS photocell. (*http://optoelectronics.perkinelmer.com/content/RelatedLinks/Brochures/BRO_PhotoconductiveCellsAndAnalogOptoiso.pdf.*)

Downloaded from Digital Engineering Library @ McGraw-Hill (www.accessengineeringlibrary.com)
Copyright © 2010 The McGraw-Hill Companies. All rights reserved.
Any use is subject to the Terms of Use as given at the website.

TABLE 3 Typical Variation of Resistance with Light History Expressed as a Ratio R_{LH}/R_{DH} at Various Test Illumination Levels in Foot Candles.

Illumination (foot candles)	0.01	0.1	1.0	10	100
R_{LH}/R_{DH} ratio	1.55	1.35	1.20	1.10	1.10

(http://optoelectronics.perkinelmer.com/content/RelatedLinks/Brochures/BRO_PhotoconductiveCellsAndAnalogOptoiso.pdf.)

R_{LH} is the resistance after "infinite" exposure to light, while R_{DH} is the resistance after "infinite" exposure to a dark environment. Infinite may be approximated by 24 hours.

CdTe Cadmium telluride and cadmium zinc telluride detectors are chemical group II-VI materials having an energy bandgap of about 1.6 eV, corresponding to a spectral cutoff in the vicinity of 775 nm. These devices, however, are principally used for gamma ray detection because of their high z number which translates into a high absorption coefficient for gamma rays. The principal advantage of CdTe in this application is its ability to operate at room temperature, in comparison with Ge gamma ray detectors which must typically be cooled to 77 K. Figure 81 illustrates the absorption of CdTe as a function of gamma ray energy out to 300 keV.

Sensitivity: See Fig. 81.

Standard sizes: Wafers in 10- and 16-mm diameter; rods 7 × 2 × 2 mm; cubes 2 × 2 × 2 mm.

Standard thickness: 1 and 2 mm.

Bias voltage: 150 to 300 V/cm.

Operating temperature range: –10 to +55°C

Leakage current: 10 to 300 nA

Capacitance: 10 pF

Response time: < 1 μs.

Manufacturers: Acrorad: http://www.acrorad.co.jp/us/index.html, Aurora, II-VI eV Products: http://www.evproducts.com/, Perkin Elmer, Radiation Monitoring Devices: http://www.rmdinc.com/products/p007.html

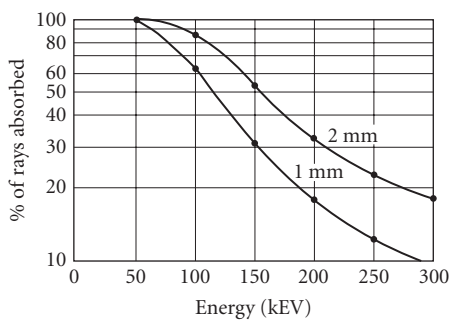

FIGURE 81 The high percentage of rays absorbed by CdTe makes these detectors highly sensitive. At 100 keV, a 2-mm-thick detector absorbs 85 percent of the rays. (*Radiation monitoring devices, Cadmium Telluride brochure.*)

Downloaded from Digital Engineering Library @ McGraw-Hill (www.accessengineeringlibrary.com)
Copyright © 2010 The McGraw-Hill Companies. All rights reserved.
Any use is subject to the Terms of Use as given at the website.

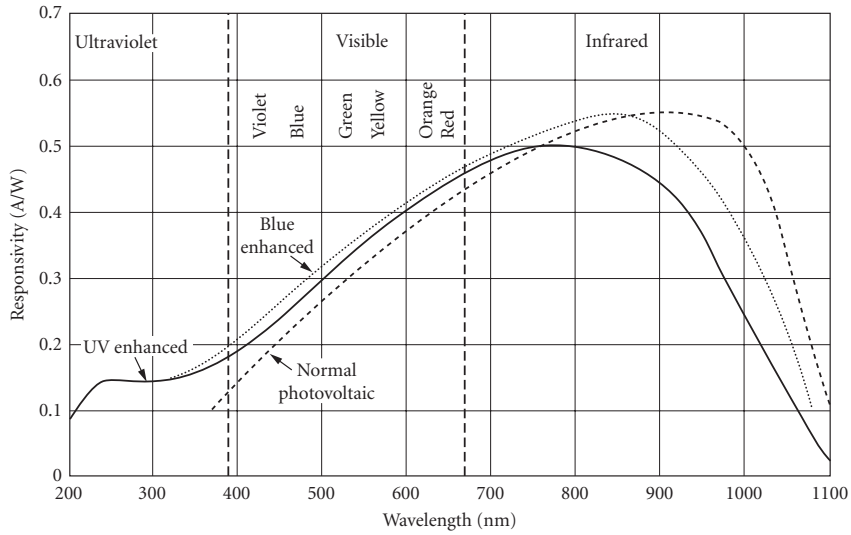

FIGURE 82 Typical spectral response for *pn* junction, blue-enhanced, and UV-enhanced silicon photodiodes. (*UDT Sensors, Inc., Optoelectronic Components Catalog.*)

Si Silicon photovoltaic detectors are widely available. They are useful at wavelengths shorter than about 1.1 μm and can even be used for x-ray and gamma-ray detection. There are four main silicon detector types:

- *pn* junction photodiodes, generally formed by diffusion, but ion implantation can also be used.
- *pin* junctions, which have lower capacitance and hence higher speed, and because of a thicker active region have enhanced near-IR spectral response.
- UV- and blue-enhanced photodiodes
- Avalanche photodiodes with significant internal gain, combining high speed and sensitivity

The main parameters of interest are spectral response (see Fig. 82), time constant, and zero-bias resistance or reverse-bias leakage current. Silicon material has an indirect bandgap and hence the spectral cutoff is not very sharp near its long-wavelength limit as shown in Fig. 82. The effective time constant of *pn* junction silicon detectors is generally limited by resistance-capacitance (RC) considerations rather than by the inherent speed of the detection mechanism (drift and/or diffusion). High reverse bias may or may not shorten charge collection time, but it generally reduces cell capacitance, and therefore the RC product, therefore, reverse bias usually results in faster response.

On the other hand, increased reverse bias causes increased noise, so that a trade-off exists between speed and sensitivity. For high-frequency applications, load resistance should be made small, although this makes Johnson (thermal) noise comparatively larger, which limits sensitivity (see Fig. 83). In order to keep sensitivity high when using these devices at high frequency, operational (current-mode) amplifiers, which can be built into the detector package, and avalanche photodiodes, which incorporate built-in gain before the load resistor is encountered, have been developed. Very careful regulation of the detector bias is required for stable operation of avalanche photodiodes.

Silicon pn junction photodiodes These are general purpose when high sensitivity is required and time constants on the order of a microsecond are permissible. The device construction is illustrated in Fig. 84. These devices are typically operated in a photovoltaic mode at zero bias, but can be used in a photoconductive mode in which the device is reverse biased.

Downloaded from Digital Engineering Library @ McGraw-Hill (www.accessengineeringlibrary.com)
Copyright © 2010 The McGraw-Hill Companies. All rights reserved.
Any use is subject to the Terms of Use as given at the website.

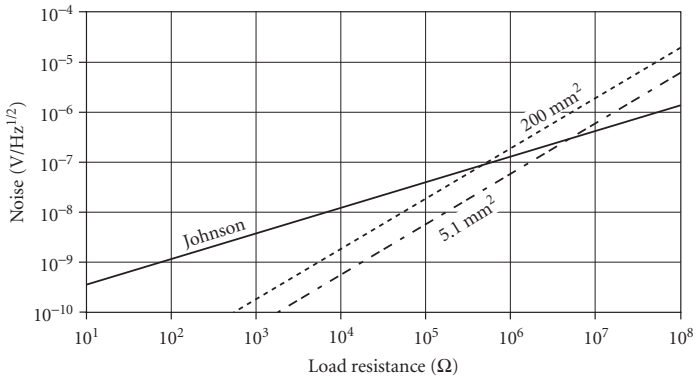

FIGURE 83 Output noise as a function of circuit load resistance for *pin* silicon photodiodes with areas of 5.1 and 200 mm^2, compared with the Johnson noise of the load resistor. Dark current measured at 10-V reverse bias for the detector with area of 5. 1 mm^2 is 10 nA, and 100 nA for the detector with an area of 200 mm^2. Note that good preamplifiers have a noise level of about 1 nV/Hz$^{1/2}$, depending upon the bandwidth. (*Detector data from UDT Sensors, Optoelectronic Components Catalog.*)

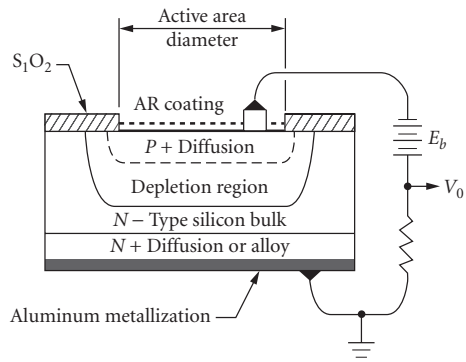

FIGURE 84 Planar diffused silicon photodiode construction. (*UDT Sensors, Inc., Optoelectronic Components Catalog.*)

Sensitivity: $D^*(\lambda_{pk}) \approx$ mid-10^{12} to 10^{13} Jones, $D^*(2800\ \text{K}) \approx 2 \times 10^4$ Jones, becoming amplifier-limited for small-area detectors (see Figs. 85 and 86). D^* can also be estimated from the R_0A product (detector zero-bias resistance or shunt resistance diode area), which is illustrated in Fig. 87, in combination with Fig. 19, which illustrates the dependence of D^* on R_0A product.

Noise: See Figs. 88 (noise vs. bias) and 89 (noise vs. temperature); as T drops, impedance rises, so that decreasing noise current produces increasing noise voltage. However, the signal increases even faster, yielding an improved signal-to-noise ratio with cooling. Figure 90 (noise vs. frequency) shows the dependence on bias.

Capacitance: Capacitance is proportional to area and increases slightly with temperature (see Fig. 91).

Responsivity: See Figs. 82 and 88.

Quantum efficiency: >90 percent quantum efficiency achievable with antireflection coating.

Sensitive area: 0. 2 to 600 mm^2 areas are readily available.

Downloaded from Digital Engineering Library @ McGraw-Hill (www.accessengineeringlibrary.com)
Copyright © 2010 The McGraw-Hill Companies. All rights reserved.
Any use is subject to the Terms of Use as given at the website.

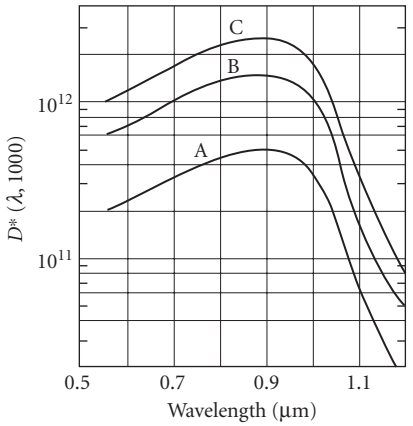

FIGURE 85 D^* versus 1 for small-area junction silicon photodiodes: curves A, B, and C correspond to areas of 0.02, 0.2, and 1 cm^2. The lower D^* for smaller area detector performance is due to amplifier limitations rather than intrinsically poorer D^*, for small-area detectors. (*Texas Instruments, Infrared Devices, SC-8385-366. Reprinted by permission of Texas Instruments.*)

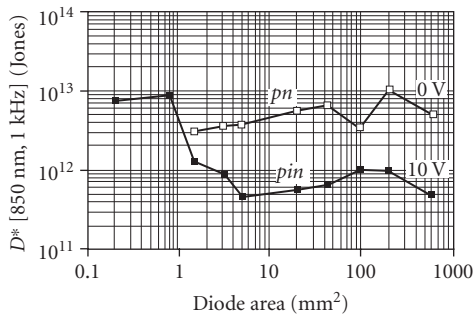

FIGURE 86 D^* as a function of diode area for *pn* junction silicon photodiodes operated in the photovoltaic mode (0 V) and *pin* junction diodes operated in the photoconductive or reverse-bias mode (10 V). (*UDT Sensors, Optoelectronic Components Catalog.*)

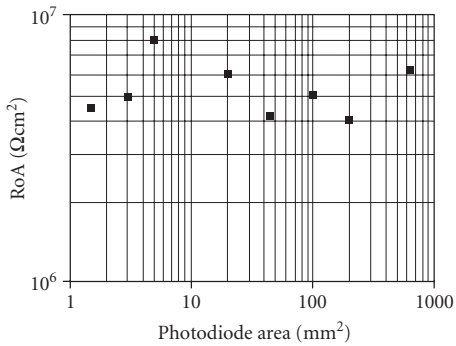

FIGURE 87 The resistance-area product (R0A) at zero bias and 295 K of silicon *pn* junction photodiodes. The lack of area dependence is evidence that intrinsic properties of the junction, rather than surface effects, are dominant in these devices.

Time constant: Inherently slow for high-sensitivity applications, generally limited by RC (depends directly on device area), but can be limited by carrier diffusion outside the depletion region or by trapping of carriers in deep impurity centers. Typical data for a circuit using a 50-Ω load resistor is illustrated in Fig. 92.

Operating temperature: Ambient, but noise (leakage current) can be reduced by operating at lower temperatures (see Fig. 76 for typical signal and noise vs. temperature).

Uniformity: Typically ±8 percent across a diode area with a 40-μm focused light spot.

Linearity: 5 percent or better over 10 orders of magnitude flux from 10^{-13} to 10^{-3} W/cm^2.

Downloaded from Digital Engineering Library @ McGraw-Hill (www.accessengineeringlibrary.com)
Copyright © 2010 The McGraw-Hill Companies. All rights reserved.
Any use is subject to the Terms of Use as given at the website.

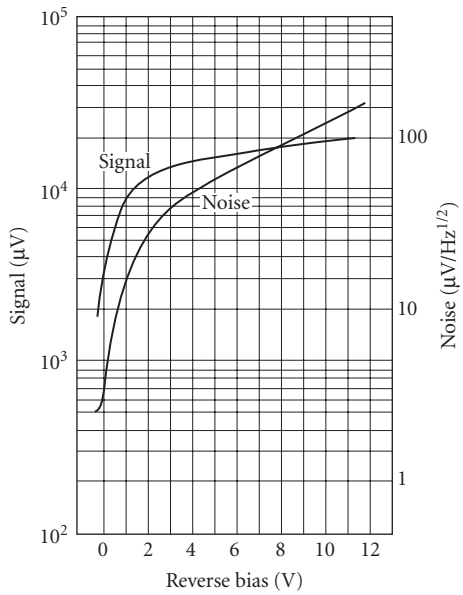

FIGURE 88 Typical *pn* junction signal and noise versus reverse bias ($R_L = 10$ MΩ). (*Electronuclear Laboratories, Bull. 1053, 1966.*)

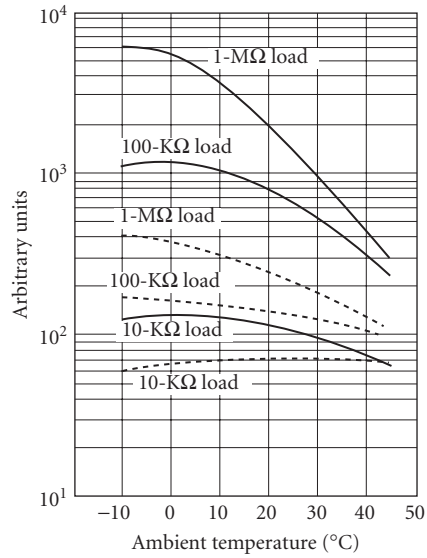

FIGURE 89 Relative signal and noise versus temperature for *pn* junction silicon photodiode at zero bias; — = signal; --- = noise. (*Electronuclear Laboratories, Bull. 1052, 1966.*)

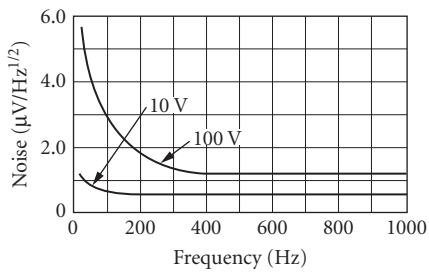

FIGURE 90 Typical *pn* junction and *pin* junction noise-frequency spectrum for different reverse bias ($A = 1 \times 1$ mm; $R_L = 1$ MΩ). (*Electronuclear Laboratories, Bull. 1078, 1966.*)

Recommended circuit: See Fig. 93. High-impedance FET current-mode amplifier to supply fixed bias voltage, regardless of current.

Stability: See Fig. 20 and section relating to stability. Check with manufacturer.

Manufacturers: Advanced Photonix, EG&G Canada, EG&G Heimann, Edmund Optics, Electro Optical Systems, Electro-Optics Technology, International Radiation Detectors, Janos Technology, Laser Precision Corp, Laser Systems Devices, Melles Griot, Newport/Klinger, Ophir Optronics, Optical Signature, Opto-Electronics, Optometrics, Oriel, Photonic Detectors, RMD, Sapidyne, Scientific Instruments, SEMICOA, Silonex, Spire, UDT Sensors.

Silicon pin junction photodiodes The *pin* junction detector is faster but is also somewhat less sensitive than conventional *pn* junction detectors. *PIN* photodiodes have slightly extended red

Downloaded from Digital Engineering Library @ McGraw-Hill (www.accessengineeringlibrary.com)
Copyright © 2010 The McGraw-Hill Companies. All rights reserved.
Any use is subject to the Terms of Use as given at the website.

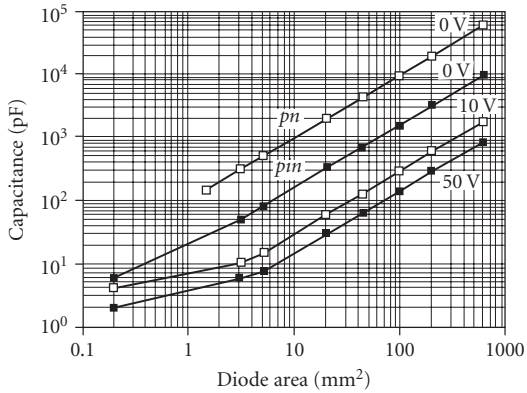

FIGURE 91 Capacitance as a function of detector area for *pn* junction silicon photodiodes operated in the photovoltaic mode (0 V) and *pin* junction photodiodes at 0-, 10-, and 50-V reverse bias. The larger depletion width, which is a consequence of the lightly doped "*i*" region in the *pin* device, gives *pin* diodes lower capacitance for the same device area. (*UDT Sensors, Optoelectronic Components Catalog.*)

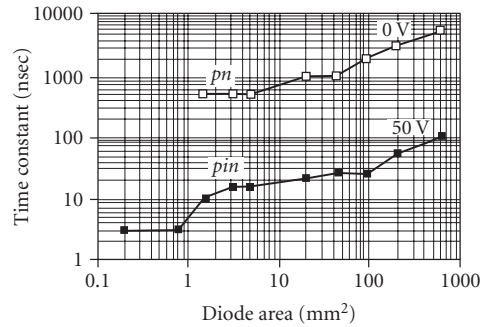

FIGURE 92 Time constant for *pn* junction silicon photodiodes operated in the photovoltaic mode (0 V) and a *pin* junction detector in the photoconductive or reverse-bias mode (50 V). A 50-Ω load was used in both cases, which limits sensitivity because of Johnson noise (see also Fig. 83). (*UDT Sensors, Optoelectronic Components Catalog.*)

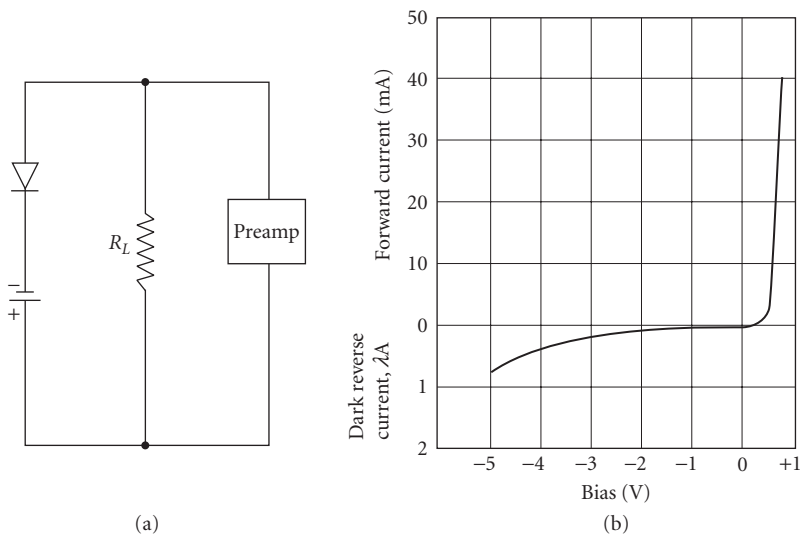

FIGURE 93 *pn* junction silicon photodiode: (*a*) recommended circuit; (*b*) typical electrical characteristics. (*Texas Instruments, Bull. SC-8385-366. Reprinted by permission of Texas Instruments.*)

response. In the normal *pn* junction, charge-collection time has a slow and a fast component. The fast component is due to photons absorbed in the depletion layer of the *pn* junction. Since the electric field in the depletion region is strong, carriers are quickly separated by drift through the electric field across the depletion region. However, photons absorbed deeper in the material, beyond the depletion region, produce carriers which must diffuse to the junction before they are collected, and diffusion times are on the order of a microsecond. This component becomes more significant near the

Downloaded from Digital Engineering Library @ McGraw-Hill (www.accessengineeringlibrary.com)
Copyright © 2010 The McGraw-Hill Companies. All rights reserved.
Any use is subject to the Terms of Use as given at the website.

long-wavelength limit of the spectral response. Application of reverse bias in an ordinary *pn* junction detector reduces the capacitance, shortening the RC time constant, and increases the width of the depletion layer thereby increasing the fraction of photons absorbed within the high field region and proportionally increasing the fraction of the fast component of the response.

However, the doping level of the ordinary *pn* junction limits the extent of the depletion layer increase to only 5 to 10 μm at a reverse bias of 50 V (this assumes an abrupt junction with a concentration of 1×10^{15} cm^{-3}). *pin* detectors incorporate a very lightly doped region between the *p*- and *n*-regions that allows a modest reverse bias to form a depletion region the full thickness of the material (500 μm for a typical silicon wafer). Extended red response in a pin device is a consequence of the extended depletion layer width, since longer wavelength photons will be absorbed in the active device region. Unfortunately, the higher dark current collected from generation within the wider depletion layer results in lower sensitivity. Generation of carriers can be minimized by minimizing the concentration of deep-level impurity centers in the detector with careful manufacturing. Operation at lower temperature will also reduce the dark current.

Sensitivity: D^*_{pk} 1×10^{12} Jones for 2-mm^2 area (depends slightly on bias, see Figs. 86 and 94). For high-speed operation, detectivity is lower (see Fig. 83).

Noise: Depends upon diode area and circuit load resistance. Johnson noise will dominate at low values of load resistance when circuit is optimized for fast response. Preamp noise may also limit. See Fig. 83.

Responsivity: Similar to *pn* junction. See Fig. 82.

Quantum efficiency: 90 percent quantum efficiency achievable with antireflection coating.

Capacitance: Proportional to detector area. See Fig. 91.

Operating temperature: See Fig. 95.

Time constant: Varies with capacitance (device area); see Fig. 92.

Sensitive area: 0. 2 to 600 mm^2 readily available.

Recommended circuit: Same as for *pn* junction photodiodes. See Figs. 93 and 96.

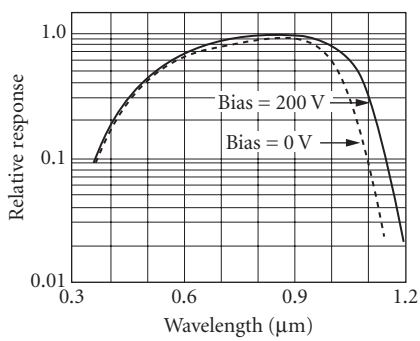

FIGURE 94 Dependence of spectral response on bias for silicon photodiodes. (*Electronuclear Laboratories, Bull. 1076, 1968.*)

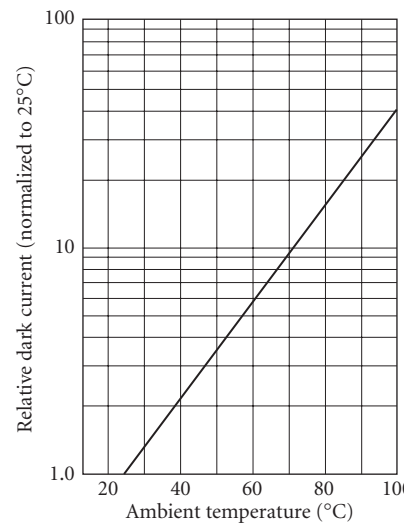

FIGURE 95 Relative dark current versus temperature for *pin* junction silicon photodiodes—bias 100 V. (*Electronuclear Laboratories, Bull. 1076, 1969.*)

Downloaded from Digital Engineering Library @ McGraw-Hill (www.accessengineeringlibrary.com)
Copyright © 2010 The McGraw-Hill Companies. All rights reserved.
Any use is subject to the Terms of Use as given at the website.

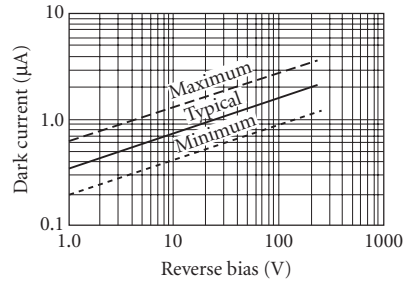

FIGURE 96 Typical dark current versus bias for *pin* silicon phototdiode ($A = 1 \times 1$ mm). (*Electronuclear Laboratories, Bull. 1078, 1968.*)

Stability: See Fig. 20 and section relating to stability. Check with manufacturer.

Manufacturers: Same as for *pn* junction photodiodes.

UV -and blue-enhanced photodiodes Blue- and UV-enhanced photodiodes may improve the quantum efficiency by 50 to 100 percent over standard photodiodes in the blue and UV spectral region. The quantum efficiency of ordinary *pn* and *pin* junction photodiodes degrades rapidly in the blue and UV spectral regions. This is because the high absorption coefficient of silicon at these wavelengths causes the photocarriers to be generated within the heavily doped *p*- (or *n*-) type contact surface where the lifetime is short due to the high doping and/or surface recombination. Blue- and UV-enhanced photodiodes optimize the response at short wavelengths by minimizing near-surface carrier recombination. This can be achieved by using very thin and highly graded *p* (or *n* or metal Schottky) contacts, by using lateral collection to minimize the percentage of the surface area which is heavily doped, and/or passivating the surface with a fixed surface charge to repel minority carriers from the surface. These devices typically have quartz windows or UV-transmissive glass, compatible with good transmission into the UV spectrum. The user should be aware that UV and higher energy radiation in particular can alter the fixed charge conditions in the surface region of silicon and other detectors (typically in the surface oxide) which can cause the detector performance to drift and/or be unstable (see Fig. 20).

Sensitivity: See Figs. 82 and 97; D^*_{pk} 3–5 $\times 10^{12}$ Jones for diodes with areas of 1–100 mm^2 at $V_R = 0$, $R_L = 40$ MΩ.

Quantum efficiency: Same as *pn* junction photodiodes, but enhanced in the UV and blue regions by 50 percent or more (see Fig. 82).

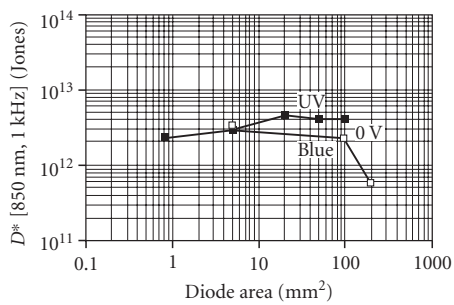

FIGURE 97 D^* as a function of diode area for blue- and UV-enhanced silicon photodiodes operating in the photovoltaic mode (0-V bias). (*UDT Sensors, Optoelectronic Components Catalog.*)

Downloaded from Digital Engineering Library @ McGraw-Hill (www.accessengineeringlibrary.com)
Copyright © 2010 The McGraw-Hill Companies. All rights reserved.
Any use is subject to the Terms of Use as given at the website.

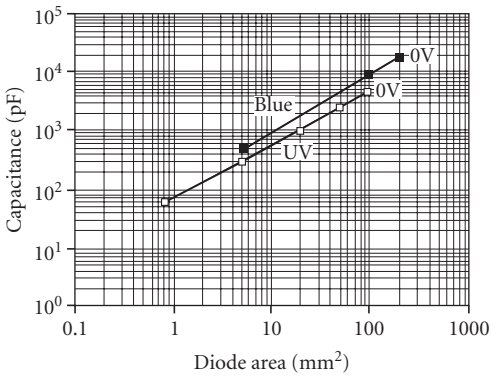

FIGURE 98 Capacitance as a function of detector area for blue- and UV-enhanced silicon photodiodes operated in the photovoltaic mode (0 V). The capacitance per unit area is close to that of *pn* junction photodiodes shown in Fig. 91. (*UDT Sensors, Opto electronic Components Catalog.*)

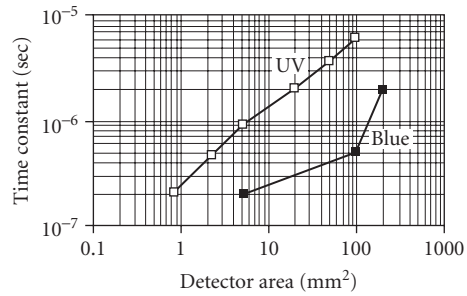

FIGURE 99 Time constant for UV- and blue-enhanced silicon photodiodes as a function of detector area at zero-volts bias. A 50-Ω load was used in both cases. (*UDT Sensors, Optoelectronic Components Catalog.*)

Responsivity: see Fig. 82.

Capacitance: Comparable to *pn* junction photodiodes (See Fig. 98).

Operating temperature: Ambient.

Time constant: Dependent upon device type. Increases with device area; 200 ns to 6 μs for areas 1 to 100 mm^2 (see Fig. 99).

Sensitive area: 1 to 200 mm^2 readily available.

Recommended circuit: Same as *pn* junction photodiodes.

Stability: See Fig. 20 and section relating to stability. Check with manufacturer.

Manufacturers: See list for silicon *pn* junction photodiodes.

Silicon avalanche photodiodes The avalanche photodiode, is especially useful where both fast response and high sensitivity are required. Whereas normal photodiodes become Johnson- or thermal-noise-limited when used with a low-impedance load resistor for fast response, avalanche photodiodes make use of internal multiplication, associated with reverse breakdown in the *pn* junction in order to keep the detector noise above the Johnson-noise level. [Because the response time is usually RC-limited, small load resistors (often 50 Ω) are used to achieve fast signal response.] However, as the load resistor is decreased, the detector noise voltage decreases in direct proportion, whereas the Johnson noise decreases only as the square root of the load resistor. Thus, the detector noise voltage can become lower than the Johnson noise for load resistance values smaller than a critical value. With an APD device, lower values of load resistors can be used without reaching the critical value because the internal gain boosts the detector noise voltage.

Stable avalanche or multiplication is made possible by a guard-ring construction using n^+pp^+, Schottky-nn^+, or $n^+p\pi p^+$ structure; beveled *pin* structure (see Fig. 100); mesa structures; or other structures which prevent surface breakdown.[25] However, very careful bias control is essential for stable performance. An optimum gain exists below which the system is limited by receiver noise and above which shot noise dominates receiver noise and the overall noise increases faster than the signal (Fig. 101).

In addition to fast-response applications, avalanche photodiodes are useful whenever amplifier noise is limiting, for example, small-area devices. Signal-to-noise-ratio improvements of one to two orders of magnitude over a nonavalanche detector can be achieved.

Downloaded from Digital Engineering Library @ McGraw-Hill (www.accessengineeringlibrary.com)
Copyright © 2010 The McGraw-Hill Companies. All rights reserved.
Any use is subject to the Terms of Use as given at the website.

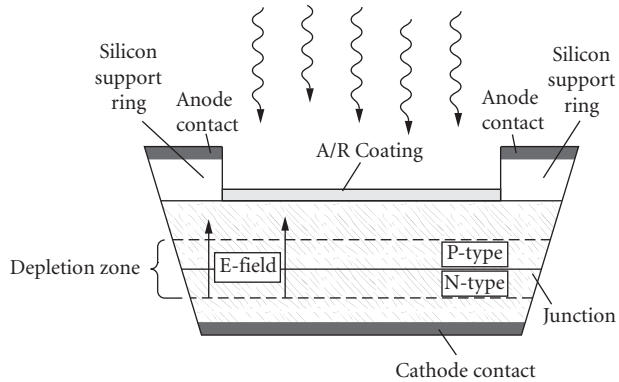

FIGURE 100 Cross section of a beveled-edge silicon avalanche photodiode. The beveled edge prevents early breakdown. (*Advanced Photonix. Avalanche Photodiode Catalog.*)

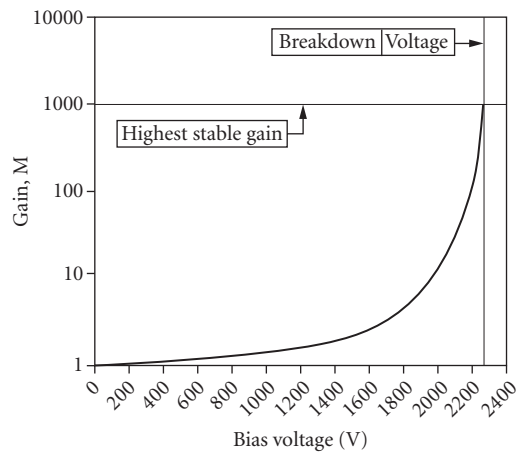

FIGURE 101 Gain as a function of reverse bias can reach 1000. This operating point is very close to breakdown and requires careful bias control. (*Advanced Photonix. Avalanche Photodiode Catalog.*)

APDs are sometimes used in combination with scintillator crystals such as CsI to detect high-energy radiation in the range of 10 to 1000 keV.

Sensitivity: D^* 3–5 × 10^{13} Jones (see Fig. 102).

Noise: Function of detector area. As gain increases, noise (dark current) increases (see Fig. 103). Optimum gain is where avalanche noise equals system noise. Thus, optimum gain is a function of system noise.

Responsivity: Photocurrent is the product of the incident optical power in watts, wavelength in micrometers, and quantum efficiency (η) divided by 1.24 and multiplied by the avalanche gain M.

$$I_{\text{photo}} = M(P\ \eta\ \lambda/1.24) \qquad \text{(See Figs. 101 and 104)}$$

Downloaded from Digital Engineering Library @ McGraw-Hill (www.accessengineeringlibrary.com)
Copyright © 2010 The McGraw-Hill Companies. All rights reserved.
Any use is subject to the Terms of Use as given at the website.

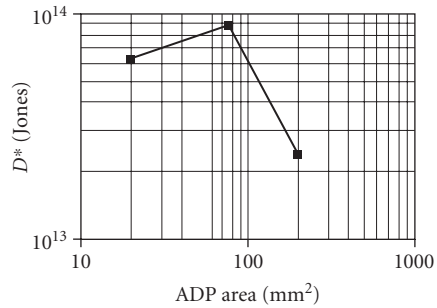

FIGURE 102 D^* for three silicon avalanche photodiodes shown as a function of diode area. (*Advanced Photonix. Avalanche Photodiode Catalog.*)

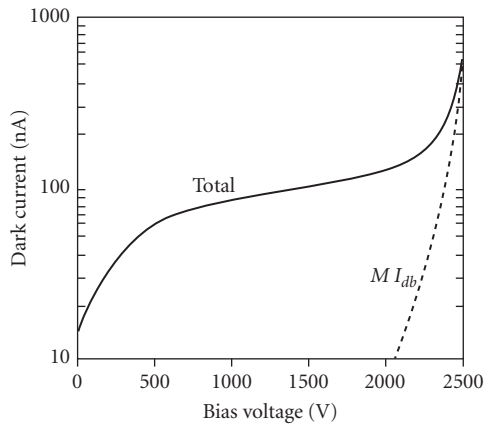

FIGURE 103 Dark current as a function of reverse bias for a 16-mm-diameter APD. At low-bias surface dark current dominates, but avalanche-multiplied bulk dark current increases rapidly as the gain increases. (*Advanced Photonix. Avalanche Photodiode Catalog.*)

Quantum efficiency: Typically 85-percent peak (see Fig. 104).

Capacitance: Depends on bias and area (see Fig. 105).

Sensitive area: 20 to 200 mm^2.

Series resistance: Depends on area; typical values are 40 Ω for 5-mm diameter to 5 Ω for 16-mm diameter

Time constant: See Fig. 106.

Recommended circuit: Requires a filtered high-voltage dc supply that itself must have very low noise and a load resistor. The output may be ac- or dc-coupled. (See Fig. 107.)

Operating temperature: 40 to 45°C.

Stability: Exposure to UV or high-energy radiation may affect dark current. See Fig. 20 and section relating to stability. Check with manufacturer.

Downloaded from Digital Engineering Library @ McGraw-Hill (www.accessengineeringlibrary.com)
Copyright © 2010 The McGraw-Hill Companies. All rights reserved.
Any use is subject to the Terms of Use as given at the website.

PHOTODETECTORS

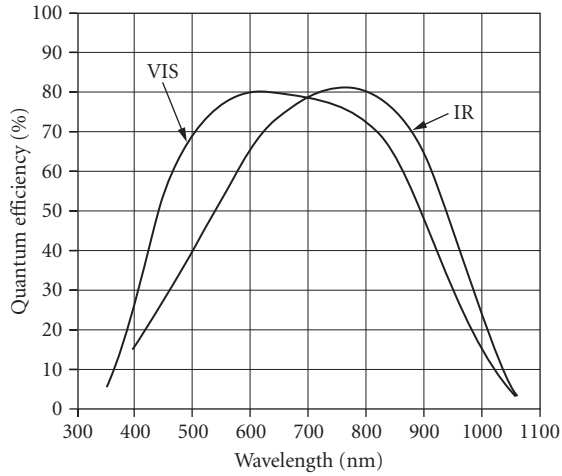

FIGURE 104 APD quantum efficiency at high gain. Adjustment of the oxide deposited on the surface produces two different curves. (*Advanced Photonix. Avalanche Photodiode Catalog.*)

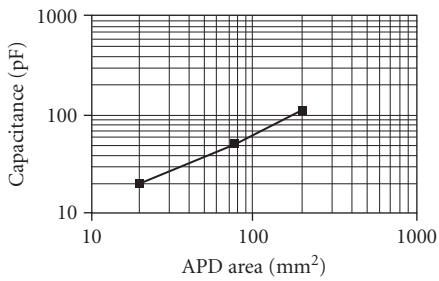

FIGURE 105 Capacitance for three silicon avalachche photodiodes shown as a function of diode area. (*Advanced Photonix. Avalanche Photodiode Catalog.*)

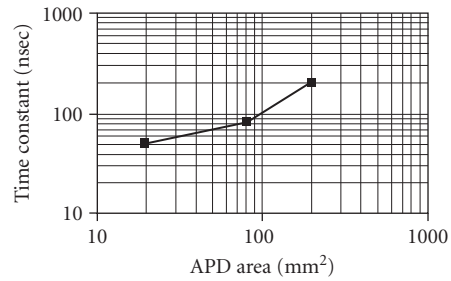

FIGURE 106 Time constant for three silicon avalanche photodiodes shown as a function of diode area. (*Advanced Photonix. Avalanche Photodiode Catalog.*)

Manufacturers: Advanced Photonix, Devar, EG&G Judson, EG&G Vactec, EG&G Canada, Edmund Optics, Electro-Optical Systems, Hamamatsu, Janos Technology, Newport/Klinger, Opto-Electronics (Ontario), Oriel, Photonic Detectors, Photonic Packaging Technologies, RMD, Texas Optoelectronics, Thorn EMI Electron Tubes.

InGaAs Indium gallium arsenide detectors have been developed for optimum performance with fiber-optic communications at 1.3 and 1.55 μm. This detector material has a direct bandgap and represents one of several compound semiconductor alloy systems specially developed for photodetectors. In the case of this alloy of two group III-V chemical compound semiconductors, the ratio of InAs to GaAs controls the spectral cutoff, allowing the detector to be optimized for a particular wavelength. InGaAs detectors have generally been specialized for high-speed applications with

Downloaded from Digital Engineering Library @ McGraw-Hill (www.accessengineeringlibrary.com)
Copyright © 2010 The McGraw-Hill Companies. All rights reserved.
Any use is subject to the Terms of Use as given at the website.

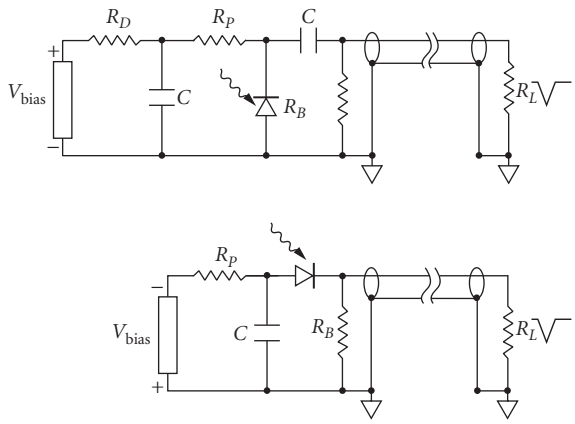

FIGURE 107 AC- and DC-coupled APD circuits with a filter following the power supply and a coaxial cable on the output. (*Adanced Photonix, Avalanche Photodiode Catalog.*)

optimum sensitivity since these performance factors can drive a fiber-optic system throughput and cost. For this reason, available devices include

- *PIN* photodiodes
- Avalanche photodiodes

The significance of these devices to fiber-optic applications is reflected in the number of vendors who sell integrated packages of InGaAs photodetectors combined with preamplifiers and fiber-optic pigtails.

The InGaAs alloy system allows the spectral response to be tailored to longer wavelengths than the quartz fiber-optic bands and devices with cutoffs of 2.2 and 2.6 μm are also available.

InGaAs pin photodiode

Sensitivity: D^* mid-10^{12} Jones for 1.67-μm cutoff; $D^* \approx 1 \times 10^{12}$ Jones for 2.2-μm cutoff, and $D^* \approx 5 \times 10^{11}$ Jones for 2.6-μm cutoff.

Responsivity: 0. 85 to 0. 95 A/W in the range of 1.3 to 1.55 μm.

Quantum efficiency: For 1.67-μm cutoff, see Fig. 108.

Dark current: See Fig. 109.

Capacitance: 0.7 to 1.2 × 10^4 pF/cm for 1.7-μm cutoff; 2.5 × 10^4 pF/cm for 1.85-μm cutoff; 3 × 10^4 pF/cm for 2.15-μm cutoff; 5 × 10^4 pF/cm for 2.65-μm cutoff. See also Fig. 110 for bias dependence.

Time constant: Varies with resistance-capacitance time (see Fig. 111). Since capacitance depends upon reverse bias, the time constant varies proportionally (see Fig. 110 for dependence of capacitance on bias).

Size: 0. 05 to 3-mm diameter.

Recommended circuit: Standard photodiode options; zero bias for best sensitivity, reverse bias for maximum speed.

InGaAs avalanche photodiode

Sensitivity: $D^* \approx 5 \times 10^{11}$ Jones for 1.7-μm cutoff. In the fiber-optics industry, the sensitivity is also given in power units of dBm. Figure 112 compares InGaAs *pin*, APD, and Ge APD sensitivities.

Downloaded from Digital Engineering Library @ McGraw-Hill (www.accessengineeringlibrary.com)
Copyright © 2010 The McGraw-Hill Companies. All rights reserved.
Any use is subject to the Terms of Use as given at the website.

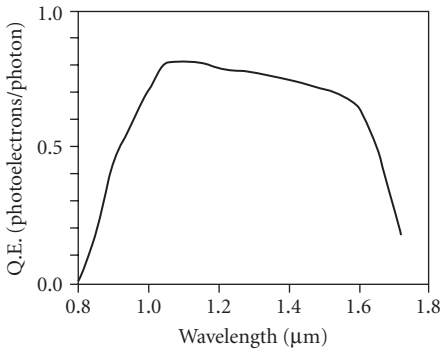

FIGURE 108 Spectral dependence of quantum efficiency for an InGaAs detector having a cutoff of 1.67 μm. (*Sensors Unlimited, data sheet.*)

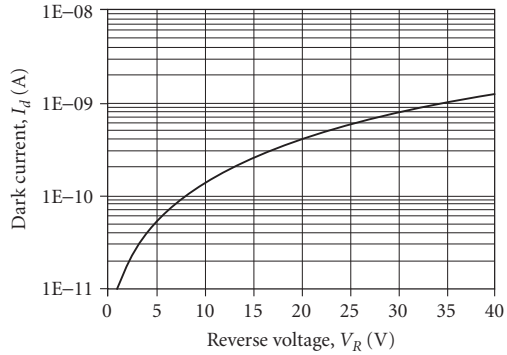

FIGURE 109 Dark current as a function of reverse-bias voltage for a 60-μm-diameter InGaAs detector having a cutoff of 1.67 μm. (*Fermionics, InGaAs Photodiodes.*)

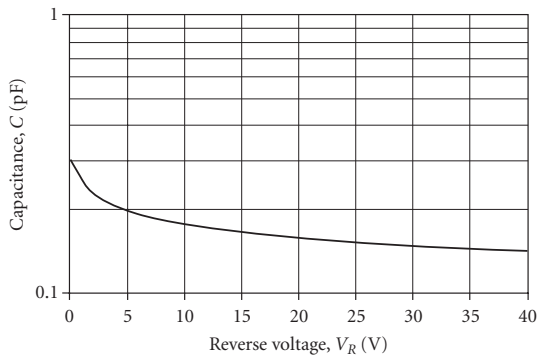

FIGURE 110 Capacitance as a function of reverse-bias voltage for a 60-μm-diameter InGaAs detector having a cutoff of 1.67 μm. (*Fermionics, InGaAs Photodiodes.*)

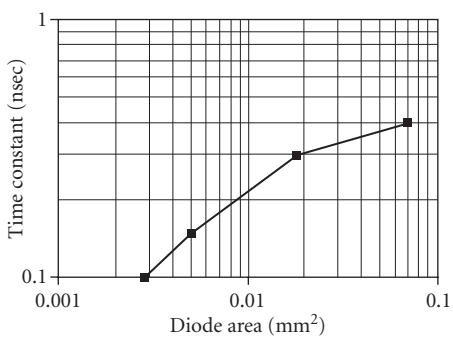

FIGURE 111 Time constant for small InGaAs *pin* photodiodes as a function of diode area measured with a 50-Ω load.

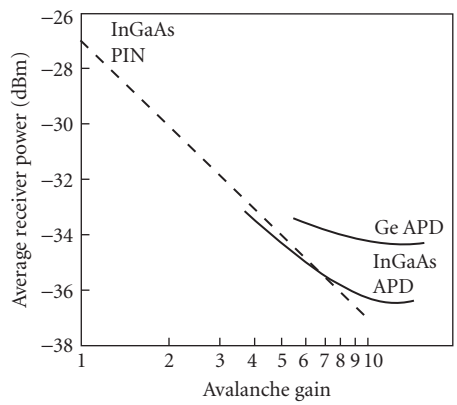

FIGURE 112 APD receiver sensitivity. Typical receiver sensitivity at a receiver rate of 1.7 Gbit/s and $\lambda = 1.3$ μm for an InGaAs pin, Ge APD, and an InGaAs APD. (*AT&T, 126A/B, C ASTROTEC InGaAs.*)

Downloaded from Digital Engineering Library @ McGraw-Hill (www.accessengineeringlibrary.com)
Copyright © 2010 The McGraw-Hill Companies. All rights reserved.
Any use is subject to the Terms of Use as given at the website.

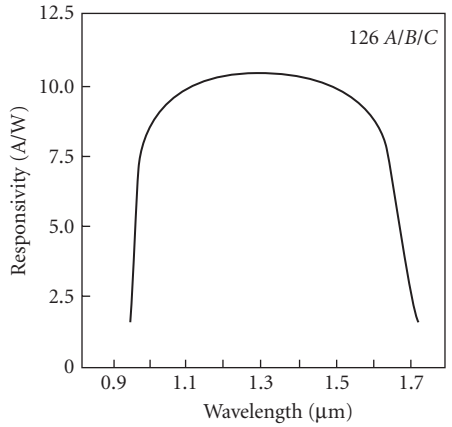

Note: Responsivity = (chip quantum efficiency) × gain × λ (μm)/1.24. The minimum chip quantum efficiency is 80%, and the minimum pigtail coupling efficiency is 90%.

FIGURE 113 Responsivity for an InGaAs avalanche photodiode versus wavelength for avalanche gain of 12. (*AT&T, 126A/B, C ASTROTEC InGaAs.*)

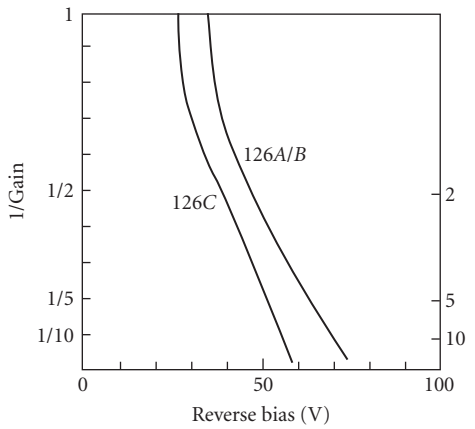

FIGURE 114 Inverse of avalanche gain for an InGaAs avalanche photodiode versus reverse bias. (*AT&T, 126A/B, C ASTROTEC InGaAs.*)

Spectral response: 1.0 to 1.65 μm; see Fig. 113.

Responsivity: 8 to 10 A/W typical.

Avalanche gain: Critically depends upon reverse bias, see Fig. 114.

Capacitance: At gain of 12, 7.5×10^4 pF/cm^2.

Bandwidth: Up to 3 GHz; see Figs. 115 and 116.

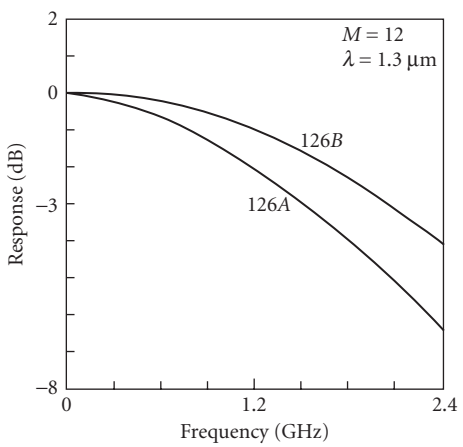

FIGURE 115 Frequency response of an InGaAs APD (126 A/B). (*AT&T, 126A/B, C ASTROTEC InGaAs.*)

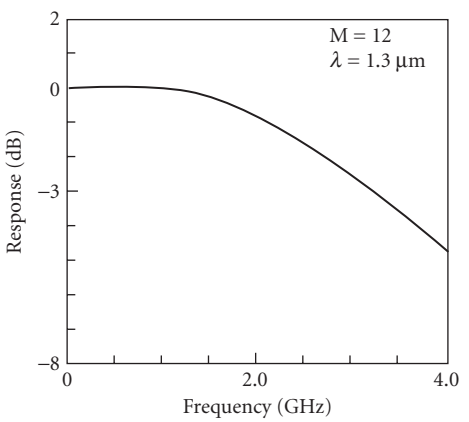

FIGURE 116 Frequency response of InGaAs APD (126C). (*AT&T, 126A/B, C ASTROTEC InGaAs.*)

Downloaded from Digital Engineering Library @ McGraw-Hill (www.accessengineeringlibrary.com)
Copyright © 2010 The McGraw-Hill Companies. All rights reserved.
Any use is subject to the Terms of Use as given at the website.

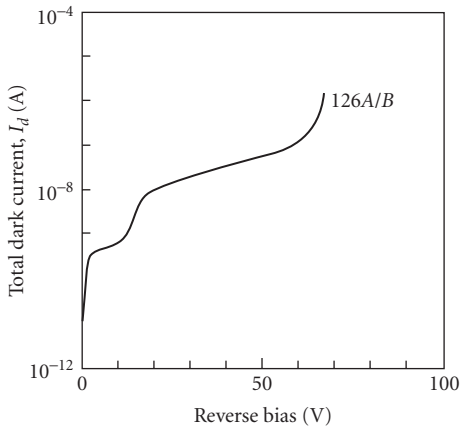

FIGURE 117 Dark current versus reverse bias of InGaAs APD (126A/B). (*AT&T, 126A/B, C ASTROTEC InGaAs.*)

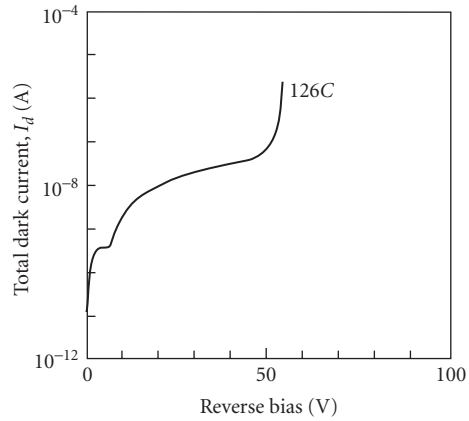

FIGURE 118 Dark current versus reverse bias of InGaAs APD (126C). (*AT&T, 126A/B, C ASTROTEC InGaAs.*)

Size: 0.04 to 0.5-mm diameter.

Dark current: Dependent upon reverse bias, device structure, and temperature. See Figs. 117, 118, and 119.

Recommended circuit: See Figs. 107 and 120.

Manufacturers: Advanced Photonix, AT&T, EG&G Canada, Edinburgh Instruments, Edmund Optics, Electro-Optical Systems, Electro-Optics Technology, Emcore, Epitaxx, Fermionics, GCA Electronics, Germanium Power Devices, Hamamatsu, New England Photoconductor, New Focus,

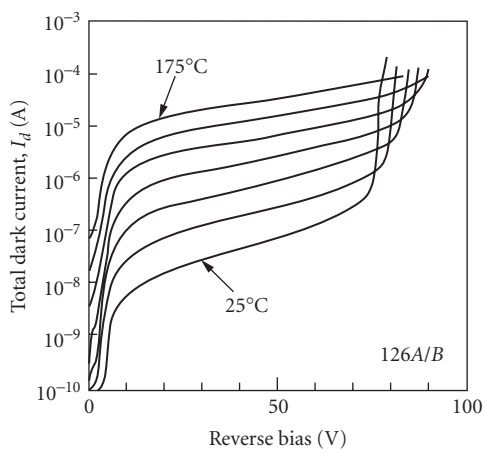

FIGURE 119 Dark current versus voltage of InGaAs APD as a function of temperature at 25°C increments. Note: The temperature dependence of the 126*C* dark current is the same as the 126*A*/*B*. (*AT&T, 126A/B, C ASTROTEC InGaAs.*)

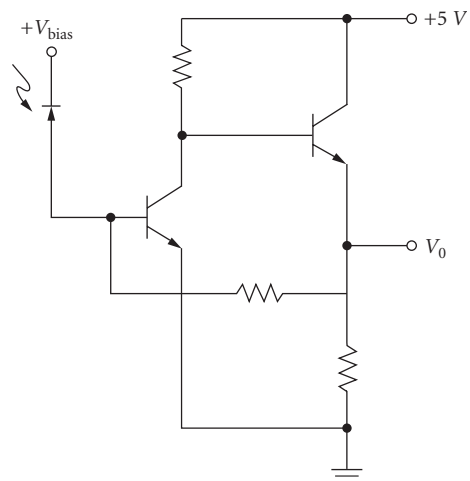

FIGURE 120 Bipolar transimpedance amplifier for InGaAs avalanche photodiode. (*AT&T, 126A/B, C ASTROTEC InGaAs; Optical Fiber Communications, John M. Senior, © 1985, Prentice-Hall; ISBN-0-13-638248-7.*)

Downloaded from Digital Engineering Library @ McGraw-Hill (www.accessengineeringlibrary.com)
Copyright © 2010 The McGraw-Hill Companies. All rights reserved.
Any use is subject to the Terms of Use as given at the website.

Newport, North Coast Scientific, Opto-Electronics, Ortel, Photonic Detectors, Goodrich Sensors Unlimited, Spire, Swan Associates, Telcom Devices, Teledyne Judson Technologies, UDT Sensors.

Ge Germanium intrinsic photodetectors are similar to intrinsic silicon detectors but offer spectral response out to 1.5 to 1.8 μm. *PN* junction photodiodes offer submicrosecond response or high sensitivity from the visible region to 1.8 μm. Zero bias is generally used for high sensitivity and large reverse bias for high speed. As in the case of silicon, germanium has an indirect bandgap and soft spectral cutoff. The previous discussion on silicon detectors applies in general, with the exception that blue- and UV-enhanced devices are not relevant to germanium detectors. Germanium detectors, because of their narrower bandgap, have higher leakage currents at room temperature, compared to silicon detectors. Detector impedance increases about an order of magnitude by cooling 20°C below room temperature. Thus, performance can improve significantly with thermoelectric cooling or cooling to liquid nitrogen temperature.

As with silicon, the device structure and bias configuration can affect spectral response and rise time. Three detector types are available:

- *pn* junction
- *pin* junction
- Avalanche photodiode

Germanium pn and pin

Sensitivity: D^*(peak, 300 Hz, room temperature) $>2 \times 10^{11}$ Jones, increases significantly with cooling by thermoelectric cooler or liquid nitrogen. (See Figs. 121, 122, and 123.)

Quantum efficiency: >50 percent with antireflection coating.

Noise: See Figs. 124 and 125.

Responsivity: 0.9 A/W at peak wavelength. See Fig. 121.

Capacitance: Lower for *pn* structure compared with *pn* diode. See Fig. 126.

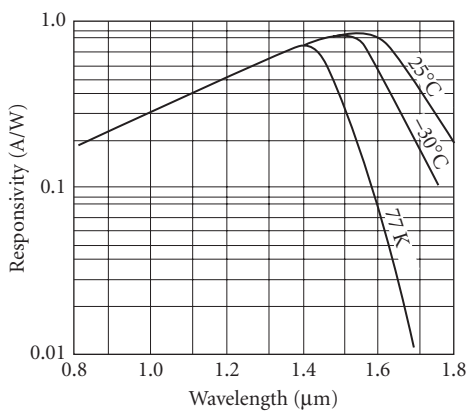

FIGURE 121 Spectral response for a germanium *pn* junction photodiode at three temperatures. (*Teledyne Judson Technologies, J16 germanium photodiodes, 2008.*)

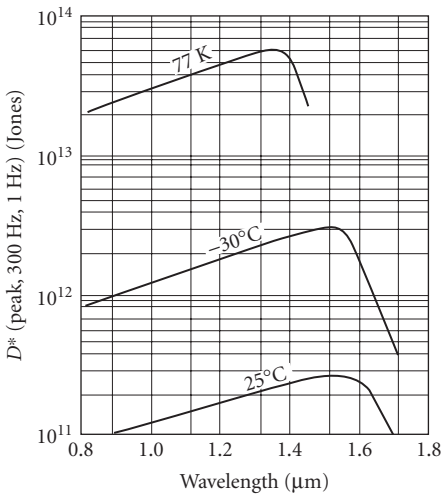

FIGURE 122 D^* as a function of wavelength for a germanium *pn* junction photodiode at three temperatures. (*EG&G Judson, Infrared Detectors, 1994.*)

Downloaded from Digital Engineering Library @ McGraw-Hill (www.accessengineeringlibrary.com)
Copyright © 2010 The McGraw-Hill Companies. All rights reserved.
Any use is subject to the Terms of Use as given at the website.

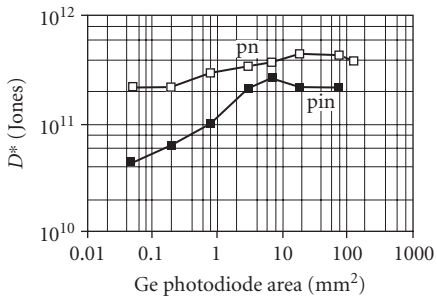

FIGURE 123 D^* for germanium *pn* and *pin* photodiodes shown as a function of diode area. (*EG&G Judson, Infrared Detectors, 1994.*)

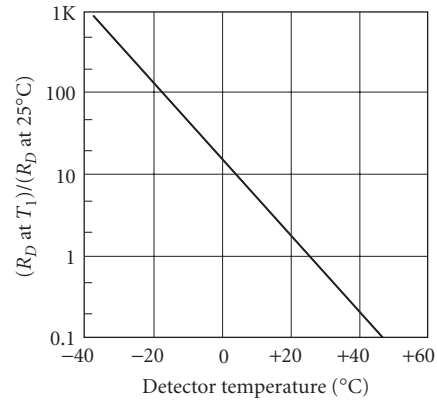

FIGURE 124 Ratio of resistance at temperature T to the resistance at 25°C for a germanium *pn* junction photodiode. (*Teledyne Judson Technologies, J16 germanium photodiodes, 2008.*)

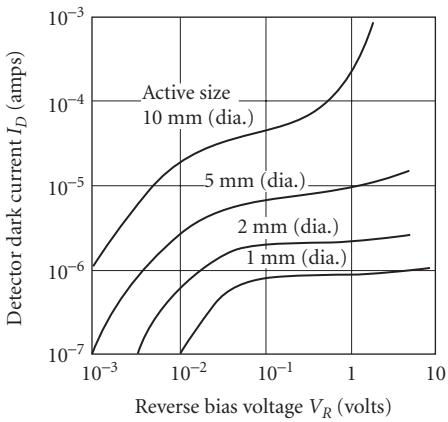

FIGURE 125 Dark current as a function of reverse bias for germanium *pn* junction photodiodes of different diameters at 25°C. (*Teledyne Judson Technologies, J16 germanium photodiodes, 2008.*)

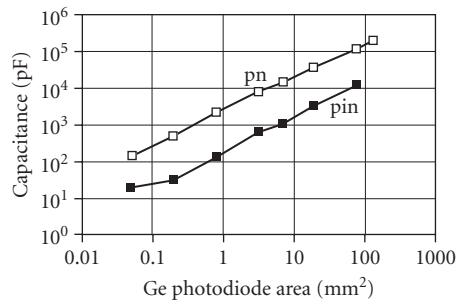

FIGURE 126 Capacitance for germanium *pn* and *pin* photodiodes shown as a function of diode area. (*EG&G Judson, Infrared Detectors, 1994.*)

Time constant: PIN diodes provide faster response. See Fig. 127.

Sensitive area: 0.25 to 13-mm diameter standard.

Operating temperature: Ambient, TE-cooled, or liquid nitrogen.

Profile: ±2 percent across active area at 1.3 μm.

Linearity: Excellent over 10 orders of magnitude. See Fig. 128.

Recommended circuit: See previous section on silicon photodiodes.

Manufacturers: Edinburgh Instruments, Electro-Optical Systems, Judson, Electro-Optical Systems, Fastpulse Technology, Germanium Power Devices, Infrared Associates, Newport, North Coast Scientific, Opto-Electronics, Oxford Instruments, Scientific Instruments.

Downloaded from Digital Engineering Library @ McGraw-Hill (www.accessengineeringlibrary.com)
Copyright © 2010 The McGraw-Hill Companies. All rights reserved.
Any use is subject to the Terms of Use as given at the website.

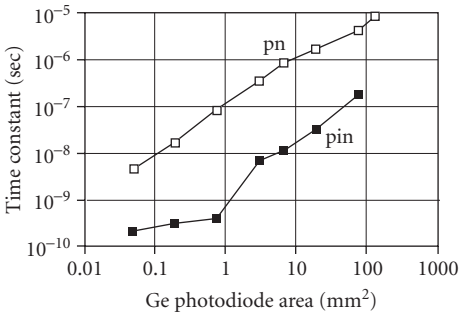

FIGURE 127 Time constant for germanium *pn* and *pin* photodiodes shown as a function of diode area. (*EG&G Judson, Infrared Detectors, 1994.*)

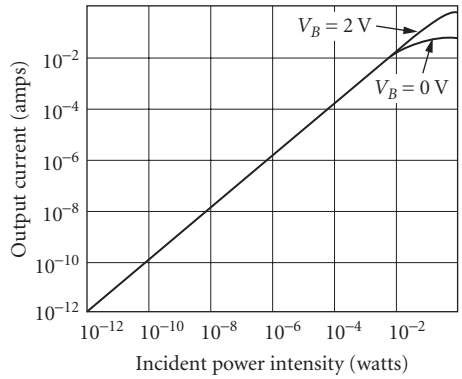

FIGURE 128 Linearity of a germanium *pn* junction photodiode. (*EG&G Judson, Infrared Detectors, 1994.*)

Germanium avalanche photodiode The germanium avalanche photodiode is similar to the silicon APD but has lower optimum gain, longer cut-off wavelength (1.7 μm), and higher leakage current. Germanium APDs combine the sensitivity of a Ge *pn* photodiode and the speed of a *pin* Ge photodiode.

Sensitivity: D^* 2×10^{11} Jones at 30 MHz for a diode with area of 5×10^{-2} mm^2 or about the same as for a *pn* Ge diode with the same area, and about a factor of 4 higher than a *pin* Ge photodiode (compare with Figs. 122 and 123). D^* depends on gain.

Gain: See Fig. 129.

Dark current: See Fig. 130.

Capacitance: 2 pF at 20-V reverse bias for 100-μm diameter, 8 pF at 20-V reverse bias for 300-μm diameter.

Quantum efficiency: 60 to 70 percent at 1.3 μm.

Responsivity: Photocurrent is the product of the incident optical power in watts, wavelength in micrometers, and quantum efficiency (η) divided by 1.24 and multiplied by the avalanche gain M. $I_{photo} = M(P\lambda\eta/1.24)$. (See Figs. 121 and 129).

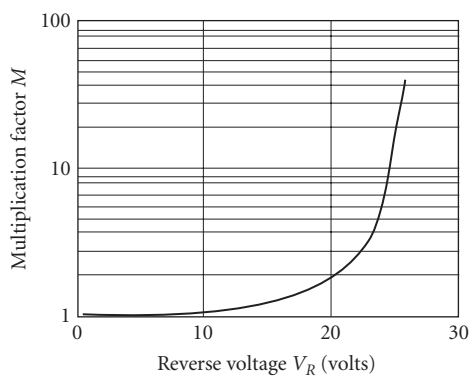

FIGURE 129 Gain as a function of reverse bias for germanium avalanche photodiode. (*EG&G Judson, Infrared Detectors, 1994.*)

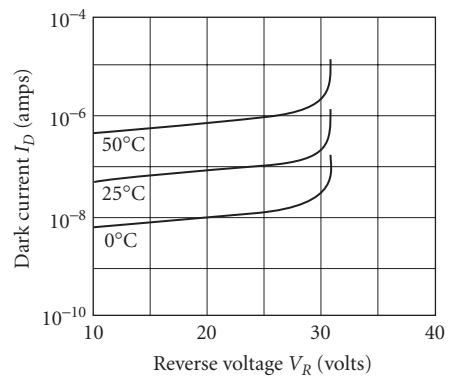

FIGURE 130 Dark current as a function of reverse bias for germanium avalanche photodiode. (*EG&G Judson, Infrared Detectors, 1994.*)

Downloaded from Digital Engineering Library @ McGraw-Hill (www.accessengineeringlibrary.com)
Copyright © 2010 The McGraw-Hill Companies. All rights reserved.
Any use is subject to the Terms of Use as given at the website.

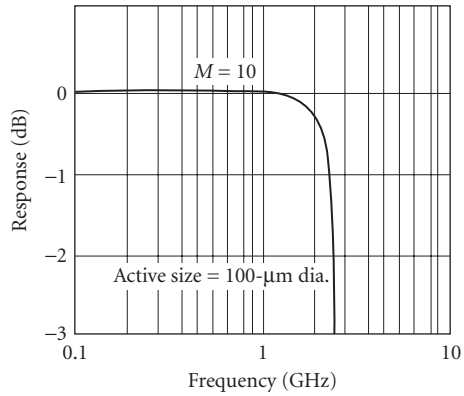

FIGURE 131 Frequency response of a germanium avalanche photodiode at two gain operating points. (*EG&G Judson, Infrared Detectors, 1994.*)

Operating temperature: Ambient or TE-cooled.

Time constant: 0.2 ns for 100-μm diameter; 0.3 ns for 300-μm diameter; both at 1.3 μm, $M = 10$ and with $R_L = 50\ \Omega$. See Fig. 131.

Sensitive area: 100- and 300-μm diameter standard.

Recommended circuit: See circuit recommended for Si APD.

Manufacturers: Edmund Optics, Metrotech, North Coast Scientific, Teledyne Judson Technologies.

PbS Photoconductive lead sulfide was one of the earliest and most successful infrared detectors. Even today it is one of the most sensitive uncooled detectors in the 1.3- to 3-μm spectral region. With cooling, PbS sensitivity is competitive with other detectors out to about 4.2 μm; however, its response time is slow.

Many PbS characteristics can be varied by adjusting the chemistry of the deposition process and/or the post-deposition heat treatment. These characteristics include spectral detectivity, time constant, resistance, and upper limit of operating temperature.[26] PbS is generally made by chemical reaction of Pb acetate and thiourea, except for high-temperature (373 K) applications, where evaporation is used. The material is deposited as a thin film (1 to 2 μm thick) on a variety of substrates, such as sapphire. With photolithographic processing, small sensitive areas can be made with comparatively high D^* values.

PbS may be tailored for ambient or room-temperature operation (ATO), intermediate or thermoelectrically cooled operation (ITO), and low-temperature or nitrogen-cooled operation (LTO). They are manufactured differently for particular temperature ranges, as shown in Table 4.

Sensitivity: D^* 1.5×10^{11} Jones at 295 K. See Figs. 132 to 137.

Responsivity: Depends on detector area, bias, resistance, and operating temperature (see Figs. 138 and 139).

Quantum efficiency: Generally limited by incomplete absorption in the thin film to 30 percent as estimated from blip D^* values.

Noise: Dominated by $1/f$ noise at low frequencies. See Figs. 135 and 140.

Time constant: Can be varied in manufacturing. Typical values are 0.2 ms at 295 K, 2 to 5 ms at 193 and 77 K. See Fig. 139.

Sensitive area: Typical sizes are square elements with dimensions of 0.5, 1, 2, and 5 mm on a side.

Downloaded from Digital Engineering Library @ McGraw-Hill (www.accessengineeringlibrary.com)
Copyright © 2010 The McGraw-Hill Companies. All rights reserved.
Any use is subject to the Terms of Use as given at the website.

TABLE 4 PbS Performance Characteristics

	Typical operating temperature, K			
	350	273 (ATO)	193 (ITO)	77 (LTO)
Sensitivity	†	Figs. 132, 138	Figs. 133, 136, 138	Figs. 134, 138
D^* (λ_{max})/D^* (500 K)		105	55	17
Noise, V/Hz$^{1/2}$		Fig. 140	Fig. 140	Fig. 140
Dark resistance, MΩ/sq	<0.3	<2	<10	<20
Time constant, μs‡	50	100–500	5000	3000

†At 350 K, cuttoff wavelength moves into ~2.4 μm, with $D^*(\lambda_{max}) \approx 10^{10}$ Jones.

‡These are typical values; the time constant can be adjusted over two orders of magnitude in fabrication, but D^* is affected.

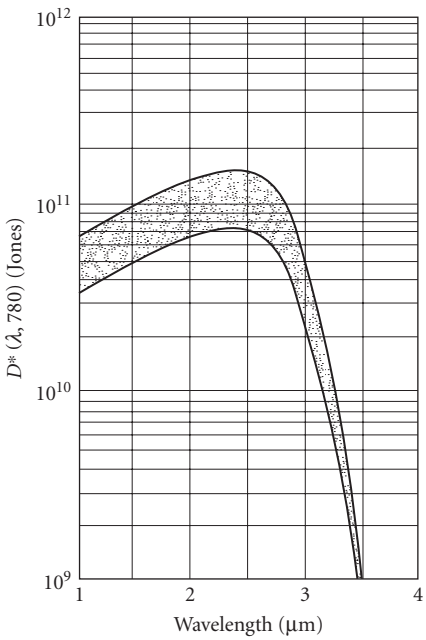

FIGURE 132 Range of spectral detectivities for PbS (ATO) at 295 K; 2π FOV, 295-K background. (*Santa Barbara Research Center.*)

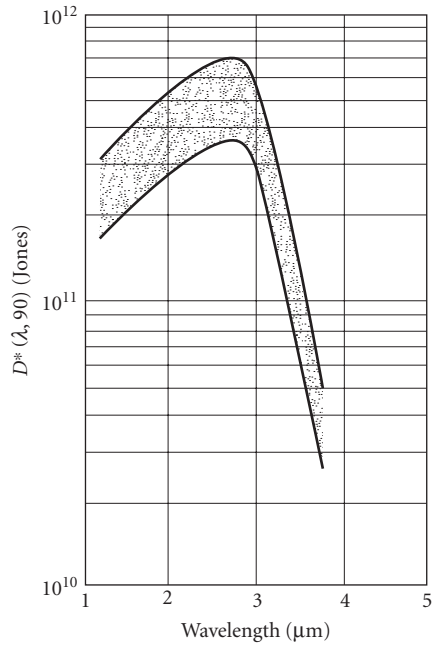

FIGURE 133 Range of spectral detectivities for PbS (ITO) at 193 K; 2π FOV, 295-K background. (*Santa Barbara Research Center.*)

Capacitance: <1 pF (limited by mounting configuration).

Recommended circuit: Standard photoconductor.

Stability: Exposure to visible and/or UV radiation can induce instability and drift. Stability will recover with storage in the dark, or by baking.

Sensitivity profile: Uniform within 10 percent.

Linearity: Excellent over broad range 10^{-8} to 10^{-3} W.

Manufacturers: Alpha Omega Instruments, Cal-Sensors, Edmund Optics, Electro-Optical Systems, Hamamatsu, New England Photoconductor, Teledyne Judson Technologies, OptoElectronics, Orielt.

Downloaded from Digital Engineering Library @ McGraw-Hill (www.accessengineeringlibrary.com)
Copyright © 2010 The McGraw-Hill Companies. All rights reserved.
Any use is subject to the Terms of Use as given at the website.

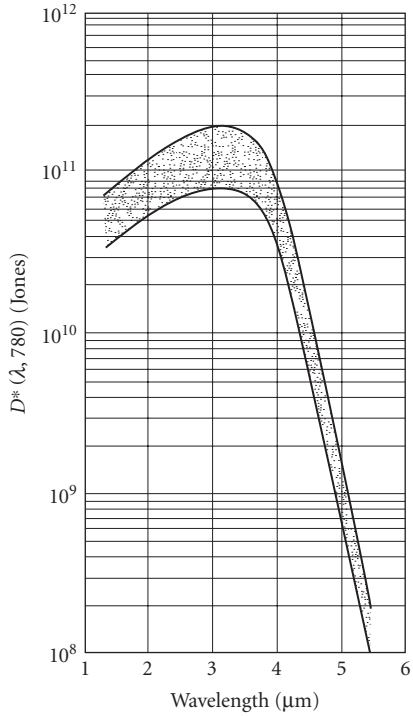

FIGURE 134 Range of spectral detectivities for PbS (LTO) at 77 K; 2π FOV, 295-K background. (*Santa Barbara Research Center.*)

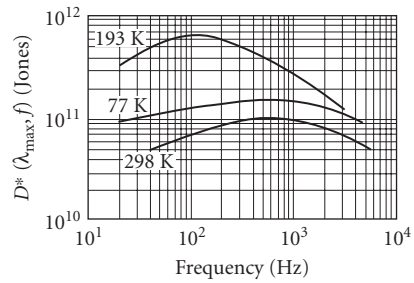

FIGURE 135 Example of detectivity vs. temperature for PbS detectors at various operating temperatures; 2π FOV, 295-K background. (*Santa Barbara Research Center.*)

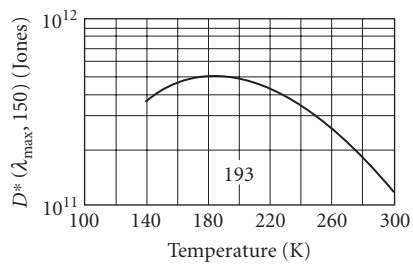

FIGURE 136 Example of detectivity versus temperature for PbS (ITO) detectors; 2π FOV, 295-K background. (*Santa Barbara Research Center.*)

Downloaded from Digital Engineering Library @ McGraw-Hill (www.accessengineeringlibrary.com)
Copyright © 2010 The McGraw-Hill Companies. All rights reserved.
Any use is subject to the Terms of Use as given at the website.

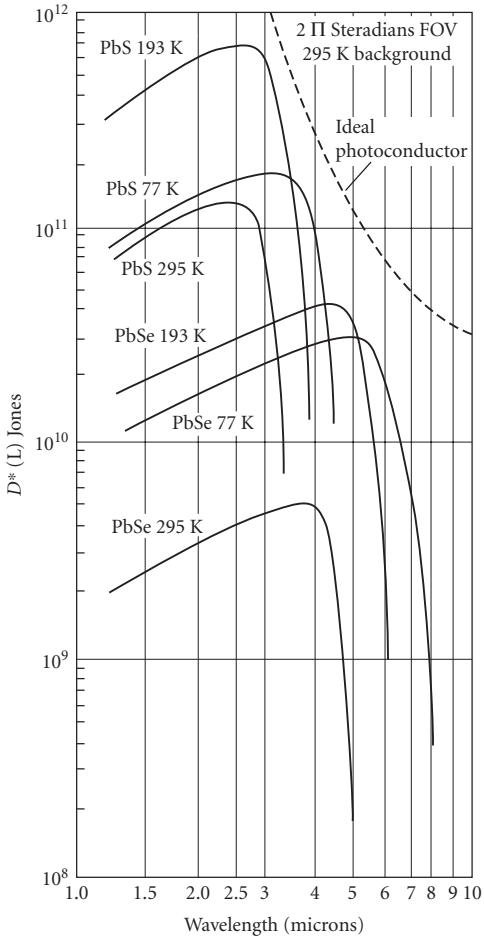

FIGURE 137 D^* versus wavelength for PbS and PbSe detectors operating at temperatures ranging between 77 K and 295 K. (*CAL-SENSORS, Infrared Detectors.*)

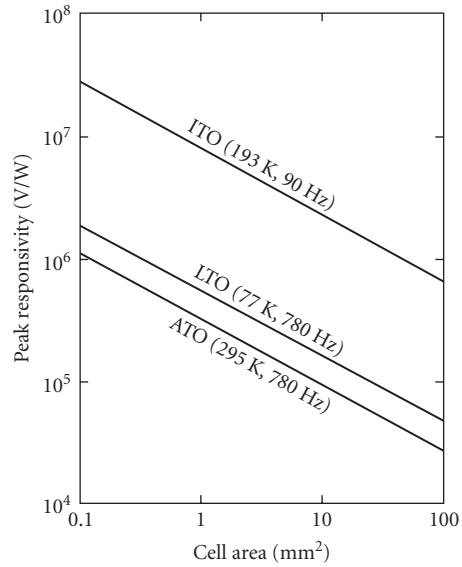

FIGURE 138 PbS typical peak responsivity versus cell area (actual values range within a factor of two of these shown.)

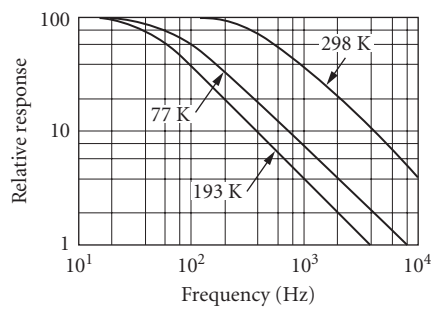

FIGURE 139 Example of signal versus frequency for PbS detectors. (*Santa Barbara Research Center.*)

Downloaded from Digital Engineering Library @ McGraw-Hill (www.accessengineeringlibrary.com)
Copyright © 2010 The McGraw-Hill Companies. All rights reserved.
Any use is subject to the Terms of Use as given at the website.

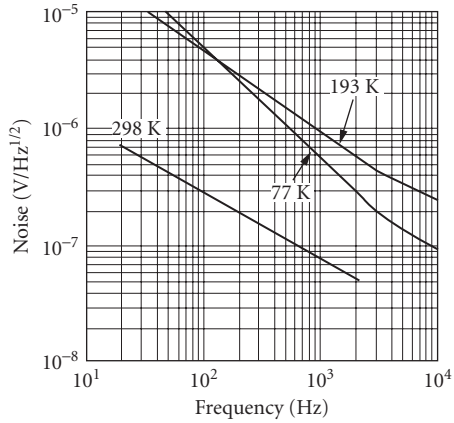

FIGURE 140 Example of noise versus frequency for PbS detectors. (*Santa Barbara Research Center.*)

InAs (Photovoltaic) InAs detectors are single-crystal, intrinsic, direct-bandgap photovoltaic devices for use in the 1- to 4-μm region (spectral cutoff varies with temperature). At room temperautre, InAs provides good sensitivity and submicrosecond response times. At 195 K, InAs performance equals or betters the sensitivity of any other detector in the 1 to 3.5-μm region. Devices with sapphire immersion lenses are available to increase signal responsivity for operation at higher temperatures where the detector is thermal-noise-limited. Compared to PbS and PbSe detectors, InAs has very little low frequency (1/f) noise if operated in the photovoltaic mode.

Sensitivity: D^*(peak) varies from 1.2×10^9 Jones at 295 K to 6×10^{11} Jones at 77 K. See Fig. 141.

Quantum efficiency: Maximum of about 75 percent without antireflection coating.

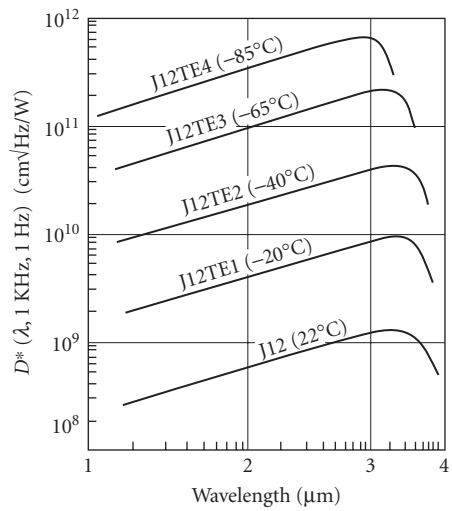

FIGURE 141 D^* versus wavelength for InAs detector operating at temperatures ranging between 77 K and 295 K. (*Teledyne Judson Technologies, 2008.*)

Downloaded from Digital Engineering Library @ McGraw-Hill (www.accessengineeringlibrary.com)
Copyright © 2010 The McGraw-Hill Companies. All rights reserved.
Any use is subject to the Terms of Use as given at the website.

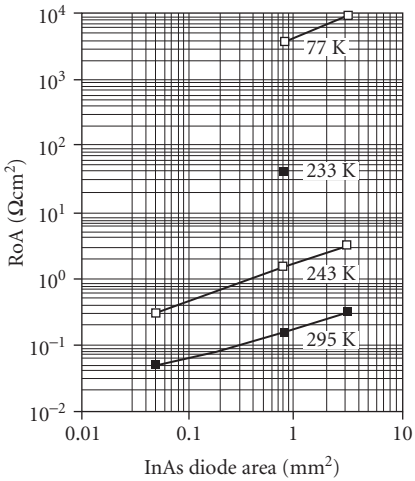

FIGURE 142 R_0A of InAs photodiodes shown as a function of diode area. Lower impedance per unit area for smaller devices indicates that these devices are surface-leakage-limited. (*Santa Barbara Research Center.*)

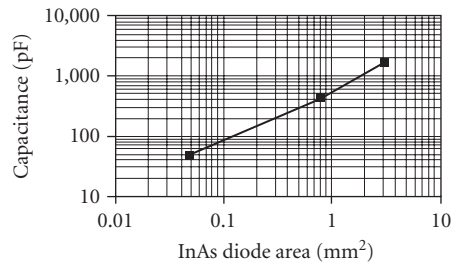

FIGURE 143 Capacitance of InAs photodiodes shown as a function of diode area. Capacitance will not change appreciably with temperature. (*Teledyne Judson Technologies, 2008.*)

Noise: Low impedance tends to make preamplifier noise dominate at room temperature; background limited (for 300 K background) at operating temperatures below 200 K.

Time constant: Less than 0.5 μs at all temperatures when low values of load resistor are used to reduce the RC time constant.

Responsivity: 0.5 to 1.25 A/W at peak.

Dynamic resistance: See Fig. 142.

Diode capacitance: See Fig. 143.

Sensitive area: Standard sizes 0.25 to 2-mm diameters.

Operating temperatures: 77 to 300 K.

Linearity: Anticipated to be very good over many decades.

Sensitivity profile: ±15 percent.

Recommended circuits:

Open circuit: PV InAs detectors with areas less than 2×10^{-2} cm require no bias when operated and can be connected directly into the input stage of amplifier (capacitor ensures elimination of dc bias from amplifier) (Fig. 144*a*).

Transformer: Useful when using InAs at zero bias, particularly at room temperature where diode impedance is low (Fig. 144*b*).

Reversed bias: At temperatures greater than 225 K considerable gain in impedance and responsivity is achieved by reverse-biasing (Fig. 144*c*).

Fast response: To utilize the short intrinsic time constant, it is sometimes necessary to load the detector to lower the RC of the overall circuit (reverse bias will also lower detector capacitance) (Fig. 144*d*).

Manufacturers: Electro-Optical Systems, Hamamatsu, Teledyne Judson Technologies.

Downloaded from Digital Engineering Library @ McGraw-Hill (www.accessengineeringlibrary.com)
Copyright © 2010 The McGraw-Hill Companies. All rights reserved.
Any use is subject to the Terms of Use as given at the website.

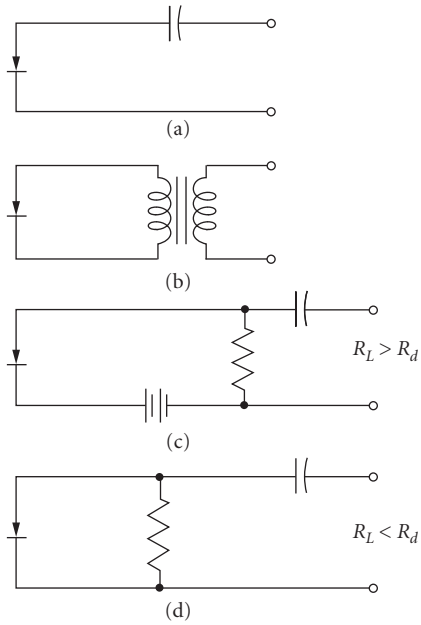

FIGURE 144 Recommended circuits for InAs detectors: (*a*) open circuit, (*b*) transformer, (*c*) reversed bias, (*d*) fast response.

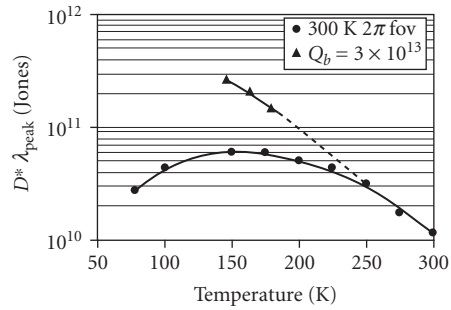

FIGURE 145 D^* of PbSe as a function of a function of temperature for two background flux conditions: high background of 2π field of view and reduced background of 3×10^{13} phtons/cm^2/s. D^* at the higher background flux reaches a maximum around 160 K because the background noise increases at lower temperatures due to the increase in long-wavelength spectral reponse of the detector. (*Santa Barbara Research Center.*)

PbSe Lead selenide is an intrinsic, thin-film photoconductor, whose long-wavelength spectral response and speed of response exceeds that of PbS. At room temperature, PbSe has peak D^* which can exceed 1×10^{10} Jones with a spectral cutoff out to 4.4 μm. At liquid-nitrogen temperature, InSb offers twice the D^*, largely because PbSe offers response out to 7 μm at 77 K, considerably longer than InSb. However, for intermediate temperatures, from 180 K to room temperature, PbSe offers competitive D^* combined with moderately fast response.[26] PbSe technology has made a significant advance in the past decade in some vendors being able to reproducibly make high-performance detectors.

Sensitivity: $D^* \approx 1 \times 10^{10}$ Jones at 300 K, increases with cooling (see Figs. 137 and 145). D^* is limited by $1/f$ noise at low frequencies (see Fig. 146).

Response: Figure 147 shows responsivity in amperes per watt for a high-quality detector with a length of 0.016 cm and width of 0. 024 cm. Responsivity in volts per watt is obtained by multiplying A/W data by resistance (see Fig. 148). Responsivity will vary inversely with detector length (see Figs. 149 and 150).

Noise: Figure 151 shows the noise as a function of temperature for a detector with a length of 0.016 cm and width of 0. 024 cm. Noise as a function of frequency is shown in Fig. 152.

Resistance: Figure 148 shows the resistance as a function of temperature for a detector with a length of 0.016 cm and width of 0. 024 cm.

Capacitance: 1 pF (limited by mounting configuration).

Time constant: See Figs. 153 and 154. Time constant will be longer when detector is operated in reduced background flux condition.

Stability: Exposure to visible and/or UV radiation can induce instability and drift. Stability will recover with storage in the dark at room temperature.

Downloaded from Digital Engineering Library @ McGraw-Hill (www.accessengineeringlibrary.com)
Copyright © 2010 The McGraw-Hill Companies. All rights reserved.
Any use is subject to the Terms of Use as given at the website.

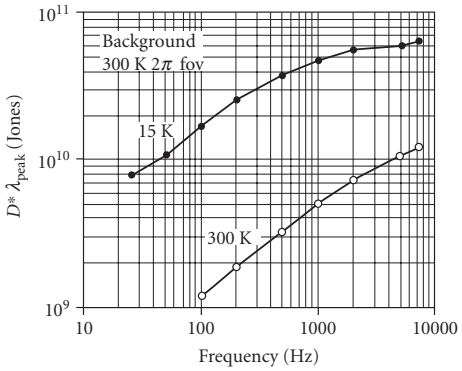

FIGURE 146 D^* of PbSe as a function of frequency for two temperatures. PbSe has considerable 1/f noise which reduces D^* at lower frequencies. (*Santa Barbara Research Center.*)

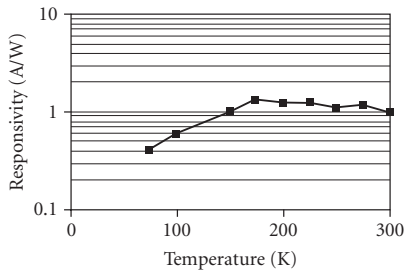

FIGURE 147 Responsivity in A/W of PbSe thin-film photoconductive detectors as a function of temperature for a high background flux level. Multiply by detector resistance to get V/W. (*Santa Barbara Research Center.*)

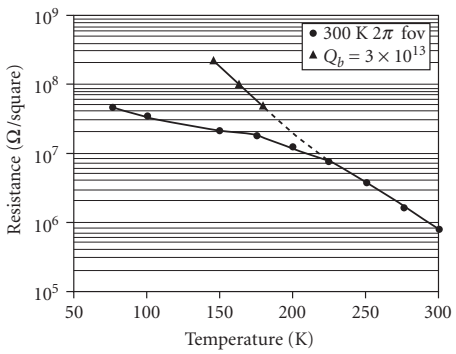

FIGURE 148 Resistance (Ω/square) of PbSe thin-films as a function of temperature for two background flux levels. At any temperature, the absolute value can be varied by altering the manufacturing process in chemical deposition and/or heat treatment. (*Santa Barbara Research Center.*)

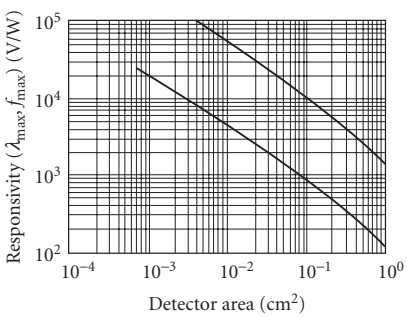

FIGURE 149 Expected range of peak responsivities versus detector size, typical PbSe (ATO) infrared detectors. (*Santa Barbara Research Center.*)

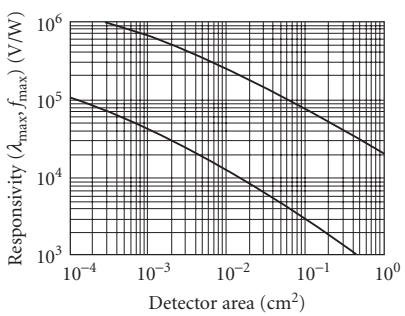

FIGURE 150 Expected range of peak responsivities versus detector size, typical PbSe (ITO and LTO) infrared detectors. (*Santa Barbara Research Center.*)

Downloaded from Digital Engineering Library @ McGraw-Hill (www.accessengineeringlibrary.com)
Copyright © 2010 The McGraw-Hill Companies. All rights reserved.
Any use is subject to the Terms of Use as given at the website.

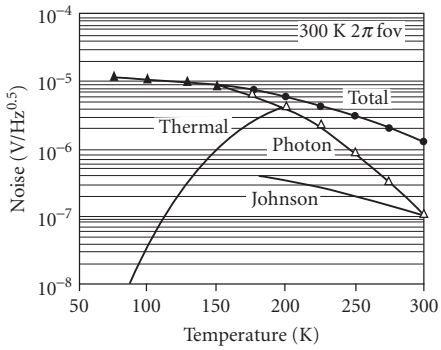

FIGURE 151 Noise voltage (per square root of bandwidth) of PbSe thin-film photoconductive detectors as a function of temperature for a high back ground flux level. Photon noise is dominant below 200 K. Thermal noise is dominant at higher temperatures. Total noise levels are well above typical preamplifier noise. (*Santa Barbara Research Center.*)

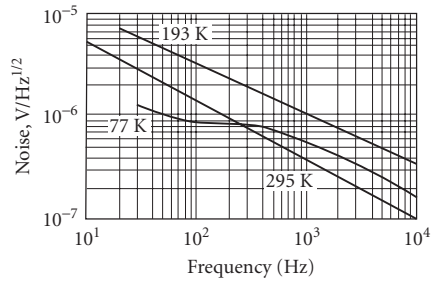

FIGURE 152 Example of noise versus frequency for PbSe detectors (ATO, ITO and LTO types) (1 × 1 mm). (*Santa Barbara Research Center.*)

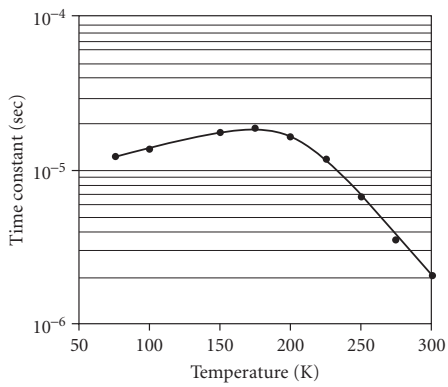

FIGURE 153 Time constant of PbSe thin-film photoconductive detectors as a function of temperature. (*Santa Barbara Research Center.*)

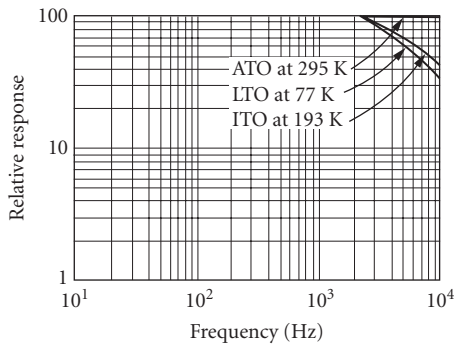

FIGURE 154 Example of signal versus frequency for PbSe detectors (ATO, ITO and LTO). (*Santa Barbara Research Center.*)

Recommended circuit: Standard photoconductor.

Operating temperature: 77 to 300 K.

Manufacturers: Cal-Sensors, Edmund Optics, Electro-Optical Systems, Hamamatsu

InSb Historically, indium antimonide material has been used for at least four different radiation detector types, two of which, the photoconductive and photoelectromagnetic types, are no longer widely used. We discuss here the intrinsic photovoltaic device. [The very far infrared bolometer (InSb bolometer) was previously discussed in Sec. 24.7.

At 77 K, InSb photodiodes offer background limited sensitivity at medium-to-high background flux conditions in the 1- to 5.5-μm spectral range. At lower temperatures, they provide sensitive detectors at low background flux levels such as in astronomy applications, but with a slightly shortened long-wavelength cutoff. Operation is possible up to as much as 145 K, but because the spectral

Downloaded from Digital Engineering Library @ McGraw-Hill (www.accessengineeringlibrary.com)
Copyright © 2010 The McGraw-Hill Companies. All rights reserved.
Any use is subject to the Terms of Use as given at the website.

response increases with increasing temperature, the detector impedance drops rapidly leading to significant thermal noise.

Sensitivity: Spectral response out to 5.5 μm at 77 K (see Fig. 155). D^* 1×10^{11} Jones, increases with reduced background flux (narrow field of view and/or cold filtering) as illustrated in Fig. 156.

Quantum efficiency: ~ 60–70 percent without antireflection coating. >90 percent with antireflection coating.

Noise: Background current limited over wide range of background flux at 77 K (see Fig. 157).

Time constant: <1 μs.

Responsivity: 3 A/W at 5 μm without antireflection coating.

Noise equivalent power (*NEP*): Frequency dependence is shown in Fig. 158 for three detector sizes.

Capacitance: Typically 0.05 F/cm^2.

Impedance: Top-grade detectors have 1–5 $\times 10^6$ Ωcm^2 R_0A product at 77 K, at zero bias, and without background flux.

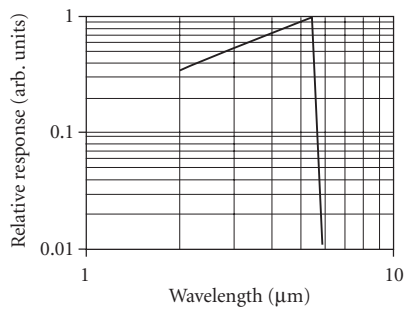

FIGURE 155 Relative spectral response per watt of an InSb photodiode without antireflection coating. the direct bandgap results in a sharp spectral cutoff. (*Santa Barbara Research Center.*)

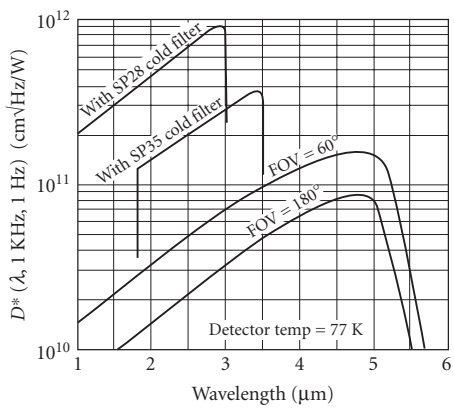

FIGURE 156 D^* as a function of wavelength for an InSb detector operating at 77 K. (*Teledyne Judson Technologies, 2008.*)

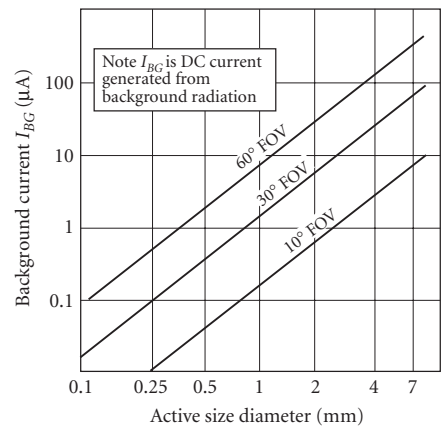

FIGURE 157 Background current as a function of photodiode area for InSb detectors operating at 77 K, shown at three values of the detector field of view. (*Teledyne Judson Technologies, 2008.*)

Downloaded from Digital Engineering Library @ McGraw-Hill (www.accessengineeringlibrary.com)
Copyright © 2010 The McGraw-Hill Companies. All rights reserved.
Any use is subject to the Terms of Use as given at the website.

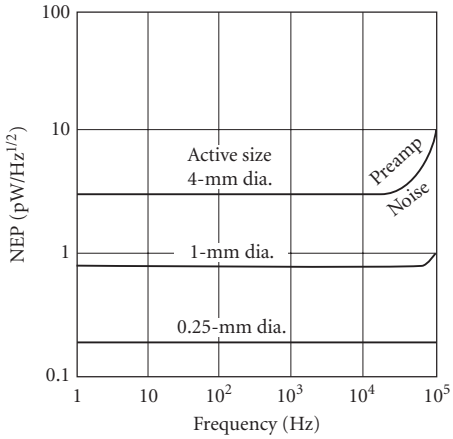

FIGURE 158 NEP as a function of frequency for three sizes of InSb photodiodes. (*Teledyne Judson Technologies, 2008.*)

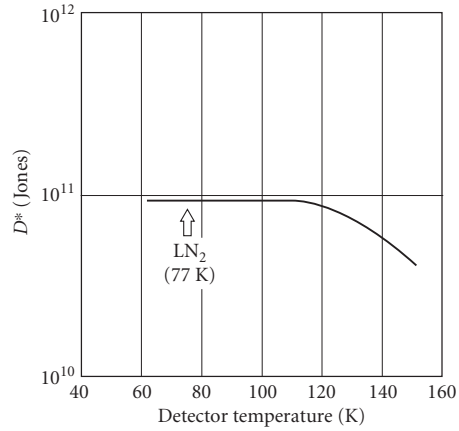

FIGURE 159 InSb photodiode D^* as a function of operating temperature between 77 K and 150 K, for a 2π (180°) FOV. (*Teledyne Judson Technologies, 2008.*)

Sensitive area: 0.04 × 0.04-mm square to 1 × 5-mm rectangle; 0.25 to 10-mm diameter.

Operating temperature: Normally 77 K; InSb can be used up to approximately 145 K (see Fig. 159).

Linearity: Linear to ~1-mW/cm^2 flux.

Sensitivity profile: ±15 percent or better.

Stability: Devices from some vendors are subject to "flashing," where exposure to visible or UV flux causes a change in the insulating surface charge thereby causing a change in the diode impedance. The detector typically recovers at room temperature.

Recommended circuit: Same as for Si and Ge photodiodes; zero or reverse bias in combination with a load resistor and low-noise preamplifier. Low-impedance load resistor can be used for obtaining fast response, with consequences of reduced sensitivity.

Manufacturers: L3 Cincinnati Electronics, Edinburgh Instruments, New England Photoconductor, Teledyne Judson Technologies, Electro-Optical Systems, Hamamatsu, Infrared Associates.

Ge:Au Gold-doped germanium detectors are relatively fast single-crystal p-type impurity-doped photoconductors for the 2- to 9-μm region. Although not the most sensitive detector anywhere in its range of spectral sensitivity, Ge:Au offers respectable sensitivity over a broad spectral region using liquid nitrogen cooling. Sensitivity can be improved by a factor of 2.5 by operating at T <65 K (pumped liquid nitrogen or other cryogen). At these temperatures, Ge:Au becomes background limited.

Sensitivity: See Figs. 160 to 163.

Quantum efficiency: Dependent on wavelength, detector geometry (absorption thickness), antireflection coating, and enclosure (integration chamber can increase absorption). $D_{\lambda pk}/D^*_{500\ K}$ = 2.7 (see Fig. 164).

Noise: See Fig. 165.

Time constant: <50 ns with full D^* [shorter response times (<2 ns) can be tailored by heavy concentration of compensating (*n*-type) dopant and suitable bias circuit (see circuit discussion to follow). Heavy compensation increases resistance, and hence the incoherent signal-to-noise ratio becomes limited by the thermal noise of the load (typically a factor of 2 degradation in the signal-to-noise ratio). Quantum efficiency, however, is not significantly altered, so that a high compensation concentration does not hurt the coherent-detection signal-to-noise ratio].

Downloaded from Digital Engineering Library @ McGraw-Hill (www.accessengineeringlibrary.com)
Copyright © 2010 The McGraw-Hill Companies. All rights reserved.
Any use is subject to the Terms of Use as given at the website.

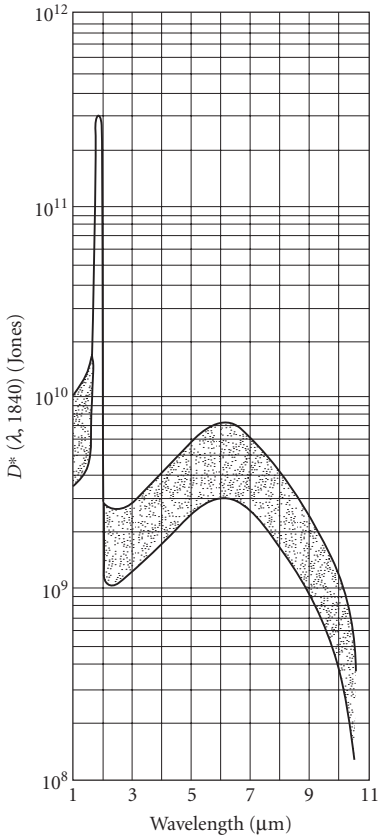

FIGURE 160 D^* versus λ for Ge:Au; T = 77 K, 2π FOV; 295-K background. (*Santa Barbara Research Center.*)

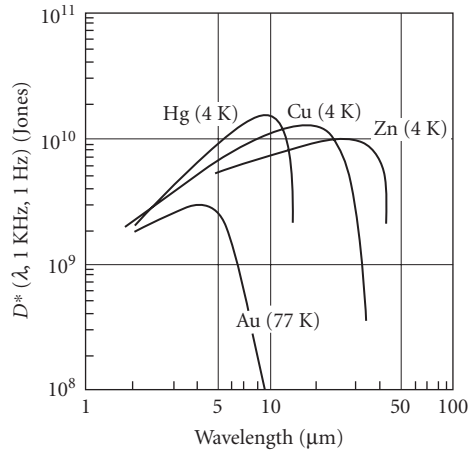

FIGURE 161 D^* as a function of wavelength for extrinsic germanium detectors doped with Au, Hg, Cu, and Zn, for a 300-K 2π (180°) FOV background flux. (*EG&G Judson, Infrared Detectors, 1994.*)

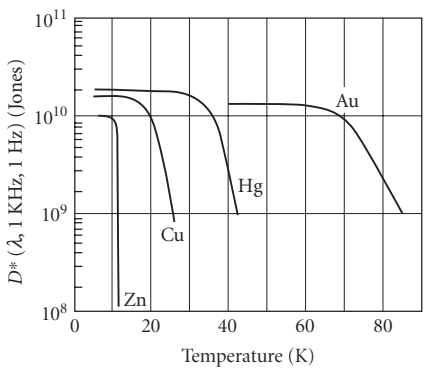

FIGURE 162 D^* as a function of operating temperature for extrinsic germanium detectors doped with Au, Hg, Cu, and Zn for a 300-K 2π (180°) FOV background flux. (*EG&G Judson, Infrared Detectors, 1994.*)

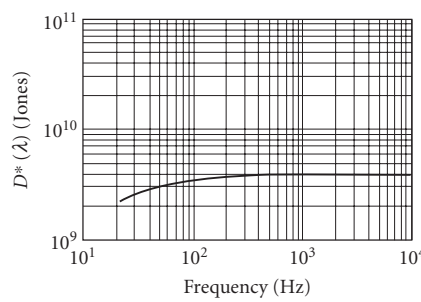

FIGURE 163 Typical D^* versus frequency (T = 77 K). (*Santa Barbara Research Center.*)

Downloaded from Digital Engineering Library @ McGraw-Hill (www.accessengineeringlibrary.com)
Copyright © 2010 The McGraw-Hill Companies. All rights reserved.
Any use is subject to the Terms of Use as given at the website.

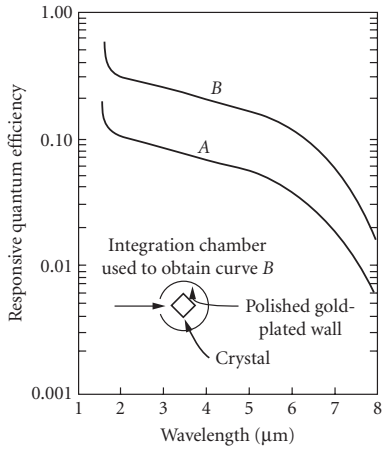

FIGURE 164 Quantum efficiency versus λ for Ge:Au (T = 78 K). (*Santa Barbara Research Center, internal report.*)

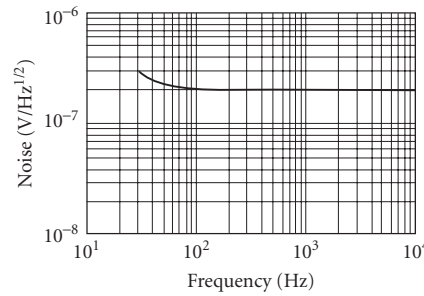

FIGURE 165 Typical noise spectrum for Ge:Au (T = 77 K, A = 1 × 1 mm). (*Santa Barbara Research Center.*)

Responsivity: Dependent upon bias and geometry, typical values are 0.1 to 0.2 A/W at 77 K. Multiply by detector resistance to get V/W.

Dark resistance: Varies with background flux and effective quantum efficiency (see previous quantum efficiency discussion), range may be 20 kΩ to 5 MΩ, or much greater under very low background flux conditions if adequately cooled to limit thermally activated conductivity. (Also see previous time-constant discussion.)

Capacitance: Depends on device geometry and mounting, typically <1 pF.

Sensitive area: 1 to 5-mm diameter standard.

Operating temperature: < 85 K (normally 77 K, but see Fig. 162).

Recommended circuit: Standard photoconductive. See Fig. 166.

Manufacturers: No suppliers are presently known.

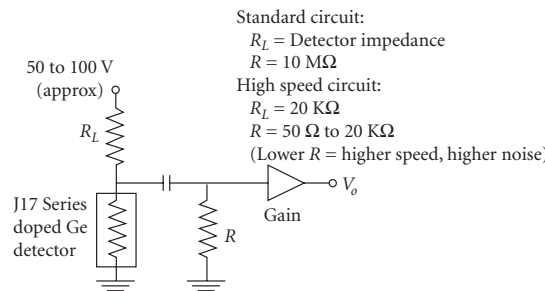

FIGURE 166 Basic operating circuit for extrinsic germanium detectors doped with Au, Hg, Cu, and Zn, for a 300-K 2π (180°) FOV high background flux. If the detector is operated in very low background flux conditions, the detector impedance can become very high. Cooled JFET (T > ≈ 50 K) or PMOS buffer amplifiers can be helpful in impedance matching under these conditions. (*EG&G Judson, Infrared Detectors, 1994.*)

Downloaded from Digital Engineering Library @ McGraw-Hill (www.accessengineeringlibrary.com)
Copyright © 2010 The McGraw-Hill Companies. All rights reserved.
Any use is subject to the Terms of Use as given at the website.

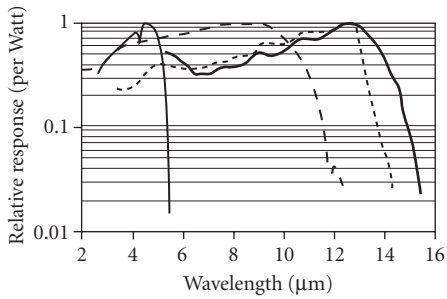

FIGURE 167 Relative spectral response per watt at 80 K for photoconductive HgCdTe detectors with antireflection coating. The curves are normalized to unity at peak value. The spectral cutoff can be adjusted by varying the ratio of HgTe to CdTe in the alloy. (*Santa Barbara Research Center.*)

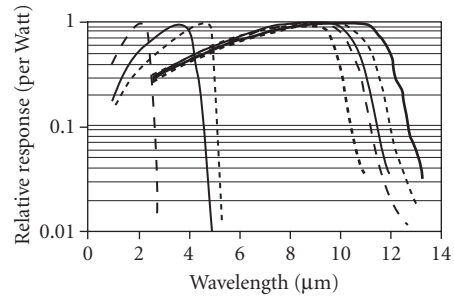

FIGURE 168 Relative spectral response per watt at 80 K for photovoltaic HgCdTe detectors without antireflection coating. The curves are normalized to unity at peak value. The spectral cutoff can be adjusted by varying the ratio of HgTe to CdTe in the alloy. (*Santa Barbara Research Center.*)

HgCdTe, HgZnTe, HgMnTe, etc. Mercury cadmium telluride is a direct-bandgap compound alloy semiconductor, made of chemical group II and VI elements, whose peak sensitivity at a particular temperature can be adjusted from 1 to 30 μm by varying the ratio of HgTe to CdTe (see Figs. 167 and 168). In addition to HgCdTe, other combinations of chemical groups II and VI elements can be used to produce similar variable spectral cutoff compound alloys, including HgZnTe, HgMnTe, HgCdZnTe, etc. For almost all purposes, HgCdTe will be as good as any other II-VI alloy detector, so we will speak here about it exclusively, but provide some data from the other alloys noted above. Both photoconductive (PC) and photovoltaic (PV) HgCdTe detectors are available for background-limited, high-speed, intrinsic photon detection in the SWIR, MWIR, and LWIR regions. Photoconductive devices with VLWIR response out to 25 μm are also available. HgCdTe detectors can be used at room temperature, with TE cooling, and at 77 K and lower temperatures. Sensitivity generally increases with cooling, depending upon the spectral cutoff and background flux. MWIR, LWIR, and VLWIR spectral range devices are generally operated at 77 K or lower temperature for maximum sensitivity, depending upon the background flux. The PC mode is advantageous when cooling is limited, since the thermal noise of a photoconductor increases less rapidly than a photodiode as the temperature is raised. Photoconductive devices with response out to 25 μm can be usefully operated at liquid nitrogen temperature and are popular for IR spectroscopy for this reason.

HgCdTe photoconductors are fabricated from thin (≈10-μm) single-crystal slices or epitaxial layers with metal contacts at each end of the element (see Fig. 8). They are low-impedance devices with 15 to 2000 Ω/square, depending upon the alloy composition, carrier concentration, operating temperature, background flux, and surface treatment. Photoconductor time constants at 77 K may be ≈ 2 μs for devices having a 12-μm cutoff, with longer time constants for shorter cutoffs, and shorter time constants for higher operating temperatures. In the case of small detector elements, the time constant may be reduced with increasing bias voltage because photoexcited carriers will be transported to the electrical contacts where they recombine. The spectral noise characteristics of PC HgCdTe typically exhibit $1/f$ noise out to a range of 50 Hz to 1 kHz or more, the value depending upon the detector quality, long-wavelength response, operating temperature, and background flux. White noise levels range from less than 1 nV/√Hz (where preamplifier noise may then dominate), up to 20 nV/√Hz, depending upon detector quality, size, geometry, applied bias, temperature, and alloy composition. Photoconductive HgCdTe detectors are typically antireflection coated with a quarter-wave ZnS film, giving a peak quantum efficiency in the range of 85 to 90 percent, although this figure is only indirectly measured because the PC gain can be much greater than unity. Without antireflection coating, the quantum efficiency is typically 70 percent, limited by the optical index of ≈ 4.

Downloaded from Digital Engineering Library @ McGraw-Hill (www.accessengineeringlibrary.com)
Copyright © 2010 The McGraw-Hill Companies. All rights reserved.
Any use is subject to the Terms of Use as given at the website.

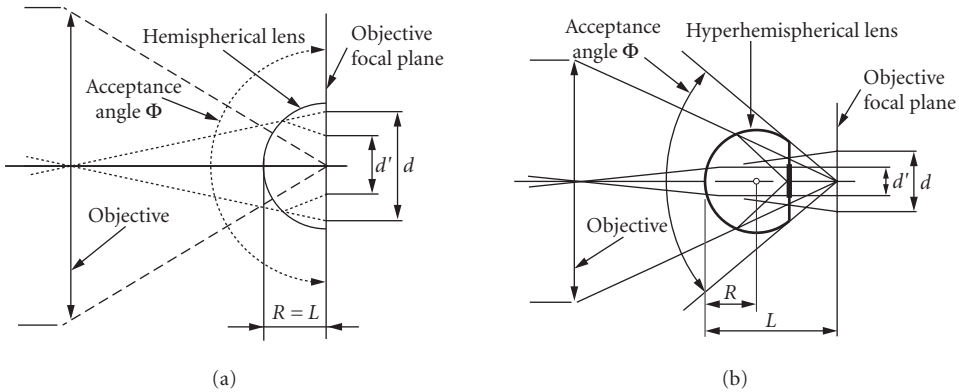

FIGURE 169 Schematic of an optically immersed HgCdZnTe detector with (*a*) hemispherical lens and (*b*) hyperhemispherical lens. Dimensions are summarized in Table 5. (*Vigo Systems.*)

TABLE 5 Summary of the Dimensions Depicted in Fig. 169, and Their Impact on D^* (Vigo Systems)

Parameter	Hemisphere	Hyperhemisphere
Distance, L	$L = R$	$L = R(n + 1)$
d/d'	n	n^2
$D^*_{\text{imm}}/D^*_{\text{non-imm}}$	n	n^2
Acceptance angle, Φ	$\Phi = 180°$	$\Phi = 2 \arcsin(1/n)$
F/#	0.5	1.55

n = index of refraction (approx. 3.3 for GaAs and 2.7 for CdTe)

A class of HgCdTe detectors is offered for detection at TE-cooled and room temperature which are optically "immersed" with a hemispherical or hyperhemispherical lens of Ge, CdTe, GaAs, or other high-index material (see Fig. 169 and Table 5). The lens increases the effective area of the detector without increasing the detector noise, provided the noise is dominated by thermal rather than photon noise as is the case for minimal cooling. The lens must be in intimate contact with the detector surface (<<1 μm spacing) to avoid total internal reflection of off-axis rays at the lens-detector interface. Immersed detectors offer up to a factor of n^2 (where n is the optical index) increased detector signal, which can mean an increase in D^* by the same factor for a thermal-noise-limited device. Operation of LWIR PC detectors at TE-cooled and room temperature is generally accompanied by increased $1/f$ noise which dominates out to higher frequencies.

Photovoltaic HgCdTe detectors ideally offer $\sqrt{2}$ higher D^* than detectors operating in the PC mode. Diodes are made in both n^+p and p^+n polarities, depending upon the manufacturer's capabilities. The R_0A product of HgCdTe photodiodes varies significantly with temperature, spectral cutoff, and device quality. It also varies with the amount of background flux incident on the device. The R_0A product defines the maximum D^* in the limit of reduced background flux (see Fig. 170 and Fig. 19). In addition to theoretically higher D^*, high-quality PV HgCdTe detectors have lower $1/f$ noise than PC HgCdTe devices, with $1/f$ knee frequencies as low as 1 Hz or less. However, the noise of PV detectors increases more rapidly with increasing temperature than for PC detectors, making photodiodes less attractive for applications where cooling is limited. Photodiodes of high quality are more difficult to make than good photoconductors and can be expected to warrant a premium price. Antireflection coating is available from some diode producers, but is not routinely offered.

Downloaded from Digital Engineering Library @ McGraw-Hill (www.accessengineeringlibrary.com)
Copyright © 2010 The McGraw-Hill Companies. All rights reserved.
Any use is subject to the Terms of Use as given at the website.

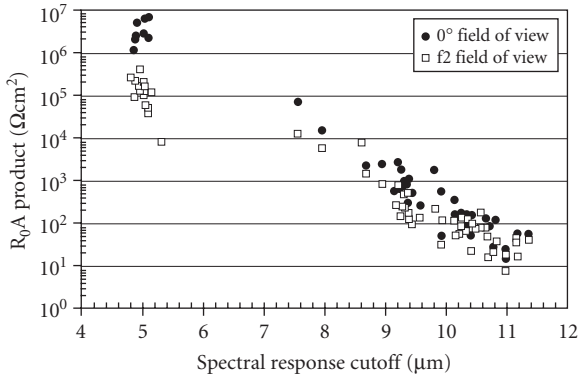

FIGURE 170 R_0A product "trendline" for small (25 × 25 to 100 × 100 μm) HgCdTe photodiodes at 77 K. Data is shown for devices with zero background flux (0° FOV) and with an F/2 field of view (29°) of a 300-K background. For 5-μm spectral cutoff material, the R_0A product is higher at 0° FOV by about an order of magnitude, compared with an F/2 background. At 10 μm, there is less of a difference between the two background conditions. Note that the R_0A product will generally be somewhat lower for larger area diodes.

Both PC and PV HgCdTe detectors are useful for infrared heterodyne detection. When sufficient local oscillator power is available, detector cooling becomes less important, since photon noise can dominate thermal noise at comparatively higher temperatures. Other things being equal, the photovoltaic detector has $\sqrt{2}$ sensitivity (signal-to-noise voltage) advantage over the photoconductor. For 10.6-μm heterodyne detection, 0.1 × 0.1-mm HgCdTe *pin* photodiodes with sensitivity near the quantum limit of $\approx 2 \times 10^{-20}$ W/ Hz are available with bandwidths up to several gigahertz. Ordinary photodiodes of the same area have bandwidths of several hundred megahertz. Photoconductors make better 10.6-μm heterodyne detectors when cooling is limited to TE-cooled temperatures of 180 K up to room temperature. At 180 K, TE-cooled photoconductors offer bandwidths of 50 to 100 MHz and heterodyne NEPs of 1 to 2×10^{-19} W/Hz. At room temperature, the NEP at 10.6 μm is limited to about 1×10^{-16} W/Hz. Immersion does not improve the performance of minimally cooled heterodyne detectors, since optical gain is already provided by the local oscillator.

Photoconductive HgCdTe

Sensitivity: Adjustable by varying alloy composition (see Figs. 167, 171 to 174).

Dark resistance: 15 to 2000 Ω/sq depending upon temperature, spectral cutoff, and surface passivation.

Responsivity: Varies with spectral cutoff, temperature, detector resistance, element length, and bias voltage or power. See Eq. (21) and Fig. 175 for detector elements with 50 × 50-μm dimensions.

Noise: *1/f* noise is dominant at frequencies below 50 to 1000 Hz for LWIR detectors at 77 K (greater for LWIR at room temperature or TE-cooled). Generation-recombination (thermal or photon) white noise is present beyond the *1/f* region at a level of less than 10^{-9} V/$\sqrt{\text{Hz}}$ to 2×10^{-8} V/$\sqrt{\text{Hz}}$, depending upon spectral cutoff, background flux, responsivity, bias, and operating temperature. Noise and signal rolloff at high frequency is determined by the time constant. See Fig. 176 for an example of the noise spectrum of an LWIR detector at 77 K.

Operating temperature: 77 K and below to 300 K and above for short spectral cutoffs and/or with significant D^* reduction for operation at higher temperatures. Detector immersion can increase D^* at elevated temperatures where thermal noise is dominate.

Downloaded from Digital Engineering Library @ McGraw-Hill (www.accessengineeringlibrary.com)
Copyright © 2010 The McGraw-Hill Companies. All rights reserved.
Any use is subject to the Terms of Use as given at the website.

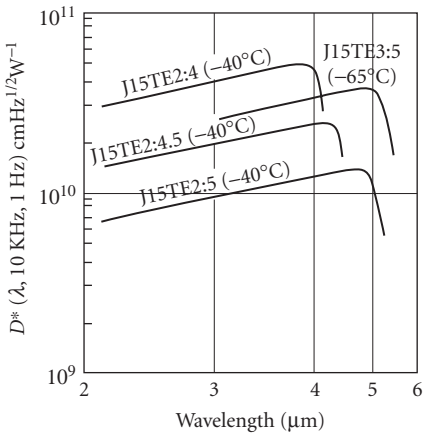

FIGURE 171 Typical D^* as a function of wavelength for a variety of MWIR HgCdTe photoconductors with thermoelectric cooling. (*Teledyne Judson Technologies.*)

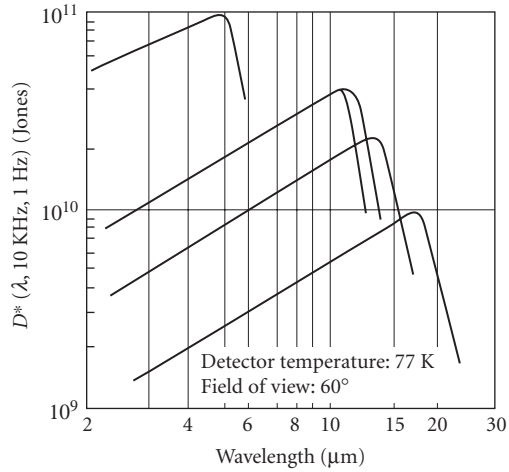

FIGURE 172 Typical D^* as a function of wavelength for a variety of LWIR and VLWIR HgCdTe photoconductors at 77 K. (*Teledyne Judson Technologies.*)

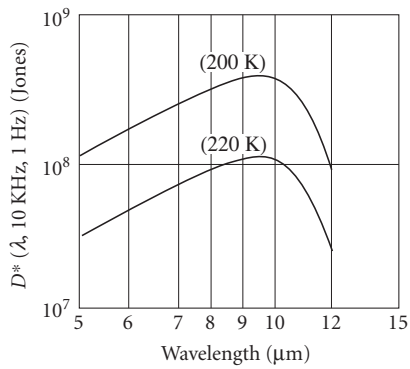

FIGURE 173 Typical D^* as a function of wavelength for LWIR HgCdTe photoconductors at 200 and 220 K. These units are cooled with three- or four-stage thermoelectric coolers. (*Teledyne Judson Technologies.*)

Linearity: At 77 K linearity begins to degrade at photon flux levels above ~ 10^{-3} W/cm^2. At 200 K linearity begins to degrade at photon flux levels above ~1 W/cm^2.

Sensitive area: 0. 025 to 4-mm linear dimensions.

Quantum efficiency: Typically >70 percent, 85 to 90 percent with antireflection coating.

Capacitance: Low, limited by mounting configuration.

Time constant: 1–2 μs for LWIR at 77 K (see Fig. 176), depends on spectral cutoff, temperature, doping, and bias.

Downloaded from Digital Engineering Library @ McGraw-Hill (www.accessengineeringlibrary.com)
Copyright © 2010 The McGraw-Hill Companies. All rights reserved.
Any use is subject to the Terms of Use as given at the website.

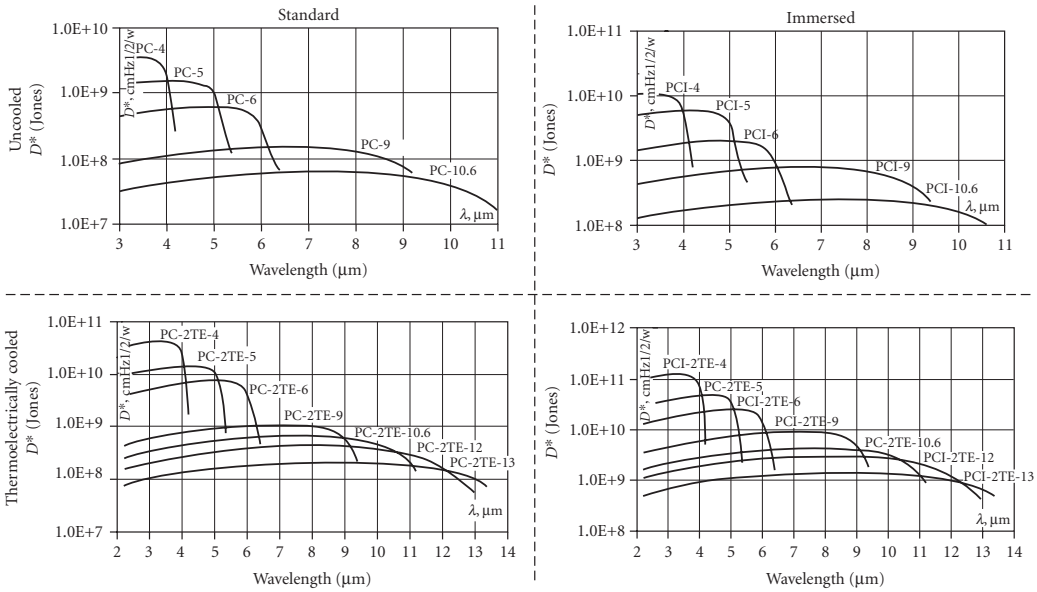

FIGURE 174 D^* for photoconductive HgCdTe detectors as a function of wavelength: *upper left*—ambient temperature operation; *upper right*—ambient temperature operation and immersed; *lower left*—thermoelectrically cooled; *lower right*—thermoelectrically cooled and immersed. (*Vigo Systems.*)

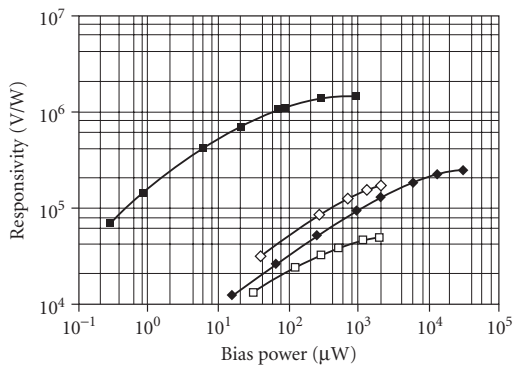

FIGURE 175 Range of peak responsivities for 12-μm cutoff HgCdTe photoconductors at 80 K. These devices have nominal dimensions of 50 × 50 μm, and resistance of 50 to 150 Ω/square. (*Santa Barbara Research Center.*)

Circuit: Standard photoconductive.

Manufacturers: Belov Technology, Boston Electronics, Hamamatsu, Infrared Associates, Kolmar Technologies, Oriel, Teledyne Judson Technologies, Vigo Systems.

Photovoltaic HgCdTe

Sensitivity: Adjustable by varying alloy composition (see Figs. 168, 170, 177, and 178). Also compare Fig. 170 with Fig. 19 for an estimate of the extent to which D^* may increase (up to the R_0A or shunt resistance limit) as the background flux is reduced.

Downloaded from Digital Engineering Library @ McGraw-Hill (www.accessengineeringlibrary.com)
Copyright © 2010 The McGraw-Hill Companies. All rights reserved.
Any use is subject to the Terms of Use as given at the website.

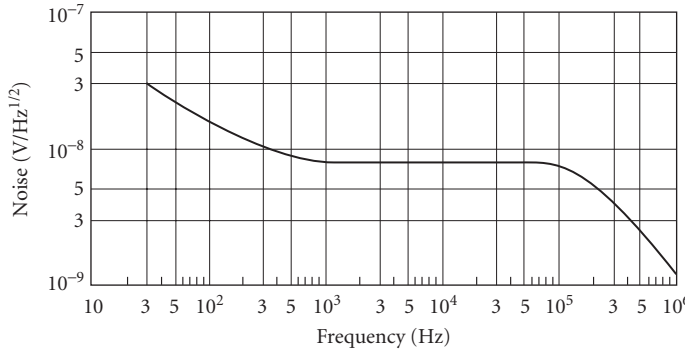

FIGURE 176 Variation of noise with frequency for photoconductive HgCdTe at 77 K. (*GEC Marconi Infrared Ltd.*)

Time constant: Depends on diode capacitance (area); 10 to 20 ns without bias; 0.5 to 3 ns with reverse bias (some trade-off of sensitivity). Low-capacitance *pin* devices with response out to several gigahertz (0.05 to 0.2-ns time constant) are also available for 10.6-μm CO_2 laser heterodyne detection.

Resistance: Refer to Fig. 170 for the R_0A product at zero bias corresponding to the detector cutoff wavelength (this figure shows very high quality diode impedances) and divide by the diode area. Large-area diodes will have somewhat lower R_0A product than shown in this figure. R_0A varies somewhat with background flux as can be noted from Fig. 170.

Operating temperature: Depends on spectral cutoff; 77 K and lower for LWIR and VLWIR detectors, up to room temperature for SWIR devices. Optical immersion and/or TE cooling will boost the performance for all spectral ranges compared with operation at ambient temperature—see Fig. 178.

Noise: High-quality devices may have flat noise response from 1 Hz out to the high-frequency limit of the time constant. 1/*f* noise may be present in lower quality devices and will increase with reverse bias.

Quantum efficiency: >50 percent (60–75 percent typical) without antireflection coating. Higher with antireflection coating.

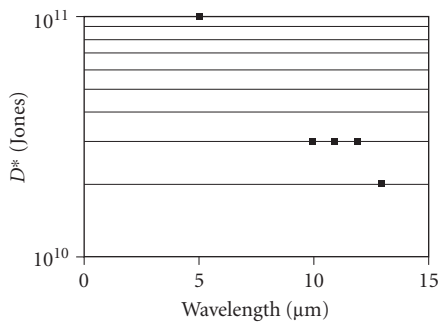

FIGURE 177 D^* specifications for small (50 × 50 to 250 × 250 μm) HgCdTe photodiodes at 77 K as a function of spectral cutoff. Data is shown for devices with 60° FOV background flux. (*Fermionics, Mercury Cadmium Telluride MWIR and LWIR Detector Series.*)

Downloaded from Digital Engineering Library @ McGraw-Hill (www.accessengineeringlibrary.com)
Copyright © 2010 The McGraw-Hill Companies. All rights reserved.
Any use is subject to the Terms of Use as given at the website.

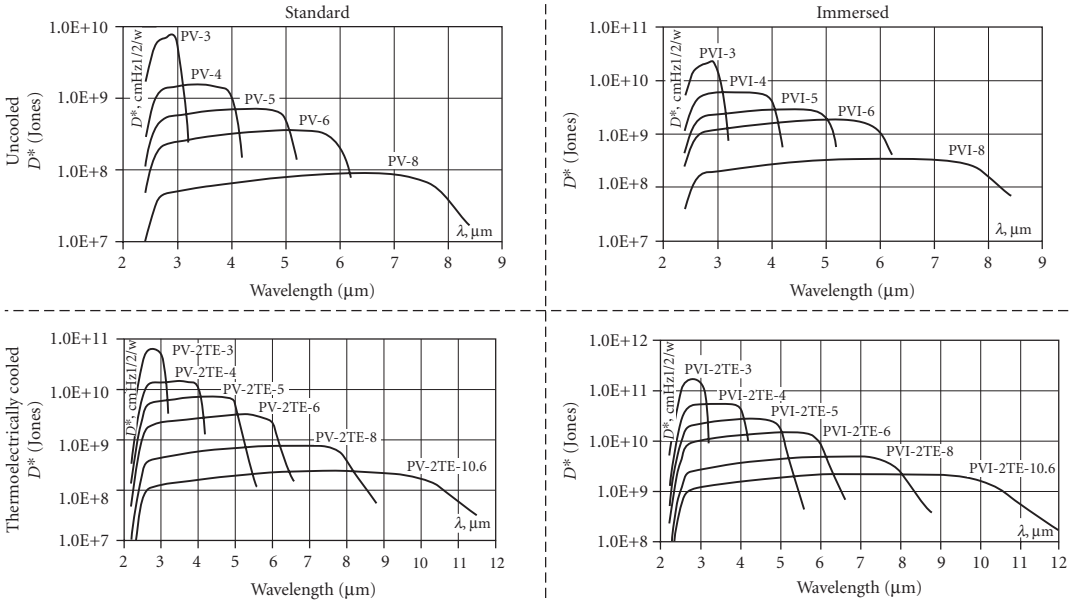

FIGURE 178 D^* for photovoltaic HgCdTe detectors as a function of wavelength: *upper left*—ambient temperature operation; *upper right*—ambient temperature operation and immersed; *lower left*—thermoelectrically cooled; *lower right*—thermoelectrically cooled and immersed. (*Vigo Systems.*)

Sensitive area: 0.0 to 0.25-mm square, 0.5- and 1-mm diameter.

Capacitance: Depends on junction doping, area, and applied bias (very slightly dependent on spectral cutoff). For standard *pn* junction devices at zero bias and 10^{15} cm^{-3} doping, capacitance is approximately 3×10^4 pF/cm. Significantly lower for *pin* junction devices.

Circuit: Standard photovoltaic circuits, reverse-bias operation to enhance speed and zero bias to maximize D^*.

Manufacturers: Boston Electronics, Kolmar Technologies, Oriel, Raytheon Vision Systems, Vigo Systems.

PbSnTe PbSnTe offers an alternative semiconductor alloy system based upon the IV-VI chemical groups to the II-VI (HgCdMnTeSe) groups previously described for fabricating variable spectral cut-off detectors. Only photovoltaic detectors are available in PbSnTe. This technology has an advantage in the ease of material growth and in the fabrication of good quality photodiode junctions. It has a disadvantage in the very high dielectric constant of the material, combined with relatively high doping concentrations giving high-capacitance (comparatively slow) detectors. For low-frequency applications this is not a disadvantage.

Sensitivity: $D^*_{peak} > 10^{10}$ Jones (see Fig. 179).

Time constant: >50 ns.

Sensitive area: 1×1 mm.

Operating temperature: 77 K.

Circuit: Standard photovoltaic.

Manufacturers: No suppliers are presently known.

Ge:Hg Mercury-doped germanium detectors are fast single-crystal impurity-doped photoconductors, sensitive out to 14 m. Ge:Hg is especially well suited for detection through the 8- to 13-μm

Downloaded from Digital Engineering Library @ McGraw-Hill (www.accessengineeringlibrary.com)
Copyright © 2010 The McGraw-Hill Companies. All rights reserved.
Any use is subject to the Terms of Use as given at the website.

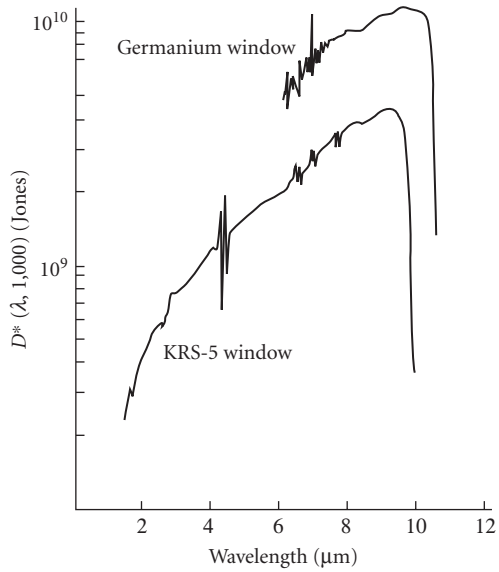

FIGURE 179 Photovoltaic PbSnTe D^* versus wavelength at 77 K and 60° FOV. (*Barnes Engineering Co.*)

atmospheric window and for detection of near-ambient sources. Unfortunately, its operating temperature must be kept less than 40 K, where it becomes 300-K background limited.

Sensitivity: See Figs. 161, 162, 180, and 181.

Quantum efficiency: 25 to 30 percent.

Noise: See Figs. 182 and 183.

Time constant: 100 ns with 50-Ω load for $T < 28$ K and electric fields < 30 V/cm. (Compensated material is available with ~5-ns time constant with a 50-Ω load. Responsivity then is reduced by 5–10× and detectivity is reduced by 2.)

Responsivity: Depends on concentration of compensating impurities, bias, area, and background flux See Figs. 183 to 185, ~10^5 V/W.

Dark resistance: Depends on area and FOV: ~100 kΩ for 180° FOV (see Fig. 186).

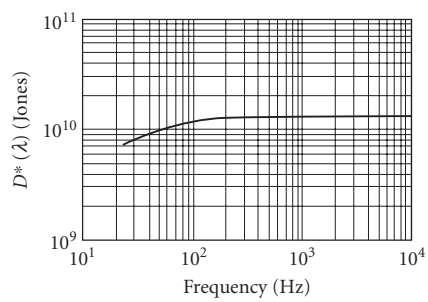

FIGURE 180 Typical D^* versus frequency at 30 K for Ge:Hg; 1 × 1-mm area; essentially constant with temperature. (*Santa Barbara Research Center.*)

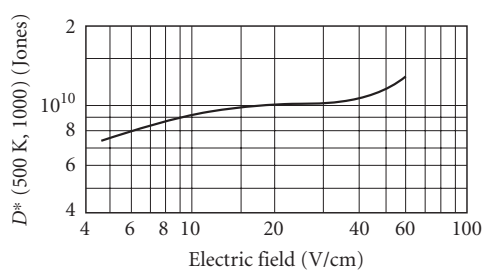

FIGURE 181 D^* versus electric field for Ge:Hg; $T = 5$ K, 90° FOV; 300-K background; 6×10^{-4} cm^{-4} area; Irtran II window. (*Reprinted by permission of Texas Instruments.*)

Downloaded from Digital Engineering Library @ McGraw-Hill (www.accessengineeringlibrary.com)
Copyright © 2010 The McGraw-Hill Companies. All rights reserved.
Any use is subject to the Terms of Use as given at the website.

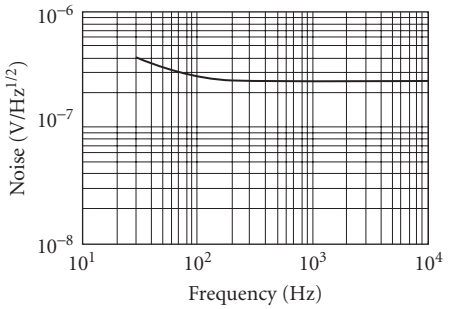

FIGURE 182 Typical noise versus frequency spectrum for Ge:Hg; 1 × 1-mm area; essentially constant with temperature. (*Santa Barbara Research Center.*)

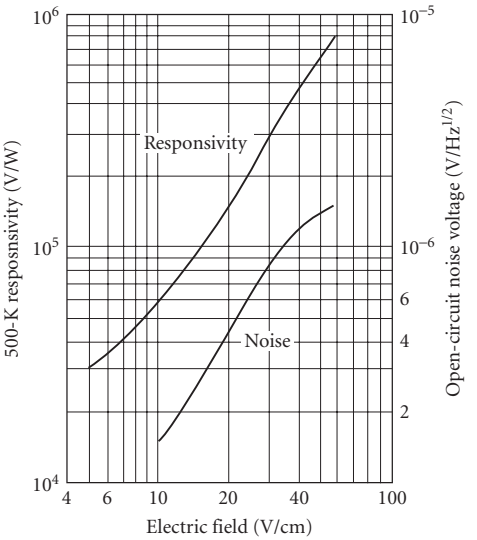

FIGURE 183 Open-circuit responsivity and noise voltage versus electric field for Ge:Hg; $T = 5$ K, 90° FOV; 300-K background; 6×10^{-4} cm^{-4} area; Irtran II window. (*Reprinted by permission of Texas Instruments.*)

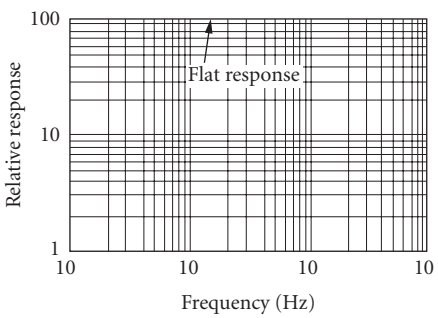

FIGURE 184 Ge:Hg typical relative response versus frequency; $T = 30$ K. (*Santa Barbara Research Center.*)

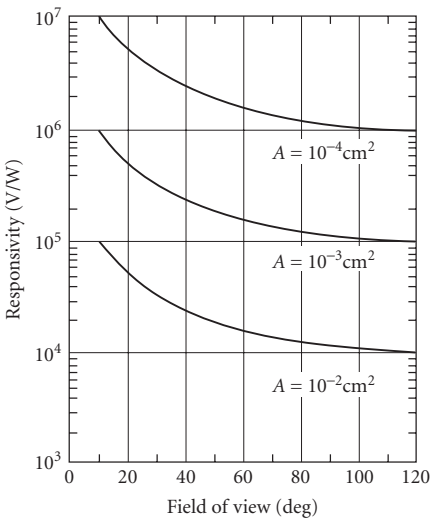

FIGURE 185 Open-circuit responsivity versus FOV for Ge:Hg at 5 K for various detector areas; 300-K background; 500-K blackbody source. (*Reprinted by permission of Texas Instruments.*)

Downloaded from Digital Engineering Library @ McGraw-Hill (www.accessengineeringlibrary.com)
Copyright © 2010 The McGraw-Hill Companies. All rights reserved.
Any use is subject to the Terms of Use as given at the website.

Capacitance: < 1 pF.

Sensitive area: 1 to 5-mm diameter.

Operating temperature: See Fig. 162.

Linearity: 10^{-3} to 10^{-8} W (size dependent).

Sensitivity profile: ±15 percent.

Recommended circuit: Standard photoconductive (see Ge:Au). See Fig. 187 for current-voltage characteristics.

Manufacturer: No suppliers are presently known.

Si:Ga Gallium in silicon forms an acceptor level with a binding energy of ~72 meV which is the basis of an infrared detector with spectral response out to approximately 17 μm, as shown in Fig. 188. The exact spectral cutoff and quantum efficiency will vary slightly with the gallium doping concentration. Gallium-doped silicon requires cooling to 20 K or lower for optimum performance. Background-limited performance associated with a quantum efficiency of about 15 percent is achievable over a wide range of background flux levels, provided the operating temperature is low enough to reduce thermal noise below the photon noise level.

Sensitivity: D^* is given by $D^* = 1.1 \times 10^{10} \times \sqrt{(A\lambda\eta)}/\sqrt{Q}$ (Jones); where A is detector area, λ is the wavelength in micrometers, η is the quantum efficiency, and Q is the background flux in watts.

Responsivity: 0.9 A/W.

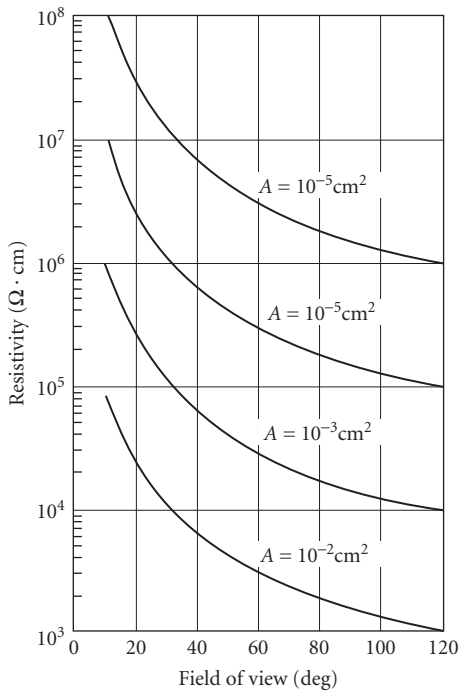

FIGURE 186 Open-circuit resistivity versus FOV for Ge:Hg at 5 K for various detector areas; 300-K background; 500-K blackbody source. (*Reprinted by permission of Texas Instruments.*)

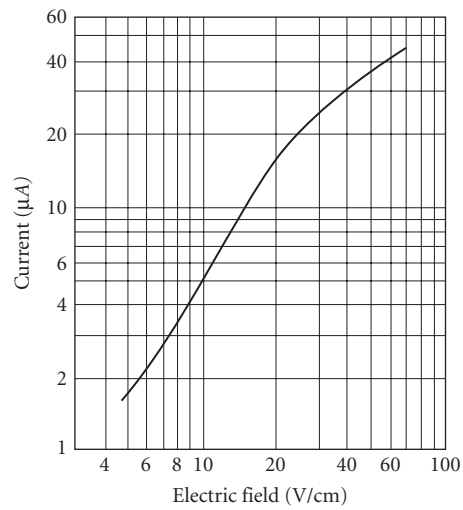

FIGURE 187 Ge:Hg bias current versus electric field; 90° FOV; T = 5 K, 300-K background; 6 × 10^{-4} cm^{-4} area; Irtran II window. (*Reprinted by permission of Texas Instruments.*)

Downloaded from Digital Engineering Library @ McGraw-Hill (www.accessengineeringlibrary.com)
Copyright © 2010 The McGraw-Hill Companies. All rights reserved.
Any use is subject to the Terms of Use as given at the website.

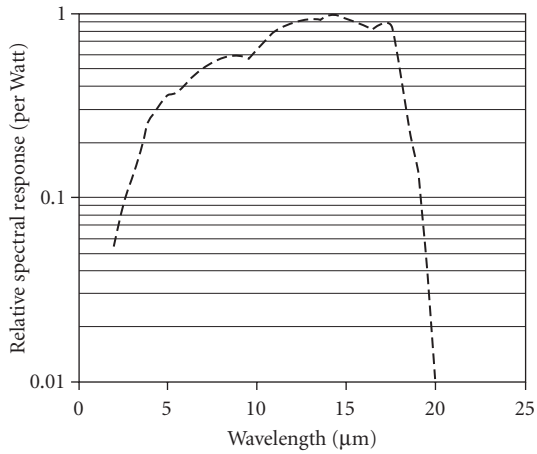

FIGURE 188 Relative spectral response per watt of Si:Ga as a function of wavelength. Data is normalized to unity at the peak response.

Time constant: <1 μs.

Resistance: Depends on background flux and detector bias (similar to Ge:Hg, see Fig. 186).

Capacitance: <1 pF (limited by mounting configuration).

Sensitive area: 0.2 to 2-mm square.

Operating temperature: <20 K.

Recommended circuit: Standard photoconductive.

Manufacturer: Infrared Laboratories.

Si:B Boron in silicon forms an acceptor level with a binding energy of ~45 meV which is the basis of this infrared detector with spectral response out to approximately 30 μm. The exact spectral cutoff and quantum efficiency will vary slightly with the boron-doping concentration. Boron-doped silicon requires cooling to about 15 K or lower for optimum performance. Background-limited performance associated with a quantum efficiency of about 10 percent is achievable over a wide range of background flux levels, provided the operating temperature is low enough to reduce thermal noise below the photon noise level.

Sensitivity: D^* is given by $D^* = 1.1 \times 10^{10} \times \sqrt{(A\lambda\eta)}/\sqrt{Q}$ (Jones); where A is detector area, λ is the wavelength in micrometers, η is the quantum efficiency, and Q is the background flux in watts.

Responsivity: 2 A/W.

Time constant: <1 μs.

Resistance: Depends on background flux and detector bias (similar to Ge:Hg, see Fig. 186).

Capacitance: <1 pF (limited by mounting configuration).

Sensitive area: 0.2 to 2-mm square.

Operating temperature: <15 K.

Recommended circuit: Standard photoconductive (see Ge:Au).

Manufacturer: Infrared Laboratories.

Ge:Cu Copper-doped germanium detectors are fast, single-crystal, impurity-doped photoconductors, with high sensitivity in the broad region 2 to 30 μm. Operating temperature must be maintained below 20 K (ideally <14 K). Ge:Cu is then 300-K background-limited, and response time <50 ns.

Downloaded from Digital Engineering Library @ McGraw-Hill (www.accessengineeringlibrary.com)
Copyright © 2010 The McGraw-Hill Companies. All rights reserved.
Any use is subject to the Terms of Use as given at the website.

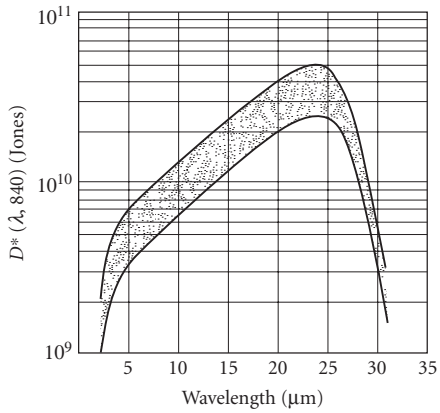

FIGURE 189 Range of spectral detectivities for Ge:Cu; 60° FOV. (*Santa Barbara Research Center.*)

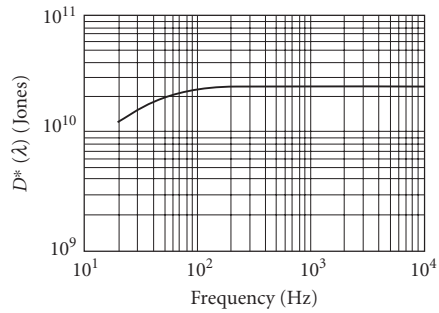

FIGURE 190 Typical D^* vs. frequency for Ge:Cu at 4.2 K. (*Santa Barbara Research Center.*)

Sensitivity: See Figs 161, 162, 189, and 190.

Noise: See Figs. 191 and 192.

Time constant: ~100 ns (can be doped to be faster, ~5 ns). (See discussion of time constant under Ge:Au).

Responsivity: 10^5 V/W (see Figs. 192 to 194).

Dark resistance: Depends on FOV (~100 kΩ for 180° FOV).

Capacitance: <1 pF.

Sensitive area: 1 to 5-mm diameter.

Operating temperature: See Figs. 162 and 194.

Linearity: 10^{-3}–10^{-8} W/cm^2 (depends on size).

Sensitivity profile: ±15 percent.

Stability: Stable in all ambient storage environments tested.

Recommended circuit: See Figs. 166 and 195.

Manufacturer: No suppliers are presently known.

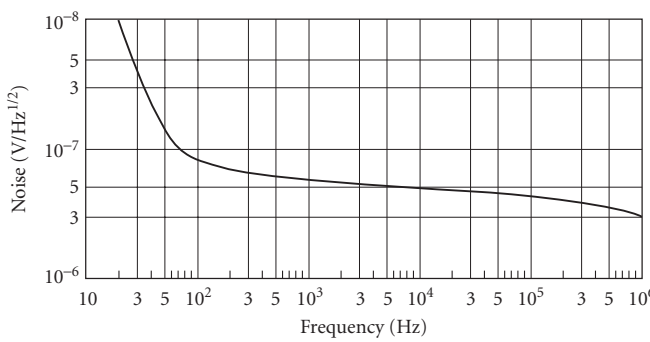

FIGURE 191 Typical noise frequency spectrum for Ge:Cu. (*GEC Marconi Infra Red Ltd.*)

Downloaded from Digital Engineering Library @ McGraw-Hill (www.accessengineeringlibrary.com)
Copyright © 2010 The McGraw-Hill Companies. All rights reserved.
Any use is subject to the Terms of Use as given at the website.

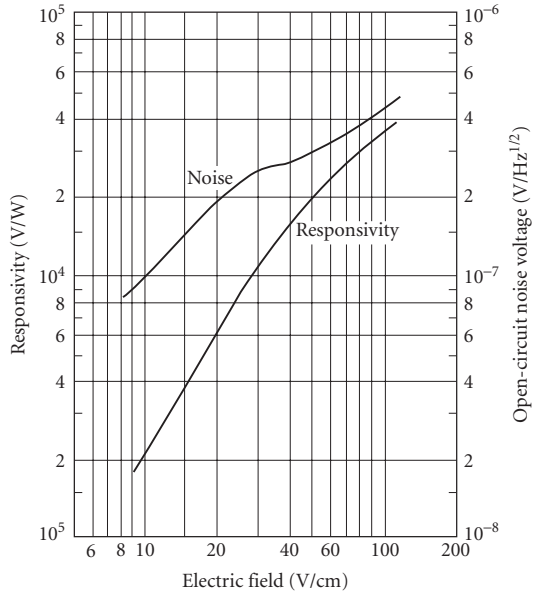

FIGURE 192 Typical noise and responsivity versus biasing field for Ge:Cu; 5 K, 60° FOV; 300-K background, A = 10^{-2} cm^2, 500-K blackbody. (*Reprinted by permission of Texas Instruments.*)

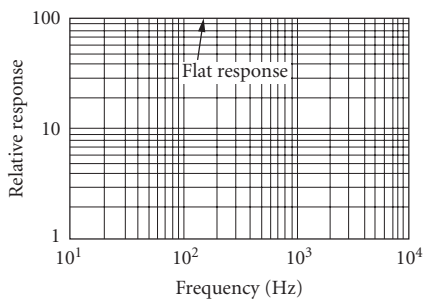

FIGURE 193 Relative response versus frequency for Ge:Cu at 4.2 K. (*Santa Barbara Research Center.*)

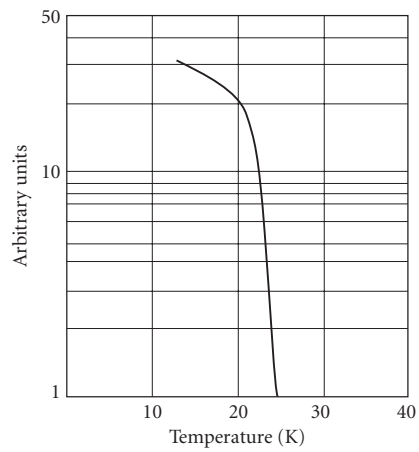

FIGURE 194 Relative responsivity versus temperature for Ge:Cu.

Ge:Zn Very similar to Ge:Cu except that cutoff wavelength moves out to 42 μm and operating temperature should be <10 K. A relatively low field breakdown limits the responsivity.

Sensitivity: See Figs 161, 162, and 196.

Noise: See Fig. 197 and 198.

Downloaded from Digital Engineering Library @ McGraw-Hill (www.accessengineeringlibrary.com)
Copyright © 2010 The McGraw-Hill Companies. All rights reserved.
Any use is subject to the Terms of Use as given at the website.

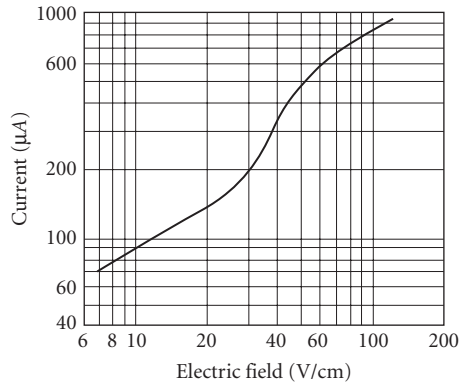

FIGURE 195 Typical current-voltage curve for Ge:Cu, 60° FOV; 300-K background: $A = 10^{-2}$ cm^{-2}. (*Reprinted by permission of Texas Instruments.*)

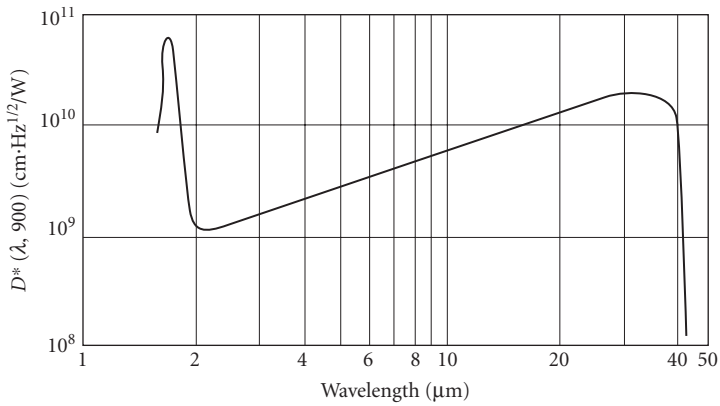

FIGURE 196 D^* versus wavelength for Ge:Zn.

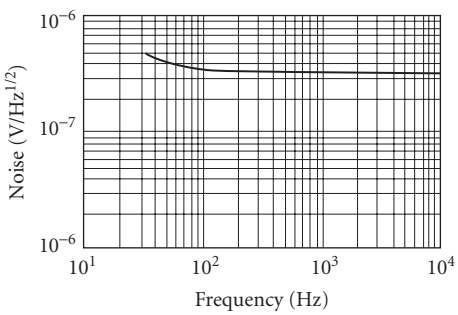

FIGURE 197 Typical noise-frequency spectrum for Ge:Zn at 4.2 K; $A = 1 \times 1$ mm. (*Santa Barbara Research Center.*)

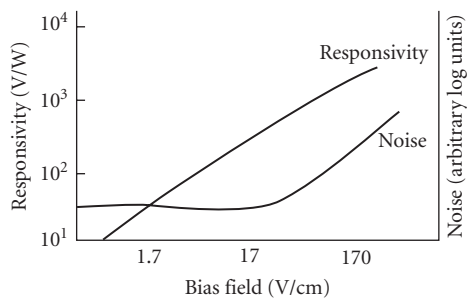

FIGURE 198 Signal and noise for Ge:Zn.

Downloaded from Digital Engineering Library @ McGraw-Hill (www.accessengineeringlibrary.com)
Copyright © 2010 The McGraw-Hill Companies. All rights reserved.
Any use is subject to the Terms of Use as given at the website.

Responsivity: 10^3 V/W (see Fig. 198).

Time constant: <50 ns. (See discussion of time constant under Ge:Au.)

Dark resistance: 0.5 to 5 MΩ/ sq (60°-FOV ambient background).

Capacitance: <1 pF (limited by mounting configuration).

Sensitive area: 1-, 2-, 3-, and 5-mm diameters.

Operating temperature: <10 K.

Recommended circuit: Standard photoconductive.

Manufacturer: No suppliers are presently known.

Ge:Ga The elements of B, Al, Ga, In, and Tl from chemical group III form shallow acceptor states (~10 meV) in germanium which are the basis of infrared detectors with spectral response out to approximately 120 μm. Currently, gallium-doped germanium is commercially available, but germanium doped with other group III elements (Ge:B, Ge:Al, Ge:In, Ge:Tl) will give similar detector performance. The small binding energies associated with this detector require cooling to liquid helium temperatures (4.2 K) or lower for optimum performance. Background-limited performance associated with a quantum efficiency of about 7 percent is achievable over a wide range of background flux levels, provided the operating temperature is low enough to reduce thermal noise below the photon noise level.

Sensitivity: D^* is given by $D^* = 1.1 \times 10^{10} \times \sqrt{(A\lambda\eta)}/\sqrt{Q}$ (Jones); where A is detector area, λ is the wavelength in μm, η is the quantum efficiency, and Q is the background flux in watts.

Responsivity: 4 A/W.

Time constant: <1 μs.

Resistance: Depends on background flux and detector bias.

Capacitance: <1 pF (limited by mounting configuration).

Sensitive area: 0.5-, 1-, and 2-mm square.

Operating temperature: <4.2 K, best below 3 K.

Recommended circuit: Standard photoconductive.

Manufacturer: Infrared Laboratories.

Photographic In this paragraph we present only the spectral sensitivity of some typical photographic emulsions. See Chap. 29, "Photographic Films," for a more extensive coverage.

The term spectral sensitivity generally has a different meaning when applied to photographic detectors than it does when applied to the other detectors described in this chapter. It comes closer to responsivity than to minimum detectable power or energy.* In Fig. 199 sensitivity is the reciprocal of exposure, expressed in ergs per centimeter, required to produce

$$\text{Density} = \log \frac{1}{\text{transmittance}} = 0.3$$

above gross fog in the emulsion when processed as recommended.

Manufacturers: AGFA, Eastman Kodak, Fuji, Polaroid.

*Work is in progress to evaluate photographic materials in terms of minimum detectable energy, a concept involving the average number of photons necessary to produce a change in density (signal) equal to that of the fog-density fluctuations (noise); see Refs. 10, 26, 27, and 28.

Downloaded from Digital Engineering Library @ McGraw-Hill (www.accessengineeringlibrary.com)
Copyright © 2010 The McGraw-Hill Companies. All rights reserved.
Any use is subject to the Terms of Use as given at the website.

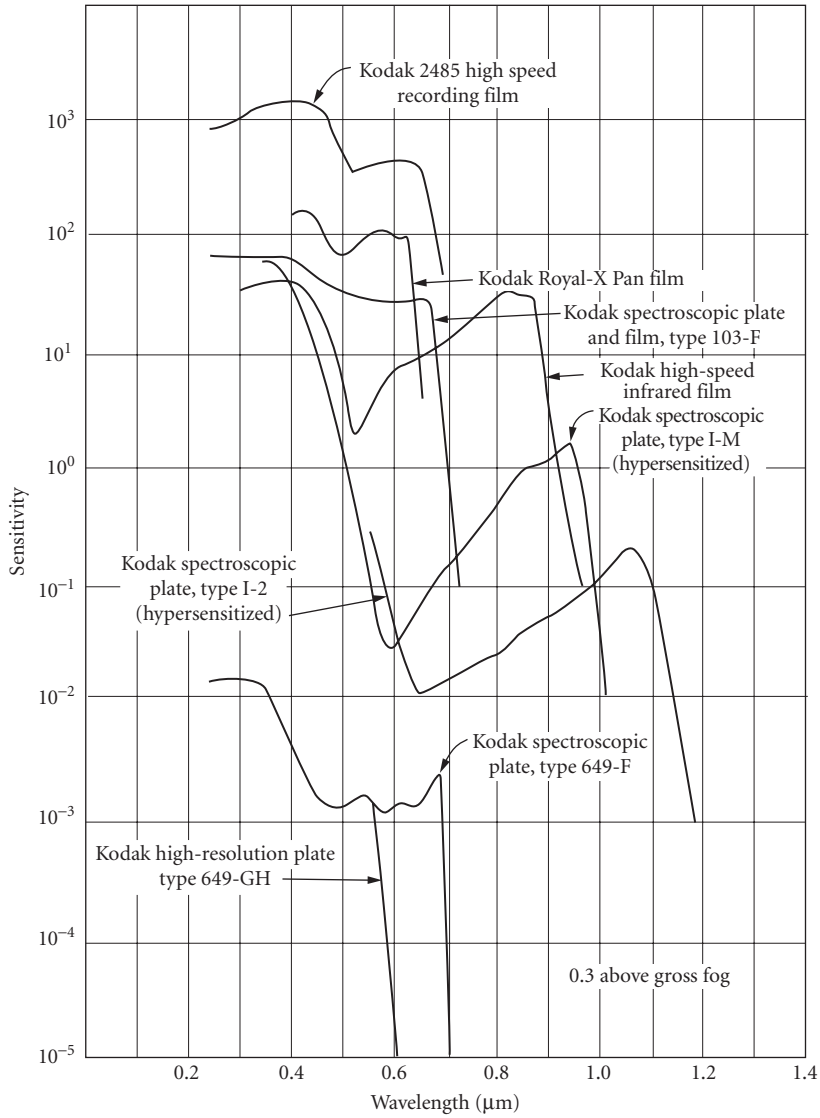

FIGURE 199 Sensitivity versus λ for typical photographic emulsions. (*Eastman Kodak.*)

24.8 REFERENCES

1. W. L. Wolfe, (ed.), *Handbook of Military and Infrared Technology*, Office of Naval Research, Washington, D.C., 1965.
2. Institute of Radio Engineers, "IRE Standards on Electron Tubes: Methods of Testing," Proceedings of the IRE 50(9): 1974–1975 (1962).
3. Radio Corporation of America, "Phototubes and Photocells," *Tech. Man.* **PT-60** (1963).

Downloaded from Digital Engineering Library @ McGraw-Hill (www.accessengineeringlibrary.com)
Copyright © 2010 The McGraw-Hill Companies. All rights reserved.
Any use is subject to the Terms of Use as given at the website.

4. D. Vincent, *Fundamentals of Infrared Detector Operation and Testing*, Wiley, New York, 1989.
5. E. L. Dereniak and D. Crowe, *Optical Radiation Detectors*, Wiley, New York, 1984.
6. W. Rogatto, ed., *The Infrared and Electro-Optical Systems Handbook*, vol. **3**, SPIE Press, Bellingham, Wash., 1993.
7. R. C. Jones, "Factors of Merit for Radiation Detectors," *J. Opt. Soc. Am.* **39**:344 (1949).
8. G. Bauer, "Ein halbleiter Hochohmbolometer mit Tafel, IV," *Phys. Z.* **44**:53 (1943).
9. J. A. R. Samson, *Techniques of Ultraviolet Spectroscopy*, Wiley, New York, 1967.
10. R. Jones, "On the Quantum Efficiency of Photographic Negatives: On the Minimum Energy Detectable by Photographic Materials," *Photogr. Sci. Eng.* **2**:57–65j, 191–204 (1958).
11. D. J. Fink, *Principles of Television Engineering*, McGraw-Hill, New York, 1940.
12. R. A. Smith, F. E. Jones, and R. P. Chasmar, *Detection and Measurement of Infrared Radiation*, Oxford University, London 1957.
13. S. F. Jacobs, and M. Sargent III, "Photon Noise Limited D^* for Low Temperature Backgrounds and Long Wavelengths," *Infrared Phys.* **10**(4):233–235 (1970).
14. P. W. Kruse, L. D. McGlaughlin, and R. B. McQuistan, *Elements of Infrared Technology*, Wiley, New York, 1962.
15. P. B. Fellgett, "On the Ultimate Sensitivity and Practical Performance of Radiation Detectors," *J. Opt. Soc. Am.* **39**:970 (1949).
16. F. J. Low, and A. R. Hoffman, "The Detectivity of Cryogenic Bolometers," *Appl. Opt.* **2**:649 (1963).
17. F. J. Low, "Low-Temperature Germanium Bolometer," *J. Opt. Soc. Am.* **51**:1300 (1961).
18. E. H. Eberhardt, "Threshold Sensitivity and Noise Ratings of Multiplier Phototubes," *Appl. Opt.* **6**:251 (1967).
19. W. C. Livingston, "Enhancement of a Photocathode Sensitivity by Total Internal Rejection as Applied to an Image Tube," *Appl. Opt.* **5**:1335 (1966).
20. W. D. Gunter, G. R. Grant, and S. A. Shaw, "Optical Devices to Increase Photocathode Quantum Efficiency," *Appl. Opt.* **9**:251 (1970).
21. M. Cole and D. Ryer, "Cooling PM Tubes for Best Spectral Response," *Electro Optical Systems Design* **4**(6):16–19 (June 1972).
22. H. E. Bennett, "Accurate Method for Determining Photometric Linearity," *Appl. Opt.* **5**:1265 (1966).
23. R. E. Simon, A. H. Sommer, J. J. Tietjen, and B. F. Williams, "New High-Gain Dynode for Photomultipliers," *Appl. Phys. Lett.* **13**:355 (1968).
24. G. A. Morton, H. M. Smith, and H. R. Krall, "Pulse Height Resolution of High Gain First Dynode Photomultipliers," *Appl. Phys. Lett.* **13**:356 (1968).
25. S. M. Sze, *Physics of Semiconductor Devices*, 2d ed., Wiley, New York, p. 773, 1981.
26. T. H. Johnson, "Lead Salt Detectors and Arrays: PbS and PbSe," *Proc. SPIE* **443**: 60–94, (1984).
27. J. C. Marchant, "Exposure Criteria for the Photographic Detection of Threshold Signals," *J. Opt. Soc. Am.* **54**:79 (1964).
28. G. R. Bird, R. C. Jones, and A. E. Ames, "The Efficiency of Radiation Detection by Photographic Films: State-of-the-Art and Methods of Improvement," *Appl. Opt.* **8**:2389 (1969).

24.9 SUGGESTED READINGS

Sommer, A. H., *Photoemissive Materials*, Wiley, New York, 1968.

Sommers, H. S., Jr. and E. K. Gritchell, "Demodulation of Low-Level Broadband Optical Signals with Semiconductors," *Proc. IEEE* **54**:1553 (1966).

Sommer, A. H., and W. B. Teusch, "Demodulation of Low-Level Broadband Optical Signals with Semiconductors, II: Analysis of the Photoconductive Detector," Proc. IEEE **52**:144 (1964).

Sun, C. and T. E. Walsh, "Performance of Broadband Microwave-Biased Extrinsic Photoconductive Detectors at 10.6 m," *IEEE J. Quantum Electron*. **6**:450 (1970).

Downloaded from Digital Engineering Library @ McGraw-Hill (www.accessengineeringlibrary.com)
Copyright © 2010 The McGraw-Hill Companies. All rights reserved.
Any use is subject to the Terms of Use as given at the website.